Surf beat and its effect on cross-shore profiles

J.A. Roelvink

Surf beat
and its effect on cross-shore profiles

PROEFSCHRIFT

ter verkrijging van de graad van doctor aan de Technische Universiteit Delft, op gezag van de Rector Magnificus, prof. drs. P.A. Schenck, in het openbaar te verdedigen ten overstaan van een Commissie aangewezen door het College van Dekanen op woensdag 16 juni 1993 te 16.00 uur

door

Jan Adriaan Roelvink
geboren 10 mei 1959 te 's Gravenhage

1993

Dit proefschrift is goedgekeurd door de promotor
prof. dr. ir. J.A. Battjes

CONTENTS

CONTENTS (continued)

SAMENVATTING

Volgens een bekende vuistregel is iedere zevende golf een hoge golf. Dit geeft aan dat de door wind opgewekte golven zich in groepen voortplanten; een golfgroep bestaat in het algemeen uit ongeveer vijf tot tien golven. Wanneer we naar de zee kijken zien we dus typisch twee soorten variaties van het wateroppervlak: de op en neer gaande korte golfbeweging en de langzame variatie van de golfhoogte.

Binnen de periode van een enkele korte golf treden fluctuaties op van drukken en snelheden, die voor een groot deel, maar niet geheel wegvallen na middeling over deze periode. Er blijft een netto bijdrage aan de waterbeweging over, die zich uit in een netto stroming en in een term die te vergelijken is met een druk op het wateroppervlak, de zogenaamde "radiation stress". Doordat de hoogte van de korte golven variëert in plaats en tijd variëren ook deze netto bijdragen; hierdoor wordt een lange golfbeweging opgewekt met perioden en lengtes die vergelijkbaar zijn met die van de golfgroepen.

Deze lange golfbeweging kan zich zowel dwars op de kust als langs de kust manifesteren. De verzamelnaam voor al dergelijke bewegingen is "surf beat", zo genoemd door Munk (1949) die ze als eerste op zee heeft waargenomen. Het "surf" slaat op de brandingszone, waar naar Munk aannam de lange golven worden gegenereerd, en "beat" (zweving) op het feit dat de lange golven een frequentiebereik hebben dat overeenkomt met de zwevings- of groepsfrequentie van de korte golven.

Door het feit dat de afmetingen van in de natuur voorkomende zandbanken en andere kustmorfologische patronen vaak overeenkomen met typische golflengten van golfgroepen en lange golven is de hypothese ontstaan dat deze patronen ook veroorzaakt worden door lange golven. In de literatuur worden twee soorten verklaringen gegeven voor een dergelijk verband.

In de eerste verklaring wordt gesteld dat aan de kust door reflecterende lange golven een staand golfpatroon ontstaat, hetgeen leidt tot een patroon van netto snelheden dat, afhankelijk van de plaats boven de bodem, naar knopen of juist naar buiken van de staande golfbeweging wijst. Afhankelijk van het transport-type ontstaan dan banken bij de knopen of bij de buiken van dit patroon.

Het probleem bij deze verklaring is, dat deze driftsnelheden zo klein zijn ten opzichte van bijvoorbeeld de onderstroom in brekende golven, dat ze niet goed waar te nemen zijn en dat ook moet worden betwijfeld of ze een grote rol spelen.

Een tweede verklaring is de volgende: de variatie van de golfhoogte wekt niet alleen lange golven op, maar ook fluctuaties in de zandconcentratie. Dit betekent dat de langegolf snelheid een sterke koppeling vertoont met de fluctuatie van de zandconcentratie.

Deze koppeling leidt tot een netto bijdrage aan het zandtransport, die van dezelfde orde van grootte is als het effect van de onderstroom.

Uit onderzoek naar het modelleren van het zandtransport dwars op de kust (bijvoorbeeld Roelvink en Stive, 1989) is duidelijk naar voren gekomen dat deze interaktie tussen korte en lange golven een wezenlijke bijdrage aan het dwarstransport vormt, die met de beschikbare modellen en concepten niet goed voorspeld kon worden. Dit is de voornaamste motivatie geweest voor het in dit proefschrift beschreven onderzoek.

Het doel van dit onderzoek is, een model te ontwikkelen waarmee de korte en lange golfbeweging in de kustnabije zone gesimuleerd kan worden, en waarmee de voor het dwarstransport relevante parameters met voldoende nauwkeurigheid kunnen worden voorspeld.

Hierbij beperken wij ons tot de situatie van loodrecht invallende golven op een in langsrichting uniform strand, omdat dit een logische eerste stap is, en omdat er genoeg aanwijzingen zijn dat de bewegingen dwars op de kust tenminste een belangrijk onderdeel vormen van het fenomeen "lange golven".

Dit proefschrift is als volgt opgebouwd: in het eerste hoofdstuk wordt aan de hand van de literatuur nader ingegaan op de achtergronden van surf beat en het effect ervan op kustprofielen.

In het tweede hoofdstuk worden modelvergelijkingen opgesteld, uitgaande van de over de korte golven gemiddelde behoudsvergelijkingen voor massa, impuls, golfaktie en golfdichtheid. Hierbij besteden we speciale aandacht aan de zogenaamde sluitingsvergelijkingen die nodig zijn om het stelsel behoudsvergelijkingen oplosbaar te maken. Een wezenlijk onderdeel hierbij is het modelleren van de dissipatie van golfenergie door het breken van gegroepte korte golven, waarvoor een nieuwe formulering wordt voorgesteld.

In het derde hoofdstuk bespreken we hoe de modelvergelijkingen worden gediscretiseerd om ze met behulp van de computer op te kunnen lossen. Hierbij treedt het probleem op, dat de vergelijkingen alleen gelden op het domein tussen de zeewaartse grens en de waterlijn. Doordat de waterlijn heen en weer beweegt is dit domein niet constant in de tijd. Het probleem wordt opgelost door de vergelijkingen te transformeren naar een rekendomein dat wel constant is in de tijd, en de getransformeerde vergelijkingen in dat domein op te lossen. Het numerieke schema wordt getest aan de hand van bekende analytische oplossingen. Ook wordt getest of het schema bestand is tegen discontinue oplossingen (brekende lange golven) van de ondiep-water vergelijkingen.

In het vierde hoofdstuk wordt de ijking van de empirische onderdelen van het model besproken. Het gaat hierbij met name om de formulering voor de dissipatie van golfenergie door het breken van korte golven. In het hoofdstuk wordt verwezen naar een als Appendix B toegevoegde publicatie over dit onderwerp.

In het volgende hoofdstuk behandelen we de validatie van het model aan de hand van door anderen uitgevoerde experimenten in golfgoten. Het eerste geval betreft regelmatige golfgroepen die zijn gegenereerd door twee golfcomponenten met verschillende frequentie en amplitude te superponeren (Kostense, 1984). Het model blijkt de variatie in de lange golfcomponenten ten gevolge van variaties in de opgelegde korte golven goed weer te geven. Het tweede geval betreft proeven met onregelmatige golven (Van Leeuwen, 1992). Hierbij wordt veel aandacht besteed aan het genereren van randvoorwaarden die goed aansluiten bij de tijdens het experiment opgewekte golven. Het model geeft de gemeten tijdseries van de korte golfenergie en de totale lange golfbeweging redelijk tot goed weer, terwijl over langere tijd gemiddelde parameters nauwkeurig worden voorspeld.

In het zesde hoofdstuk bespreken we de invloed van kustdwarse lange golven op kustprofielen. Eerst wordt teruggegrepen op proeven die door Roelvink en Stive (1989) geanalyseerd zijn, en waarin het effect van lange golven duidelijk is aangetoond. De daarin beschreven effecten blijken nu goed voorspeld te worden door het model. Vervolgens wordt aan de hand van een groot aantal simulaties voor realistische omstandigheden en kustprofielen onderzocht wat de rol van lange golven in het genereren van zandbanken is. Hieruit komt als conclusie naar voren dat de kustdwarse lange golven een belangrijke, doch voornamelijk destructieve rol spelen: het effect van lange golven is, dat gevormde banken zeewaarts verplaatst worden en daarbij afgevlakt worden.

In hoofdstuk zeven worden tenslotte de conclusies samengevat en aanbevelingen voor verder onderzoek gedaan.

ABSTRACT

In this thesis we describe the development, calibration and validation of a predictive model, code named "SURFBEAT", which describes the propagation of normally incident wave groups through the surf zone and their associated long wave motions.

The model formulations are based on the short wave averaged conservation equations for mass, momentum, wave action and wave density. Closure relations are derived from linear theory, except for those concerning dissipation terms. A new formulation for the time-varying, short wave averaged wave energy dissipation due to breaking is proposed.

The applied numerical method is tested against known analytical solutions of the non-linear shallow water equations. The scheme is capable of accurately representing bore solutions of the shallow water equations; hence the model automatically represents the breaking of long waves.

Special attention is paid to the calibration of the parameters in the breaker formulation, and a set of constant parameter values is found for which the formulation is valid over a wide range of conditions.

The complete model is validated against data from three different wave flume experiments. The first dataset concerns bichromatic waves incident on a plane sloping beach (Kostense, 1984). The measured quantities are the incident bound long wave amplitude and the reflected free long wave amplitude. The second dataset was presented by Van Leeuwen (1992) and concerns random waves incident on a plane sloping beach. Here, time series of the water elevation measured in a number of points both on the horizontal stretch near the wave maker and on the sloping beach are available. The third dataset was presented by Roelvink and Stive (1989) and concerns surface elevation and near-bed velocity measurements in a wave flume with random waves incident on a sandy beach of an initially plane slope which develops into a barred profile. The data available are time-averaged parameters of the incident wave field, the long waves and the interaction between short waves and long waves.

We conclude that in the context of cross-shore transport modelling the model presented here is an accurate enough predictive model for the propagation and decay of normally incident random wave groups and their associated long wave motions over an arbitrary beach profile. The use of the non-linear shallow water equations for the long wave motion enables application of the model to severe conditions where the long waves have high amplitudes or may even be breaking.

The role of the cross-shore long wave motions on cross-shore profiles is investigated by numerical experiments over a large number of realistic profiles and incident wave conditions. We conclude that, at least in the purely cross-shore case, the interaction between short waves and long waves plays an important, but mainly destructive role in the behaviour of longshore bars.

1. INTRODUCTION

1.1 Surf beat

According to a popular rule-of-thumb, every seventh wave is a high wave. The truth in this saying is the fact that the heights of wind-generated waves are not completely unrelated to those of previous waves, but that we often see coherent groups of high waves.

In a system of waves we thus have two characteristic time-scales: that of the individual waves and that of the wave groups. On the time-scale of individual waves we see an approximately sinusoidal fluctuation of the water level and the velocity field; on the time-scale of the wave groups we see the slow variation of the amplitudes of these fluctuations.

The fluxes of momentum and mass fluctuate within an individual wave period, but do not average out; on the time scale of wave groups the short wave averaged momentum flux ("radiation stress") and mass flux ("wave-induced mass flux") vary slowly. The variation in time and space of the radiation stress and mass flux generates long waves with periods and wave lengths similar to the group periods and lengths. These long waves may travel with the wave groups or they may be released as free waves if the wave groups forcing them change rapidly, e.g. due to breaking in the surf zone. The free waves generally reflect on the beach, and either escape to deep water ("leaky modes") or are trapped to the shoreline by refraction as "edge waves".

The collective name for long wave motions on the time-scale of the wave groups is "surf beat", a term conceived by Munk (1949) which carries the suggestion that the long waves are generated in the surf zone and which indicates that it is a phenomenon at the "beat" frequency of the wind waves, the characteristic frequency of the wave groups.

Tucker (1950) measured long waves well outside the surf zone. He determined the correlation between the short wave envelope and the long wave elevation, for different time lags, and found a significant negative correlation near zero time lag, but an even greater, mostly positive correlation at a lag corresponding to the time it takes for a short wave group to travel to the beach and for a free wave to travel back (for an example see Figure 1.1). He concluded that the diagrams indicated free waves travelling in offshore direction, produced by groups of high waves breaking on the beach.

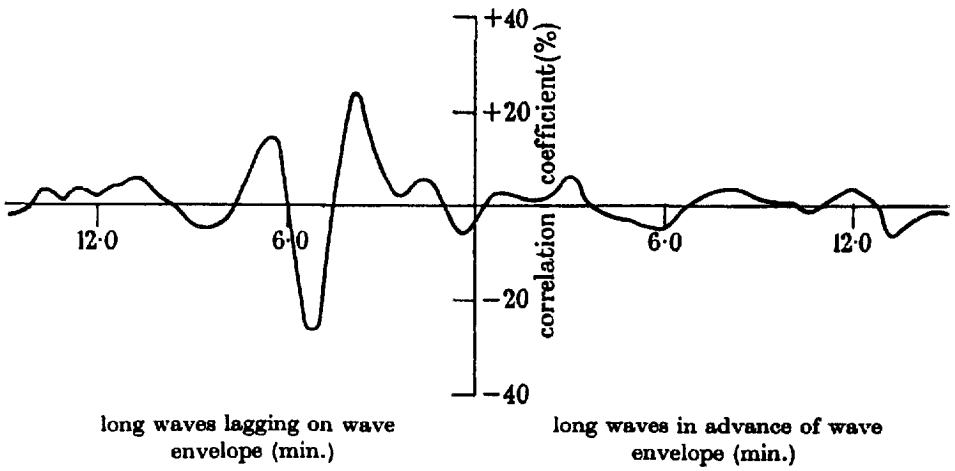

Figure 1.1 *"Correlogram" depicting correlation between short wave envelope and long wave elevation, at different time lags; a high correlation at time lag τ means, that the long wave signal resembles the short wave envelope an interval τ earlier (From Tucker, 1950)*

Longuet-Higgins and Stewart (1962) explained the negative correlation at zero time lag by the presence of "bound long waves", long waves that are forced by the variations on wave group scale of the radiation stress and mass flux, and travel at the same speed as the groups that force them. They also hypothesize that the observed free waves radiated from the beach are due to reflection of the bound waves, which are somehow released in the surf zone. At first sight, this would imply that (in contrast with the observations) the correlation between bound waves and the wave envelope that forces it must be much stronger than that between reflected waves and the envelope that forced it some minutes earlier; however, their theory shows that the shoaling of bound waves is much more spectacular than the "inverse shoaling" of free waves; hence, if the bound waves are released close to shore, the reflected free waves would have a higher amplitude at the offshore location than the bound waves, which would explain their higher correlation with the wave envelope. Still, the mechanism by which the bound waves are released is not explained by this theory.

Symonds et al. (1982) focus on a different mechanism, which is more in line with the original hypothesis by Munk (1949) and Tucker (1950). They assume that within the inner surf zone, the short waves are "saturated", meaning that the variations on wave group scale have vanished and the radiation stress gradients are constant in time. Outside the surfzone, they assume that the horizontal variation of the radiation stress is negligible (and thereby do not include the effect of bound waves). In the transition

region, the break-point moves back and forth; in this region there is a radiation stress gradient varying in time. This gradient acts as a local forcing, comparable to a wave maker which generates waves both in onshore direction and (with opposite sign) in offshore direction. The onshore directed wave is subsequently reflected off the beach and interferes with the offshore directed wave. Depending on the dimensionless width of the surf zone, the relative phase of the two free outgoing wave components changes, resulting in an enhancing or damping of the total free wave radiated from the surf zone. The fact that such an amplitude variation with the dimensionless surf zone width exists was confirmed in laboratory experiments by Kostense (1984); however, the quantitative agreement between the model and his experiments was not convincing.

Schäffer and Svendsen (1988) improved this model concept by including the forcing outside the surf zone responsible for the bound long waves. In their model this forcing is reduced in the surf zone but does not vanish completely since they relax the rigid assumption of a saturated inner surf zone. Schäffer and Jonsson (1990) compared this model with Kostense's (1984) data and now found considerably better agreement; remaining discrepancies can be ascribed to the lack of bottom friction and the use of linearized equations in their model.

Apparently bound waves are released in the surf zone and reflected off the beach. Similarly, bound waves travelling over an uneven bathymetry can be partially released as free waves; examples are given in Dingemans et al. (1991).

The amplitude of surf beat can be enhanced significantly if resonance conditions occur. For cross-shore modes, this can happen by partial wave trapping on barred profiles, as shown theoretically by Symonds and Bowen (1984), or on shallow reefs, as shown in the field by Nakaza et al. (1990) and confirmed in numerical and laboratory experiments by Nakaza and Hino (1991). Under these conditions, breaking of the long waves may be expected to occur, and linearized shallow water equations cannot be used quantitatively.

Long waves generated by obliquely incident wave groups can be trapped to the shoreline by refraction; the ensuing wave patterns are called "edge waves". Edge waves can be described as cross-shore standing wave patterns propagating alongshore; combinations of edge waves can produce alongshore standing edge waves. Ursell (1952) has shown for a plane sloping beach that a discrete number of edge-wave modes and longshore wave numbers are possible for a given frequency; the number of zero crossings in cross-shore direction is given by the mode number. The amplitude envelope decays exponentially with distance offshore from the water line.

Resonant excitation of edge waves by wave groups is possible if the forcing has an alongshore wave number corresponding with one of the edge wave modes at the group frequency. This was shown by Gallagher (1971) for low-mode edge waves. Bowen and Guza (1978) showed that on gently sloping beaches high modes are likely to be excited at resonance.

The relative importance of edge waves as compared with cross-shore long wave modes is not quite clear. There are some indications in favour of cross-shore modes. Huntley et al. (1981) report on field observations that indicate a concentration of energy in edge waves for the velocity parallel to the shore, but do not find this for the cross-shore velocity, indicating that other cross-shore modes are more important for these motions. A study by Lippmann and Holman (1992) describes analyses of bar motions based on two years of daily video time-exposures. One of their important conclusions is that 76% of the variability of the bar crest is explained by cross-shore motions, against 14% explained by the longshore structure of the bar, which may indicate a dominance of cross-shore wave modes.

A practical problem with most existing analytical models is that they use an idealized bottom geometry (e.g. a plane sloping beach), idealized incident waves (e.g. bichromatic waves) or simplified equations that preclude their use in predicting the propagation and decay of wave groups and the accompanying long waves. Models specifically aiming at producing practical predictions sofar have been presented by Lo (1981), List (1986, 1992). Both use linearized equations and a schematized description of the forcing due to random waves, which does not include the influence of long waves on the forcing. These models are formulated in the time domain. Qualitatively, promising results are reported by List (1992). A spectral approach for long wave generation on arbitrary beaches is presented by Van Leeuwen (1992), who presents comparisons with prototype measurements which are promising, but finds less agreement for laboratory experiments. This may be due to a rather crude treatment of the short wave breaking.

At this moment, the major physical problem in quantitatively predicting the generation of both cross-shore and edge wave modes of surf beat is the description of the short wave induced forcing terms, especially inside the surf zone. In random waves the concept of a saturated zone fails, as was shown e.g. in Thornton and Guza (1983). The study of Schäffer and Jonsson (1990) clearly shows the influence of including modulation of short waves within the surf zone. A formulation which describes the propagation of wave groups into the surf zone, the dissipation by breaking and the effect of long wave velocity and water level fluctuations on the wave groups is sofar lacking.

Developments towards incorporation of a more sophisticated treatment of the short wave breaking in time-domain models are presented in Sato and Mitsunobu (1991), Symonds and Black (1991) and Roelvink (1991). The latter is treated extensively in this thesis. Reniers (1992) presents a model for the generation of long waves due to obliquely incident waves on arbitrary profiles, which uses a short wave description similar to Roelvink (1991). His model is still restricted to periodic (in time and longshore space) wave groups and long waves, but may perhaps be extended to a fully spectral model.

1.2 Effect of surf beat on morphology

The hypothesis that surf beat has an important effect on cross-shore profiles originates from the fact that the typical length scales of many morphological features on natural beaches are similar to the length scales of long waves. Two types of explanations have been offered for the influence of long waves.

In the first type the long wave motion itself is responsible for introducing net transport effects through drift velocities that occur in the case of standing long waves. In cross-shore direction, it is quite likely for standing waves to occur, since most of the long waves incident on a beach will be reflected almost fully. Often, long waves are trapped to the shoreline on a sloping beach as "edge waves", which form a cross-shore standing wave pattern which propagates in longshore direction. For a standing wave pattern in longshore direction to be possible, different edge waves of the same frequency must occur simulta-neously. In this case, net drift velocities are again possible. Most existing bar patterns have been explained by various combinations of edge waves; Holman and Bowen (1982) give an excellent review of all previous studies, and present a generalised model concept for all possible interactions between two or three edge wave modes, which is able to generate all of the previously reported topographies. However, some important questions remain unanswered. First of all, the long wave amplitudes are small compared to the short waves, except very close to the shoreline. Since the drift velocities generated by standing long wave patterns scale with the amplitude squared, this means that they must be very small compared to the drift velocities related to the wind waves. Another point is that the interfering edge waves must have a significant phase coupling, which is difficult to imagine on an uninterrupted beach, but conceivable in cases of beaches between headlands.

The rôle of the short waves in the above models is limited to enhancing the time-averaged level of suspension of sediment. As was first pointed out by Shi and Larsen (1984), a much more important effect of short waves may be that the amount of suspended sediment is related to the amplitude of the short waves and therefore varies on the time-scale of the wave groups. Since the long waves act on the same time-scale as

the wave groups, and often are caused directly by these groups, a strong correlation between the suspended load and the long wave velocity is bound to exist, and thus a significant net transport effect. This effect scales with the short wave velocity variance times the long wave velocity amplitude and must therefore be much larger than the effect of the drift velocities in standing long waves. Indeed, it has been shown both in the laboratory (Roelvink and Stive, 1989) and in the field (e.g. Osborne and Greenwood, 1992a,b) that this net transport term is of the same order of magnitude as for instance those related to the return flow under breaking waves or to the asymmetry of short waves.

Roelvink and Stive (1989) use a simple formulation to estimate the effect of this term. The direction and magnitude of the interaction term between short wave velocity variance and the long wave velocity is indicated by their cross-correlation coefficient and both amplitudes. In laboratory tests and in field data (e.g. Abdelrahman and Thornton, 1987) this correlation coefficient is seen to change from negative values at offshore locations to less negative or even positive values near the shoreline. The negative values offshore are explained by a dominance of the bound long wave effect; the positive values must be due to short wave modulation caused by depth variations induced by long waves. In the preliminary model presented by Roelvink and Stive (1989), a simple empirical formulation is used for the correlation coefficient, which does not have a general applicability.

1.3 Aim and scope of the present study

The aim of the study presented in this thesis is to develop a predictive model of the propagation and decay of groups of short waves and the long waves generated by these groups, and to investigate with this model the effect of long waves on the development of cross-shore profiles.

We restrict ourselves to the case of normally incident waves, since this is a necessary first step in the development, and since there are clear indications of the importance of cross-shore long wave modes. However, the obstacles to extending the model concept presented here to two dimensions are mainly prac-tical.

The general lay-out of the thesis is as follows. In Chapter 2, the model formulations are derived from the basic short wave averaged conservation equations. The numerical scheme used to solve the resulting set of differential equations is discussed in Chapter 3.

The model contains some coefficients that need to be calibrated, mainly in the formulation of the dissipation through wave breaking. This is presented in Chapter 4. The overall model is then validated against laboratory experiments of bichromatic waves (Kostense, 1984) and random waves (Van Leeuwen, 1992), results of which are presented in Chapter 5.

In Chapter 6, effects of the interaction between long waves and short wave groups on cross-shore profile evolution are investigated for a range of incident wave parameters and profile shapes. These effects are also quantitatively compared with other profile-shaping mechanisms.

Conclusions are finally presented in Chapter 7.

2. MODEL FORMULATIONS

2.1 Introduction

Several models have been presented in literature which describe one or more aspects of long-wave generation and propagation on the time-scale of wave groups (Longuet-Higgins and Stewart, 1962; Symonds et al., 1982; Symonds and Bowen, 1984; Abdelrahman and Thornton, 1987; Schäffer et al., 1990; List, 1986, 1992). These models are well suited to clarify specific aspects, but generally use strong schematizations in either the hydrodynamic equations or the bottom geometry and therefore cannot be used as an accurate predictive model for the interacting wave group/long wave system on an arbitrary profile. The main schematizations in the present literature are in the description of the wave group propagation and attenuation, in the (linearized) form of the long wave equations or in the profile shape. The model presented here is aimed at improving this situation.

In this Chapter, we discuss the basic conservation equations, schematizations applied to these equations, closure relations that are required to solve these equations and the general behaviour of the resulting system of equations.

Parts of this Chapter have been published in slightly different form in Roelvink (1991). Parallel to the development of this model, other researchers have been developing similar models, e.g. Sato and Mitsunobu (1991), Symonds and Black (1991).

2.2 Basic equations

The basic equations applied in the model are derived from Phillips (1977); they are based partly on work by others (Longuet-Higgins and Stewart, 1964; Whitham, 1974). We consider the case of wave groups normally incident on an arbitrary beach which is uniform alongshore. As was discussed in Chapter 1, we consider two characteristic time scales: that of the individual waves and that of the wave groups and associated long waves. We assume that the time scale of the short wave fluctuations is much shorter than that of the wave groups. The behaviour of wave groups and associated mean flows and long waves is then described by the following short wave averaged conservation equations:

Conservation of momentum:

Phillips' equation 3.6.7 for the one-dimensional case reduces to:

$$\frac{\partial}{\partial t}\overline{\int_{-d}^{z_s} \rho u\,dz} + \frac{\partial}{\partial x}\overline{\int_{-d}^{z_s} (\rho u^2 + p)\,dz} - \overline{p_b \frac{d}{dx} d} + \overline{\tau_b} = 0 \tag{2.1}$$

where d is the still water depth, z_s is the water level, ρ the density of water (assumed constant), u the horizontal velocity averaged over turbulence, p the pressure, p_b the pressure at the bottom and $\overline{\tau_b}$ the bottom shear stress. The overbar denotes averaging applied to the fluctuations associated with the short waves, which are assumed to be much shorter than the long waves. Let:

$$u = U + u' \tag{2.2a}$$

where U is the long wave component, invariant with depth, and u' is the fluctuating component of the velocity;

$$h = d + \overline{z_s} \tag{2.2b}$$

where h is the total water depth, averaged over the short waves;

$$Q_t = hU + Q_w \text{ or } U = \frac{Q_t}{h} - \frac{Q_w}{h} \tag{2.2c}$$

where Q_t is the total average flux:

$$Q_t = \overline{\int_{-d}^{z_s} u\,dz} \tag{2.2d}$$

and Q_w is the wave-induced flux:

$$Q_w = \overline{\int_{-d}^{z_s} u'\,dz} \tag{2.2e}$$

The first term in equation (2.1) can now be written as:

$$\frac{\partial}{\partial t}\overline{\int_{-d}^{z_s} \rho u\,dz} = \frac{\partial}{\partial t}\left(\rho U (d + \overline{z_s}) + \rho Q_w\right) = \frac{\partial}{\partial t}\rho Q_t \tag{2.3}$$

The second term in equation (2.1) can be elaborated to:

$$\frac{\partial}{\partial x}\overline{\int_{-d}^{z_s}(\rho u^2+p)\,dz} = \frac{\partial}{\partial x}\overline{\int_{-d}^{z_s}\rho U^2+2\rho Uu'+\rho u'^2+p)\,dz} =$$

$$\frac{\partial}{\partial x}\left[\rho h U^2+2\rho UQ_w + \overline{\int_{-d}^{z_s}(\rho u'^2+p)\,dz}\right] =$$

$$\frac{\partial}{\partial x}\left[\rho\frac{\left(Q_t^2-Q_w^2\right)}{h} + \overline{\int_{-d}^{z_s}(\rho u'^2+p)\,dz}\right] \qquad (2.4)$$

Under the assumption that the vertical accelerations in the long waves are negligible compared to the acceleration of gravity (the "shallow water approximation"), the third term is reduced to:

$$\overline{p_b\frac{d}{dx}d} = \overline{p_b}\frac{d}{dx}d = \rho g h\frac{d}{dx}d \qquad (2.5)$$

Substitution of equations (2.3) to (2.5) into (2.1) yields:

$$\frac{\partial}{\partial t}\rho Q_t + \frac{\partial}{\partial x}\rho\frac{\left(Q_t^2-Q_w^2\right)}{h} + \frac{\partial}{\partial x}\overline{\int_{-d}^{z_s}(\rho u'^2+p)\,dz} = \rho g h\frac{\partial d}{\partial x} - \overline{\tau_b} \qquad (2.6)$$

Using the common definition of radiation stress:

$$S_{xx} = \overline{\int_{-d}^{z_s}(\rho u'^2+p)\,dz} - \frac{1}{2}\rho g h^2 \qquad (2.7)$$

and neglecting variations of the density ρ, we get:

$$\frac{\partial}{\partial t}Q_t + \frac{\partial}{\partial x}\left[\frac{\left(Q_t^2-Q_w^2\right)}{h} + \frac{S_{xx}}{\rho} + \frac{1}{2}gh^2\right] = gh\frac{\partial d}{\partial x} - \frac{\overline{\tau_b}}{\rho} \qquad (2.8)$$

Conservation of mass:

The short wave averaged mass conservation equation, because of the definition of Q_t, and again neglecting variations in density ρ, simply reads as:

$$\frac{\partial}{\partial t} h + \frac{\partial}{\partial x} Q_t = 0 \tag{2.9}$$

Conservation of wave action:

The conservation of wave action is described by:

$$\frac{\partial}{\partial t} \frac{E}{\omega_r} + \frac{\partial}{\partial x} (C_g + U) \frac{E}{\omega_r} = - \frac{D}{\omega_r} \tag{2.10}$$

where E is the short wave energy, C_g is the group velocity at which the wave action E/ω_r propagates in the absence of a long wave velocity, ω_r is the intrinsic frequency of the waves, viz. the short wave frequency observed when travelling at the velocity U, and D is the rate of wave energy dissipation. All these properties are slowly varying on the time scale of wave groups.

Conservation of waves:

The kinematical conservation equation for the waves reads:

$$\frac{\partial k}{\partial t} + \frac{\partial \omega}{\partial x} = 0 \tag{2.11}$$

where k is the wave number of the short waves and ω the absolute frequency.

2.3 Simplified set of equations

The set of equations (2.8) through (2.11) can be simplified by neglecting all kinematic and dynamic effects of the long waves on the short waves, except for depth variations. This is reasonable since in most cases the long wave particle velocity is much smaller than the group velocity. We further assume that the spectrum is sufficiently narrow-banded that we can neglect the variation in time and space of the frequency ω.

The primary motivation for making these assumptions is that the system becomes much more manageable and the behaviour more predictable. Near the shoreline, current

refraction effects will have an influence on the short wave energy modulations, but we assume that the water depth variations related to the long waves are much more important for the (depth-limited) short waves. The prediction of the propagation of short wave groups will be less accurate if the group velocity is modulated in time, as is the case with broad-banded spectra; however, if the area of interest is only in the order of some wave lengths, this effect will be limited.

It will be shown in Chapter 4 that these assumptions do not lead to unacceptable errors; for the purpose of this study, we restrict ourselves to the following reduced set of equations:

$$\frac{\partial}{\partial t} Q_t + \frac{\partial}{\partial x} \left[\frac{\left(Q_t^2 - Q_w^2\right)}{h} + \frac{S_{xx}}{\rho} + \frac{1}{2} g h^2 \right] = g h \frac{\partial d}{\partial x} - \frac{\overline{\tau_b}}{\rho} \tag{2.8}$$

$$\frac{\partial}{\partial t} h + \frac{\partial}{\partial x} Q_t = 0 \tag{2.9}$$

$$\frac{\partial}{\partial t} E + \frac{\partial}{\partial x} C_g E = -D \tag{2.12}$$

$$\frac{\partial \omega}{\partial x} = 0 \tag{2.13}$$

We see that the wave action equation has now been reduced to a wave energy balance equation, and that equation (2.11) has been reduced to equation (2.13).

2.4 Closure relations

We now have a system of three time-dependent first order differential equations in Q_t, h and E, respectively and known variables ρ, g and d. We therefore need additional equations for Q_w, S_{xx}, C_g, $\overline{\tau_b}$ and D.

2.4.1 Short wave parameters

The first three parameters can be derived from linear short wave theory for progressive waves. The choice for linear theory is defendable in view of other schematizations that are made, and since we are not interested in the particulars of the short waves, but only in integral properties. The expressions provided by linear theory are robust and do not 'explode' in shallow water as many non-linear expressions do. The restriction to

progressive short waves is justified since on gently sloping beaches most short wave energy is dissipated rather than reflected.

We solve k from the linear dispersion relation:

$$\omega^2 = gk \tanh kh \tag{2.14}$$

for given $\omega = \omega_r$ and h; the propagation speed C is solved from:

$$C = \omega / k \tag{2.15}$$

The group velocity is given by:

$$C_g = \frac{g}{2\omega} \left(\tanh kh + kh (1 - \tanh^2 kh) \right) \tag{2.16}$$

The radiation stress S_{xx} can now be computed from:

$$S_{xx} = (2 \frac{C_g}{C} - \frac{1}{2}) E \tag{2.17}$$

and the wave-induced flux Q_w is given by:

$$Q_w = \frac{E}{\rho C} \tag{2.18}$$

Note that E and h in these expressions still vary on the wave group scale. The angular frequency ω in these expressions is a constant representative frequency, usually close to the angular peak frequency $\omega_p = 2\pi f_p$.

2.4.2 Bottom friction

The description of the bottom shear stress under combined breaking or non-breaking short waves and long waves is extremely complex. At present, no satisfactory formulation is available. In view of the fact that we expect bottom friction to play a secondary role in our problem, we take the simple formulation:

$$\overline{\tau_b} = \frac{1}{2} \rho f_w |U| U = \frac{1}{2} \rho f_w \frac{|Q_t - Q_w| (Q_t - Q_w)}{h^2} \tag{2.19}$$

where f_w is a friction coefficient that has to be determined through calibration.

2.4.3 Wave energy dissipation

Basic concept

In a random wave train, the process of energy dissipation due to wave breaking is extremely complex. If it were possible to plot a time series of the instantaneous dissipation rate at a given location and water depth, this would show intermittent peaks with random height and spacing, which cannot be described in a deterministic way. Even when a moving average is applied over some short wave periods, the slowly varying dissipation rate will still have a random component. However, we can expect that this slowly varying dissipation rate will also have a systematic component which depends on slowly varying characteristics of the short waves, in particular the wave energy. This systematic component, which is the expected value of the dissipation rate per unit area, D, for given E, can itself be seen as the product of two components:

$$D = P_b D_b \tag{2.20}$$

where P_b is the probability that a wave of a given energy density E is breaking in the given water depth and D_b the expected value of the dissipation rate in a breaking wave, given that its energy density is E. Both P_b and D_b vary on the time-scale of the wave groups and so does D.

Dissipation in a breaking wave

In order to model the dissipation D_b in a breaking wave, we use the well-known analogy between breaking waves and bores, which results in the following approximate expression (Battjes and Janssen, 1978):

$$D_b = \frac{\alpha}{4} \rho g f \frac{H^3}{h} \tag{2.21}$$

where f is the frequency, H is the height of the breaking wave, h the water depth and α a calibration coefficient. Battjes and Janssen assume all breaking waves to have the maximum wave height H_m; as this maximum wave height is of the order of the water depth, the expression reduces to:

$$D_b = \frac{\alpha}{4} \rho g f H_m^2 \tag{2.22}$$

As in our case the height of breaking waves is allowed to be considerably smaller than the maximum wave height, equation (2.21) should be used in principle. However, it can be argued (Stive and Dingemans, 1984), that the water depth in equation (2.21) should

rather be seen as a depth to which the breaking-induced turbulence penetrates, which is of the order of the wave height. In this case, the dissipation can be written as a simple function of the energy of the breaking waves:

$$D_b = 2\alpha f_p E \tag{2.23}$$

where the peak frequency f_p has been taken as a characteristic measure of the frequency.

Probability of breaking

In general, waves break when locally the wave front becomes too steep. For irregular waves this may be the result of several mechanisms, such as interaction between short waves, interaction between wave and bottom or between wave and current or wind. For simplicity, we shall not consider the effects of current or wind on wave breaking. Even then, the processes involved are extremely complex and no accurate model is available to predict the probability of breaking in irregular waves. Therefore, a simple empirical approach is chosen, based on some crude assumptions.

These assumptions are:

1. The probability of breaking depends only on local and instantaneous wave parameters. In reality, it also depends on the history of the individual waves, but the breaking process, especially in random waves, has a time-scale which is short compared to the wave group scale, so this effect can be neglected.

2. The basic parameters governing the probability of breaking are the local and instantaneous wave energy and the water depth.

3. In principle, waves of any energy may be breaking or non-breaking. However, the probability of breaking should increase monotonically towards 1 for increasing energy or decreasing water depth.

Thornton and Guza (1983) propose the following empirical 'weighting function', which can be interpreted as the probability that a wave of height H, in a wave train with overall root-mean-square wave height equal to H_{rms}, is breaking in a water depth h:

$$P_b = \left[\frac{H_{rms}}{\gamma h}\right] \left[1 - \exp\left[-(\frac{H}{\gamma h})^2\right]\right] \leq 1 \tag{2.24}$$

According to this expression, the probability that a particular wave in an irregular wave train is breaking not only depends on the height of this wave relative to the water depth, but also on a characteristic height parameter of the whole wave train (i.e. H_{rms}). This would imply that the breaking process in a given wave group is influenced by events on a much greater time-scale, which seems unlikely and is in contradiction with our assumption 1. We therefore propose a different form:

$$P_b(E,h) = 1 - \exp\left[-\left[\frac{H}{\gamma h}\right]^n\right] \tag{2.25}$$

where $H = \sqrt{8E/\rho g}$, γ is a coefficient and n is an exponent. In Figure 2.1 this function is plotted for several values of n. It can be seen that the steepness of the function increases with increasing n. The optimal values of γ and n will have to be determined empirically.

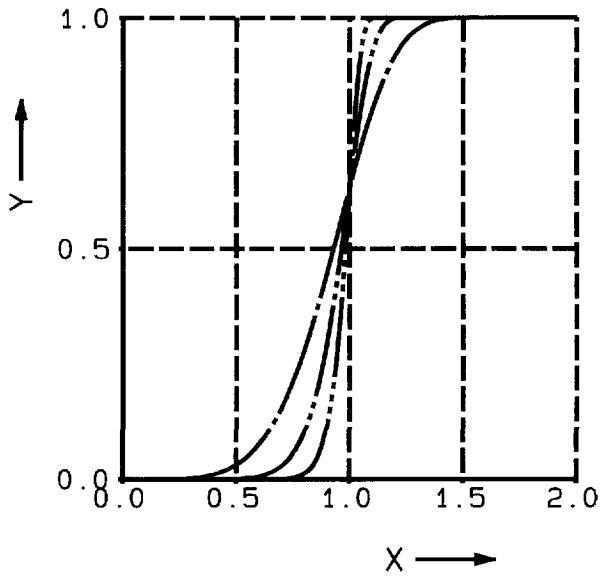

Figure 2.1 *Plot of the function* $Y = 1 - \exp(-X^n)$ *for* $n = 5$ *(line interrupted by one dot), 10 (two dots), 20 (three dots)*

Conditional expected dissipation rate for waves with given energy

The expected dissipation rate, given a specific value of E, is now simply found by substituting equations (2.23) and (2.25) into equation (2.20), which leads to:

$$D(E,h) = \left[1 - \exp\left[-\left[\frac{H}{\gamma h}\right]^n\right]\right] 2\alpha f_p E \qquad (2.26)$$

This equation describes the dissipation rate for a given (random) wave energy and water depth. The calibration of the coefficients α, γ and n and the verification of the formulation as such is described in Chapter 4.

2.5 Discussion of the system of equations

The set of equations is now complete. Here, it is useful to discuss some aspects of its characteristic properties. The combination of equations (2.8) and (2.9), apart from short wave terms, describes the propagation of free non-linear shallow water waves, which travel at a propagation speed of approximately $\sqrt{gh}$ and which may be reflected on the beach slope. The equations also allow for breaking of these long waves (see e.g. Hibberd and Peregrine, 1979), although this will not usually happen.

The wave energy balance (2.12) describes the propagation and dissipation of the time-varying short wave energy over the profile; a fluctuation of the wave energy at the seaward boundary will propagate towards the shore at the group velocity C_g. In the surf zone both the fluctuations and the mean energy are damped by dissipation, although some fluctuations remain because of the water level variations associated with the long waves.

The fluctuation of the short wave energy both in time and in space directly implies a fluctuation of the radiation stress S_{xx}, which results in a forcing term in the long wave equations that induces so-called bound long waves that travel at the group velocity (e.g. Longuet-Higgins and Stewart, 1962). The average radiation stresses also drive a mean water level set-up.

The water level fluctuations due to long waves influence the group velocity and the dissipation term in the short wave energy balance. This means that the system is interacting and that the three equations must be solved simultaneously.

2.6 Boundary and initial conditions

The boundary conditions for the three variables E, Q_t and h at the seaward and the landward boundaries are discussed in the following Sections.

2.6.1 Seaward boundary

At the seaward boundary, the (constant) frequency ω is prescribed and the incoming short wave energy E is specified as a function of time. The related incoming bound long wave is computed from the linearized solution for a horizontal bottom as given by Longuet-Higgins and Stewart (1964):

$$Q_t - <Q_t> = \frac{C_g}{\rho}(E - <E>)\frac{(2C_g/C - 0.5)}{(gh - C_g^2)} \tag{2.27}$$

$$h - <h> = \frac{1}{\rho}(E - <E>)\frac{(2C_g/C - 0.5)}{(gh - C_g^2)} \tag{2.28}$$

where the $<>$ denote averaging over the wave groups. Since within our model area long waves are generated and reflected as free waves, which cannot be prescribed beforehand, we have to ensure that these free waves can propagate out of the model area undisturbed. This is achieved by using a so-called weakly reflective boundary condition. We use the fact that the incoming bound waves travel at the known group velocity C_g, whereas the out-going free waves travel at velocity $\sqrt{gh}$, so for each parameter p, where p is Q_t or h, we can write:

$$\frac{\partial}{\partial t}p_{incoming} + C_g \frac{\partial}{\partial x}p_{incoming} = 0 \tag{2.29}$$

$$\frac{\partial}{\partial t}p_{outgoing} - \sqrt{gh}\frac{\partial}{\partial x}p_{outgoing} = 0 \tag{2.30}$$

Since p equals the sum of $p_{incoming}$ and $p_{outgoing}$, it follows that:

$$\frac{\partial}{\partial t}p = (1 + \sqrt{gh}/C_g)\frac{\partial}{\partial t}p_{incoming} + \sqrt{gh}\frac{\partial}{\partial x}p \tag{2.31}$$

This provides an adequate boundary condition for both Q_t and h.

2.6.2 Landward boundary

The landward boundary is defined at the "water line", a moving point where the water depth h has a small fixed value δ. The water line moves at a velocity $U_t = Q_t/\delta$. Here, the short wave energy E can be set to zero, since most energy will have been dissipated. The boundary condition for Q_t then follows from:

$$\frac{Dh}{Dt} = \frac{\partial h}{\partial t} + U_t\frac{\partial h}{\partial x} = 0 \tag{2.32}$$

Since from equation (2.9) we have:

$$\frac{\partial h}{\partial t} + U_t \frac{\partial h}{\partial x} + h \frac{\partial U_t}{\partial x} = 0 \tag{2.33}$$

and since $h = \delta$ at the water line, we get the simple condition:

$$\frac{\partial}{\partial x} U_t = 0 \text{ or } \frac{\partial}{\partial x} Q_t/h = 0 \tag{2.34}$$

2.6.3 Initial conditions

Since the long waves are allowed to propagate out of the model area, the effect of initial conditions vanishes after the time required for long waves to travel from the seaward boundary to the shore and back. As initial conditions, we set E and Q_t to zero and set h at the still water depth $-d$.

3. NUMERICAL SCHEME

3.1 Introduction

In this Chapter we discuss the numerical scheme used to solve the set of differential equations (2.8), (2.9) and (2.12). First, the equations are transformed from the physical domain, which has a moving landward boundary, to a fixed computational domain. We then describe the discretization of the transformed equations, and the stability condition. The scheme is validated against known analytical solutions of the non-linear shallow water equations, and its ability to represent bore solutions of the non-linear shallow water equations is verified. The method has been implemented in a computer program with code name "SURFBEAT".

The author gratefully acknowledges the help of his colleague H.A.H. Petit, who designed the numerical method.

3.2 Transformation of the equations

The physical domain in which the equations are valid ranges from the seaward boundary to the water line. The fact that the water line moves up and down poses a problem in defining the boundary conditions at the water line. This problem can be tackled in two ways. Hibberd and Peregrine (1979) describe a solution for the case of shallow water equations that uses a fixed computational grid. Although good results are obtained, the method is complicated and is difficult to convert to efficient and transparent computer code. An alternative is to transform the equations from the physical domain where the landward boundary moves, to a fixed computational domain. This greatly simplifies the description of the landward boundary. An additional advantage is, that the transformation can be designed in such a way, that an efficient, non-equidistant grid spacing in the physical domain is transformed to an equidistant grid spacing in the computational domain. A standard numerical scheme with second-order accuracy can then be applied to solve the tranformed equations.

The set of equations (2.8), (2.9) and (2.12) is of the following form, in vector notation:

$$\frac{\partial v}{\partial t} + \frac{\partial f(v)}{\partial x} = o(v)\frac{dp}{dx} + q(v) \tag{3.1}$$

The functions f and q need not be linear in their arguments.

We now use a transformation to general time dependent coordinates of the following form:

$$\tau = t \tag{3.2}$$

$$\xi = \frac{\int_0^x W(\zeta)\,d\zeta}{\int_0^{X_r(t)} W(\zeta)\,d\zeta} \tag{3.3}$$

in which W is a one-dimensional weighting function. This transformation transforms the interval in the x-domain: $[0,X_r(t)]$ which depends on the time coordinate t, to the fixed interval [0,1] in the ξ domain. The transformation to the τ domain is trivial. By choosing an appropriate weighting function W we can affect the distribution of grid points in the physical domain. As will be discussed in Section 3.3, we aim at a distribution that yields an almost uniform stability condition for the time step throughout the domain. For now, in order that the inverse transformation functions $x(\tau,\xi)$ and $t(\tau)$ exist the function W has to meet the requirement that it does not change sign in the interval $[0,X_r(t)]$.

The position of the water line $X_r(t)$ is the solution of an ordinary differential equation:

$$\frac{dX_r(t)}{dt} = U_t(t,X_r(t)) \tag{3.4}$$

since the water line moves at a speed equal to the long wave velocity $U_t = Q_t/h$.

In Appendix A we describe how the set of differential equations is transformed to the new coordinate system. Here we produce the result:

$$\begin{aligned} &\frac{\partial}{\partial\tau}\left(T_1(\tau,\xi)\,\hat{v}(\tau,\xi)\right) + \frac{\partial}{\partial\xi}\left(T_2(\tau,\xi)\,\hat{v}(\tau,\xi) + \boldsymbol{f}(v(\tau,\xi))\right) = \\ &\quad T_1(\tau,\xi)\left(\boldsymbol{o}(\hat{v}(\tau,\xi))\hat{\boldsymbol{p}}_x(\tau,\xi) + \boldsymbol{q}(\hat{v}(\tau,\xi))\right) \end{aligned} \tag{3.5}$$

$$\frac{dX_r(\tau)}{d\tau} = \hat{U}_t(\tau,1) \tag{3.6}$$

where,

$$T_1(\tau,\xi) = \frac{\int_0^{X_r(\tau)} W(\zeta)\,d\zeta}{W(x(\tau,\zeta))}, \qquad T_2(\tau,\xi) = -\frac{\xi\,W(X_r(\tau))}{W(x(\tau,\xi))}\frac{dX_r(\tau)}{d\tau}$$

$\hat{v}(\tau,\xi) = v(\tau,x(\tau,\xi))$ and $\hat{p}_x(\tau,\xi) = \frac{dp}{dx}(x(\tau,\xi))$.

Equation (3.5) can be written as:

$$\frac{\partial V}{\partial \tau} + \frac{\partial F(V,\tau,\xi)}{\partial \xi} = R(V,\tau,\xi), \tag{3.7}$$

so it has exactly the same structure as Eq.(3.1).

3.3 Discretization of transformed equations

The set of differential equations (3.5) in the (τ,ξ) domain is integrated numerically on an equidistant spatial grid:

$$\xi_i = \frac{i}{N} \text{ for } i = 0(1)N.$$

The time steps are constant as well: $\tau_j = j\Delta\tau$ and therefore $t_j = j\Delta\tau$.
In the physical domain (t,x) this introduces a time-varying, non-equidistant grid with grid points x_i^j which satisfy the equation:

$$\xi_i = \frac{i}{N} = \frac{\int_0^{x_i^j} W(\zeta)\,d\zeta}{\int_0^{x_r(\tau_j)} W(\zeta)\,d\zeta} \quad \text{for } i = 0(1)N \tag{3.8}$$

The scheme we use is Richtmeyer's predictor corrector scheme; the discretization of Eq.(3.7) now becomes:

Predictor:

$$V_{i+1/2}^{j+1/2} = \frac{1}{2}(V_{i+1}^j + V_i^j) - \frac{\Delta\tau}{2\Delta\xi}(F_{i+1}^j - F_i^j) + \frac{\Delta\tau}{4}(R_{i+1}^j + R_i^j) \tag{3.9}$$

where $F_{i+1}^j = F(V_{i+1}^j, \tau_j, \xi_{i+1})$, $R_{i+1}^j = R(V_{i+1}^j, \tau_j, \xi_{i+1})$,

$F_{i+1/2}^{j+1/2} = F(V_{i+1/2}^{j+1/2}, \tau_{j+1/2}, \xi_{i+1/2})$ and $R_{i+1/2}^{j+1/2} = R(V_{i+1/2}^{j+1/2}, \tau_{j+1/2}, \xi_{i+1/2})$

$$X_r^{j+1/2} = X_r^j + \frac{\Delta\tau}{48}(34\,\hat{U}_t(\tau_j,1) - 14\,\hat{U}_t(\tau_{j-1},1) + 4\,\hat{U}_t(\tau_{j-2},1)) \tag{3.10}$$

$x_{i+1/2}^{j+1/2}$ is solved from $\xi_{i+1/2} = \dfrac{i+1/2}{N} = \dfrac{\int_0^{x_{i+1/2}^{j+1/2}} W(\zeta)d\zeta}{\int_0^{x_r^{j+1/2}} W(\zeta)d\zeta}$ for $i = 0\,(1)\,[N-1]$.

Corrector:

$$\boldsymbol{V}_i^{j+1} = \boldsymbol{V}_i^j - \frac{\Delta\tau}{\Delta\xi}(\boldsymbol{F}_{i+1/2}^{j+1/2} - \boldsymbol{F}_{i-1/2}^{j+1/2}) + \frac{\Delta\tau}{2}(\boldsymbol{R}_{i+1/2}^{j+1/2} + \boldsymbol{R}_{i-1/2}^{j+1/2}) \tag{3.11}$$

$$X_r^{j+1} = X_r^j + \frac{\Delta\tau}{12}(23\,\hat{U}_t(\tau_j,1) - 16\,\hat{U}_t(\tau_{j-1},1) + 5\,\hat{U}_t(\tau_{j-2},1)) \tag{3.12}$$

x_i^{j+1} is solved from: $\xi_i = \dfrac{i}{N} = \dfrac{\int_0^{x_i^{j+1}} W(\zeta)d\zeta}{\int_0^{x_r^{j+1}} W(\zeta)d\zeta}$, for $i = 0\,(1)\,[N-1]$.

The schemes that are used to solve Eq. (3.6) are (3.10) and (3.12), these are both third order Adams-Bashforth methods.

3.4 Stability condition

The linear stability condition for the Richtmeyer scheme is

$$\frac{\lambda\Delta\tau}{\Delta\xi} \le 1 \tag{3.13}$$

where λ is the largest eigenvalue of $\partial\boldsymbol{F}/\partial\boldsymbol{V}$ in absolute sense.

The largest eigenvalue of $\partial f/\partial v$ in equation (3.1) can be approximated by $u + \sqrt{gh}$. Since T_1 and T_2 are both scalar functions, the largest eigenvalue in the transformed problem (3.5) becomes:

$$\lambda = \frac{T_2}{T_1} + \frac{\hat{u} + \sqrt{g\hat{h}}}{T_1}$$

Stability condition (3.13) can now be written as:

$$W(x(\tau,\xi))\,\hat{u}(\tau,\xi) - \xi\, W(X_r(\tau))\,\frac{dX_r}{d\tau} + W(x(\tau,\xi))\sqrt{g\hat{h}(\tau,\xi)} \le \frac{\Delta\xi}{\Delta\tau}\int_0^{X_r(\tau)} W(\zeta)\,d\zeta \tag{3.14}$$

The condition we use to replace Eq.(3.14) is:

$$W(x(\tau,\xi))\sqrt{g(\hat{h}(0,\xi)+\epsilon)} \le \frac{\Delta\xi}{\Delta\tau}\int_0^{X_r(\tau)} W(\zeta)\,d\zeta \tag{3.15}$$

where $\hat{h}(0,\xi)$ is the still water depth and ϵ is a small positive number. A convenient weight function now becomes:

$$W(x) = \frac{1}{\sqrt{g\,(h(0,x)+\epsilon)}} \tag{3.16}$$

With this choice the CFL stability condition (3.14) can now be replaced by:

$$\Delta\tau \le \Delta\xi \int_0^{X_r(\tau)} \frac{1}{\sqrt{g\,(h(0,x)+\epsilon)}}\,dx \tag{3.17}$$

By replacing $X_r(\tau)$ in Eq.(3.17) by a lower boundary of $X_r(\tau)$ we found a constant value for $\Delta\tau$.

3.5 Validation of the numerical scheme

3.5.1 Comparison with analytical solution

The scheme has been compared with analytical solutions of standing long waves on a plane beach as given by Carrier and Greenspan (1958); a first example is given in Figure 3.1. In this example, a sinusoidal wave with period of 10 s is generated in a water depth of 0.50 m, and propagates and reflects on a plane 1:25 slope. The amplitude is chosen such that it is half the amplitude at which wave breaking would occur on the slope. The numerical grid consists of 50 points, and the weighting function W is chosen according to equation (3.16). The value of ϵ in this function is chosen as small as possible; in this case ϵ = **0.025** m. The time step is set at .1 s, at which value the

Courant number is in the order of 0.7 throughout the domain. The fixed water depth at the water line, δ, is set at a value of 0.001 m. To facilitate the comparison with the analytical solution, the computed water level and velocity are non-dimensionalized with the bottom slope s, the acceleration of gravity g, the period T and the shoreline amplitude A according to the solution for linear shallow water waves. Very small deviations in the water level occur at the shoreline; the velocity exhibits small wiggles in the uprush-phase. These deviations disappear if the number of grid points is increased, as is shown in Figure 3.2, where the number of grid points is doubled to 100 points, and the time step reduced to .05 s.

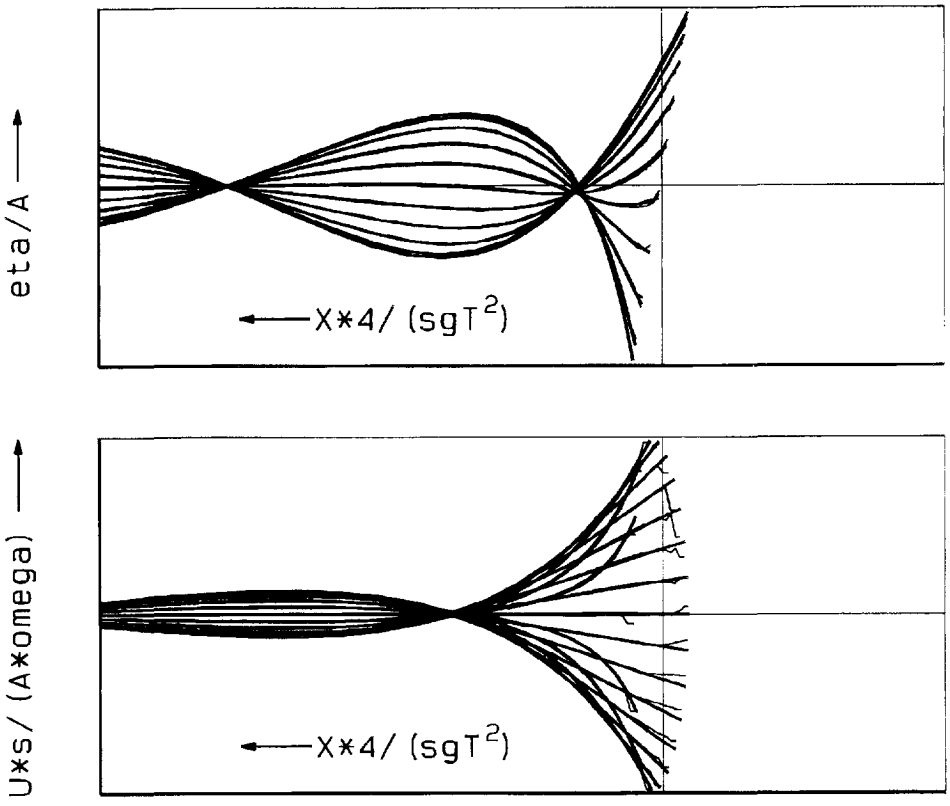

Figure 3.1 *Comparison of numerical (thin lines) and analytical (thick lines) solution of standing long wave on a plane sloping beach; dimensionless elevation (top) and velocity (bottom). 50 Grid points*

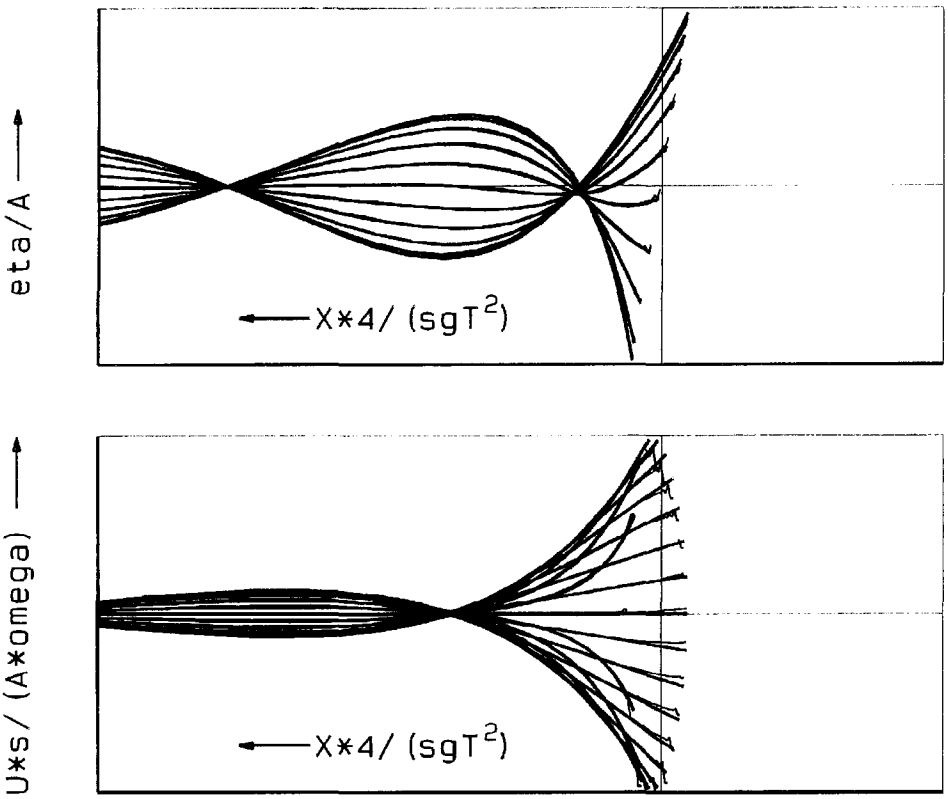

Figure 3.2 *Comparison of numerical (thin lines) and analytical (thick lines) solution of standing long wave on a plane sloping beach; dimensionless elevation (top) and velocity (bottom). 100 Grid points*

3.5.2 Breaking long waves

The non-linear shallow water equations by which the long waves in our model are described allow for discontinuous solutions or bores, and thereby automatically capture breaking of shallow water waves; see Hibberd and Peregrine (1979). Although in many cases the long waves associated with surf beat are very long, low-amplitude waves, under severe circumstances they may be breaking, as was shown in a dramatic way by Nakaza et al. (1990). We must therefore require that the scheme is capable of representing breaking waves reasonably accurately. Since the scheme we have chosen is increasingly dissipative for higher frequencies, it is well suited to capture shocks, as is shown by the example in Figure 3.3. Here we have prescribed an incident wave amplitude of 0.10 m at a water depth of 10 m, for waves with a period of 60 s which subsequently break on a plane 1:50 beach. This can be seen as an extreme case for natural beach conditions; a friction factor f_w = 0.02 was applied. In the upper part of

the Figure, the solution is shown for 50 grid points and a time step of 1.0 s; the middle part is for 100 grid points and a time step of 0.5 s. Apart from the fact that the shock is sharper for 100 grid points, the differences are negligible; the minor oscillations at the breaking wave front are kept in check by the fact that the scheme is dissipative for high frequencies.

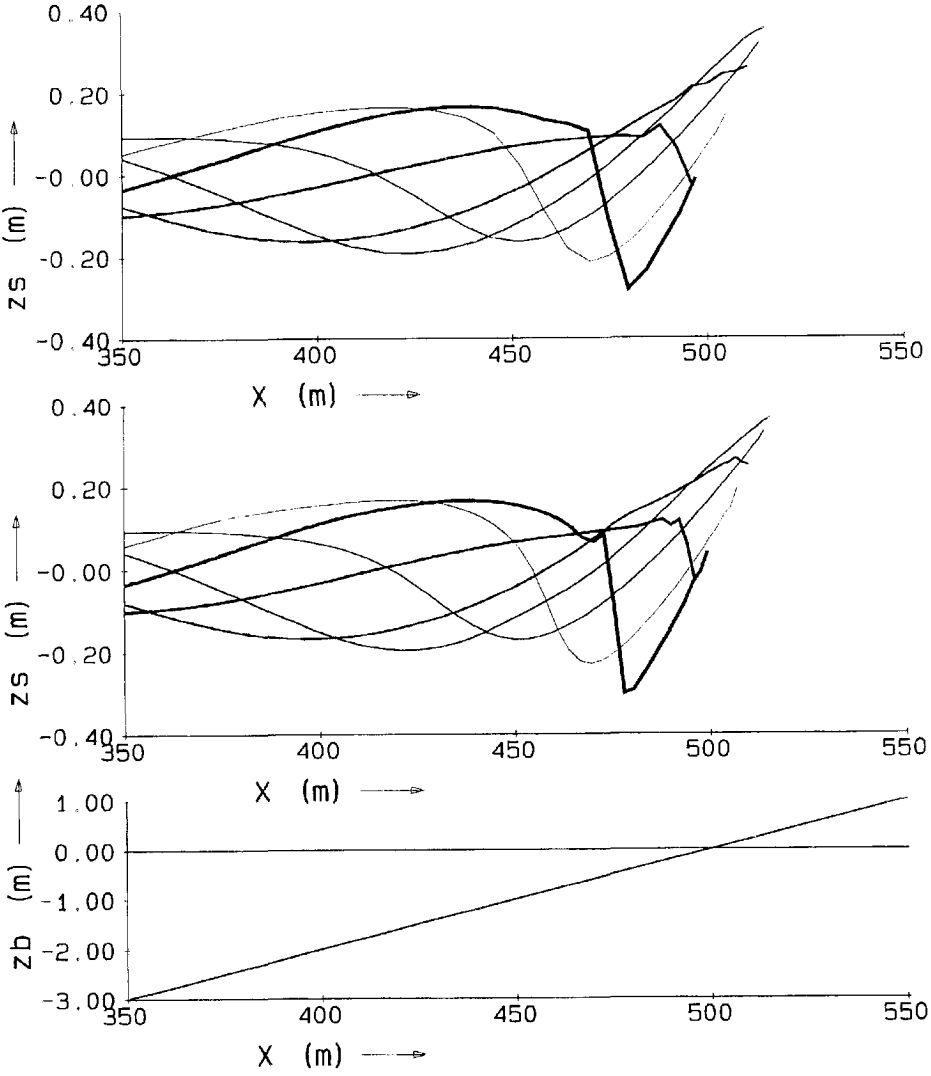

Figure 3.3 *Surface elevation at intervals of 1/6 wave period for a breaking shallow water wave on a plane beach; upper: 50 grid points, 1 s time step; middle: 100 grid points, .5 s time step; lower: (part of) bathymetry and initial water level*

3.6 Conclusions

A numerical method was designed for the non-linear system of equations (2.8), (2.9) and (2.12). In order to avoid a complicated treatment of the water line, the system of equations is transformed from a non-equidistant and time-varying physical domain to an equidistant and constant computational domain. A standard scheme of second-order accuracy is used to solve the transformed equations.

The numerical method which is applied has been tested against known analytical solutions of the non-linear shallow water equations. These solutions are reproduced accurately; small oscillations may occur near the water line; these disappear when the number of grid points is increased. The scheme is capable of accurately representing bore solutions of the shallow water equations; hence the model automatically represents the breaking of long waves.

4. CALIBRATION OF THE MODEL COEFFICIENTS

The model formulations given in Chapter 3 contain a number of empirical coefficients that have to be determined through calibration. These coefficients are related to the dissipation of short wave energy by breaking, and to the bottom friction term in the long wave momentum equation.

4.1 Dissipation by short wave breaking

The slowly varying dissipation of short wave energy by short wave breaking, D is modelled as the product of the conditional probability that waves are breaking P_b, given the energy E and the water depth h, and the expected value of the dissipation D_b in breaking waves of given energy E:

$$D(E,h) = \left[1 - \exp\left[-\left[\frac{H}{\gamma h}\right]^n\right]\right] 2\alpha f_p E \tag{2.25}$$

Here, P_b is the factor in the outer brackets. The formula contains three empirical coefficients: two, namely γ and n related to the probability of breaking, and one, α, related to the dissipation in breaking waves.

A problem in calibrating these coefficients is, that the time-varying dissipation rate D cannot be measured directly. The only way to overcome this problem is to build the formulation into models that predict measurable quantities, such as the average dissipation, the fraction of breaking waves and the mean wave energy, and by verifying these models both externally and internally. This process is described in detail in Appendix B. Here, we reproduce the main line of thought.

In order to compute the measurable parameters mentioned, the formulation (2.25) was incorporated in two types of models that describe the transformation of the mean wave energy across a profile. In the first, *probabilistic* approach, a given probability distribution of the wave energy at the seawardmost point is divided into a number of classes; the transformation of each class across the profile is then computed by:

$$\frac{d}{dx} EC_g = -D \tag{4.1}$$

This approach is equivalent to our model, if long wave effects on the short wave transformation are neglected. The mean energy at a given point is computed by combining the solutions of (4.1) for all classes.

In the second, *parametric* approach, the energy balance equation is averaged over a time which is long compared to the wave groups; this time-averaged energy balance is solved directly:

$$\frac{d}{dx}\langle EC_g\rangle = -\langle D\rangle \tag{4.2}$$

In this case, we have to give an expression for the time-averaged dissipation $\langle D\rangle$. This is obtained by assuming that the probability distribution of the short wave energy has a shape that is constant or depends only on time-averaged parameters. In this case,

$$\langle D\rangle = \int_0^\infty p(E)\,D(E)\,dE \tag{4.3}$$

Three different shape functions for $p(E)$ used in the literature have been tried, viz. a Weibull distribution, a Rayleigh distribution and a clipped Rayleigh distribution (see Appendix B). It turns out, that if we define:

$$H_E = \sqrt{\frac{8\langle E\rangle}{\rho g}} \tag{4.4}$$

we can in all three cases write for the time-averaged dissipation:

$$\langle D\rangle = f\left(\frac{H_E}{\gamma h}, n\right) 2\alpha f_p \langle E\rangle \tag{4.5}$$

where the function f depends on the choice of the shape function for the probability distribution of the short wave energy.

Since there are many data sets available on the transformation of H_E (often termed H_{rms}) across the surf zone, this parameter was used for the calibration.

A total of 11 data sets containing 159 measuring points of H_E were used for the calibration. Two overall measures of the accuracy of the models were applied, viz. the mean and root-mean-square error of H_E, made dimensionless with its value at the seawardmost point. These measures were computed for a number of combinations of n, α and γ, for the probabilistic model as well as for the three parametric models.

For different values of n, the optimum combination of α and γ was obtained by drawing isolines of the error indicators in the α,γ-plane and visually determining the approximate location of zero mean error and minimum rms-error (see Appendix B, Figure 2 a-g). By refining the α,γ-grid locally a more accurate location of this optimum was then found. It turns out that the results are not very sensitive to the value of n. The best results were obtained for n near to 10. Therefore, in the following the value $n = 10$ has been used. The probabilistic model gave the most accurate overall results for the combination of α=1.0, γ=0.55 and n=10 (Appendix B, Figure 3 a-z).

Additional data sets were added for independent verification, with reasonable result. The overall rms error over 28 data sets containing 389 data points was approximately 9% for these fixed coefficient values. Visual inspection of the individual data sets shows that the computed curves of H_E generally follow the data points quite well. Additional verification of the model against data on internal parameters is discussed in Appendix B.

The dependence of the coefficient γ on the incident wave steepness in the model presented by Battjes and Janssen (1978) and calibrated and verified by Battjes and Stive (1985) was not found in the present formulations, in which the limiting water depth is the only mechanism that causes wave breaking. Apparently, including a limiting wave steepness as a cause for wave breaking does not improve the model, at least in near-shore applications.

The conclusion is, that the dissipation formulation produces accurate results over a range of conditions with random waves, for constant values of the coefficients. It can therefore be expected that no in situ calibration of these coefficients will be required for practical applications.

4.2 Bottom friction

The problem of describing the effect of bottom friction under a combination of long waves and non-breaking or breaking short waves on the long wave motion is as yet unsolved. It is unlikely that the bottom friction coefficient f_w in the simple formulation in equation (2.19) has a constant value for a wide range of circumstances, so a calibration procedure similar to that for the dissipation formulation is not meaningful; besides, no data of similar quality are available to compare the model against. However, based on the comparison of the overall model with laboratory experiments, discussed in Chapter 5, we can tentatively recommend a value in the order of 0.02 if no data are available.

5. VALIDATION OF THE MODEL AGAINST LABORATORY DATA

Except for the friction coefficient, for which no calibration data are available, the coefficients in the model have now been determined. A validation against measurements to ensure that the basic mechanisms are represented in the model, and to assess the accuracy is described in this Chapter. We restrict ourselves to laboratory cases that are basically one-dimensional, in accordance with the main restriction of our model. Two data sets are used for validation: one presented by Kostense (1984), which concerns bichromatic waves, and one described in Van Leeuwen (1992), with random waves.

5.1 Bichromatic waves

5.1.1 Experiments

We start the validation of the SURFBEAT model by comparing results with laboratory experiments by Kostense (1984), which refer to wave channel tests of bichromatic waves on a plane beach. The experiments were carried out with active wave absorption and second order wave generation, enabling undisturbed, stable and accurate measurements. They cover a range of primary frequencies, group frequencies, amplitudes and modulation rates and are therefore well suited to verify the predictive ability of the model. The primary waves in these tests were made up of two frequencies generated in a water depth of 0.50 m and broke on a plane cemented beach of a 1:20 slope after travelling over a horizontal stretch. In Table 5.1 the ranges of amplitude and frequency of the primary waves are given.

Series	$\hat{\eta}_1$ (m)	$\frac{\hat{\eta}_2}{\hat{\eta}_1}$ (m)	ω_1 (rad/s)	$\Delta\omega$ (rad/s)
A	0.055	0.2	3.1	0.3-0.9
B	0.055	0.2	4.1	0.3-0.9
C	0.035-0.080	0.2	4.1	0.77
D	0.030-0.085	0.2	3.1	0.61
E	0.035	0.8	4.3	0.3-0.9

Table 5.1 *Ranges of primary wave parameters in Kostense experiments*

In series A, B and E, the effect of varying the difference frequency is studied for fixed primary wave amplitudes; in series C and D the effect of varying the primary wave amplitude is shown for a fixed difference frequency. Series A through D were carried out with weakly modulated waves; series E with strongly modulated primary waves.

5.1.2 Boundary conditions

For a given set of primary waves, the input boundary conditions for the numerical model are defined by:

$$E = \rho g \left[\frac{1}{2}(\hat{\eta}_1^2 + \hat{\eta}_2^2) + \hat{\eta}_1 \hat{\eta}_2 \cos(\Delta\omega\, t) \right] \tag{5.1}$$

The accompanying bound long wave, which is also generated in the experiment, is given by Longuet-Higgins and Stewart (1964):

$$h - \bar{h} = - g \left[(2\frac{C_g}{C} - 0.5) \,/\, (gh - C_g^2) \right] \hat{\eta}_1 \hat{\eta}_2 \cos(\Delta\omega\, t) \tag{5.2}$$

$$Q_t = - g\, C_g \left[(2\frac{C_g}{C} - 0.5) / (gh - C_g^2) \right] \hat{\eta}_1 \hat{\eta}_2 \cos(\Delta\omega\, t) \tag{5.3}$$

In order to prevent re-reflection of long waves at the seaward boundary, a weakly reflective boundary condition is used as described in Chapter 2.

5.1.3 Simulation procedure

The procedure to simulate the experiments with the model is as follows. For a given set of primary waves, the model is run until a periodic solution is reached. The surface elevation time series are then split into three components, viz. the incoming bound wave, the reflected free wave and an incoming free wave. Incoming free waves are negligible since they are not generated and since the weakly reflective boundary condition allows waves reflected from the beach to propagate out of the model area. The amplitudes of the incoming bound wave and the reflected free wave are determined by harmonic analysis. Per series A through E, approximately twenty such runs are carried out to cover the range of the free parameter for each series.

The numerical model contains empirical coefficients in the description of the dissipation of short waves by wave breaking, and of the dissipation of long waves by bottom friction. For random waves, a standard set of values for the wave breaking coefficients can be applied, as is shown in Chapter 4. A key factor here is the coefficient γ, which is proportional to the average breaking wave height over water depth ratio, and is set at 0.55 for random waves.

For bichromatic waves, we first have to assess whether or not the probabilistic approach towards wave breaking is justified. On the one hand, the short wave envelope varies regularly, so we can expect a quite predictable fluctuation of the breaker point. However, unless ω_1/ω_2 is rational, the surface elevation time series will not repeat itself; thus the exact position of the breaker point is unknown if only the envelope time series is given. This perhaps explains the wide scatter in experimental data on breaking wave heights, even for bichromatic waves (see for instance Sato et al., 1990). Our probabilistic approach is therefore still appropriate; however, the calibration for random waves does not apply here. According to Sato et al. (1990, Fig.6), the average breaking wave height over water depth ratio should be significantly higher than 0.55; a reasonable estimate appears to be 0.75 . Because of the uncertainty in this value, computations are performed for γ-values of 0.55, 0.75 and 0.90.

Since there is no accurate description of the bottom friction under combined short and long waves, the simplest possible formulation as in eq. (2.19) is applied. Computations are performed for three values of f_w: 0.00, 0.02 and 0.05. The variations in f_w are applied for a fixed γ-value of 0.75; the variations in γ for a fixed f_w-value of 0.02.

5.1.4 Results

The results for series A through E are shown in Figures 5.1 through 5.5, respectively. In all cases, the bound long wave amplitude is predicted accurately; it does not depend on either of the coefficients. The increase in the bound wave amplitude for increasing difference frequency is due to the slight decrease in the mean of the primary frequencies. As expected, the bound wave amplitude increases quadratically with increasing primary wave amplitude.

The amplitudes of the reflected free waves show interesting interference patterns which are represented quite well by the model. Schäffer and Jonsson (1990) already concluded, based on a comparison between their model and these data, that frictional effects must be important. Especially for the higher group frequencies this appears to be the case. A reasonable value for the friction factor of 0.02 appears to give acceptable quantitative agreement for all series.

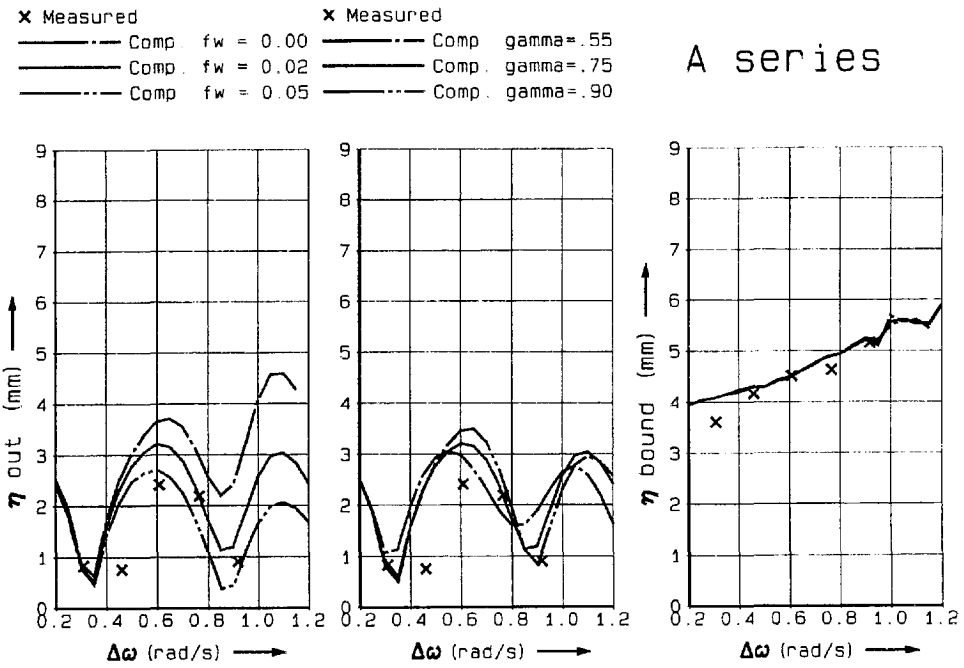

Figure 5.1 *Measured and computed amplitudes of free reflected and bound long wave elevation against difference frequency $\Delta\omega$; series A*

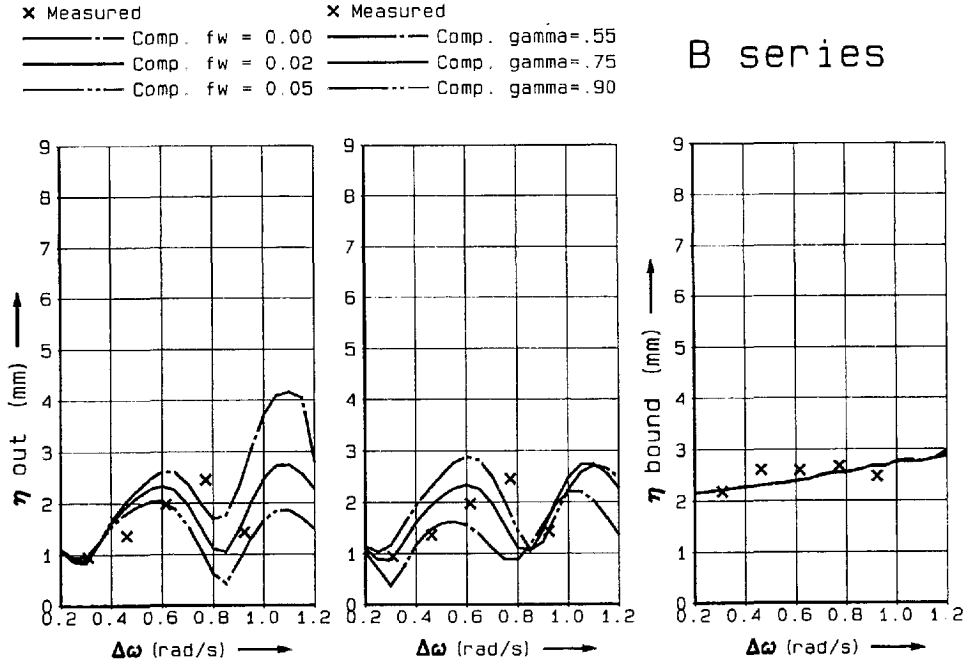

Figure 5.2 *Measured and computed amplitudes of free reflected and bound long wave elevation against difference frequency $\Delta\omega$; series B*

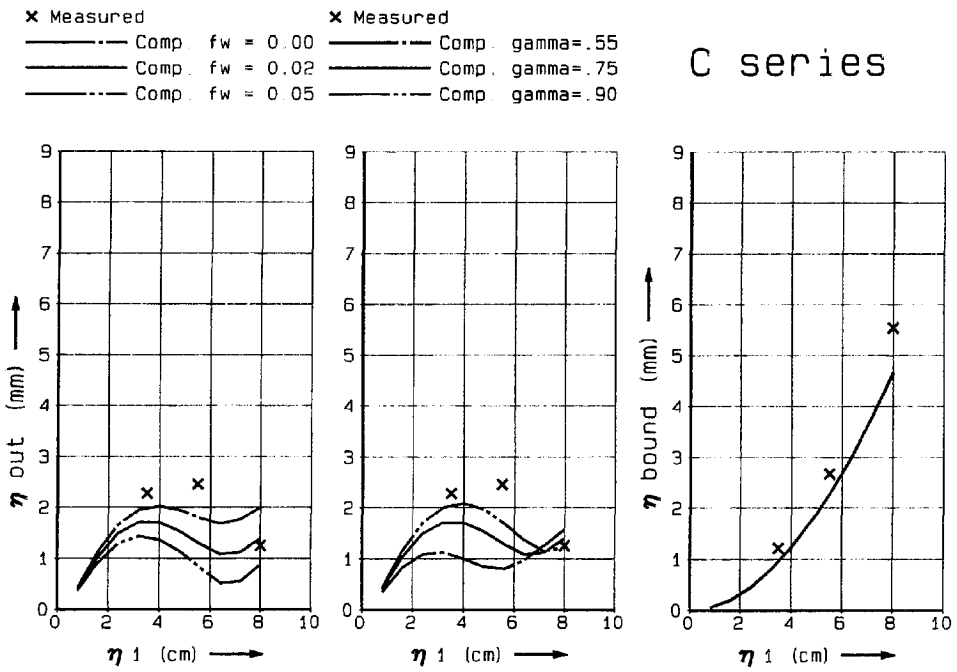

Figure 5.3 *Measured and computed amplitudes of free reflected and bound long wave elevation against primary wave amplitude $\hat{\eta}_1$; series C*

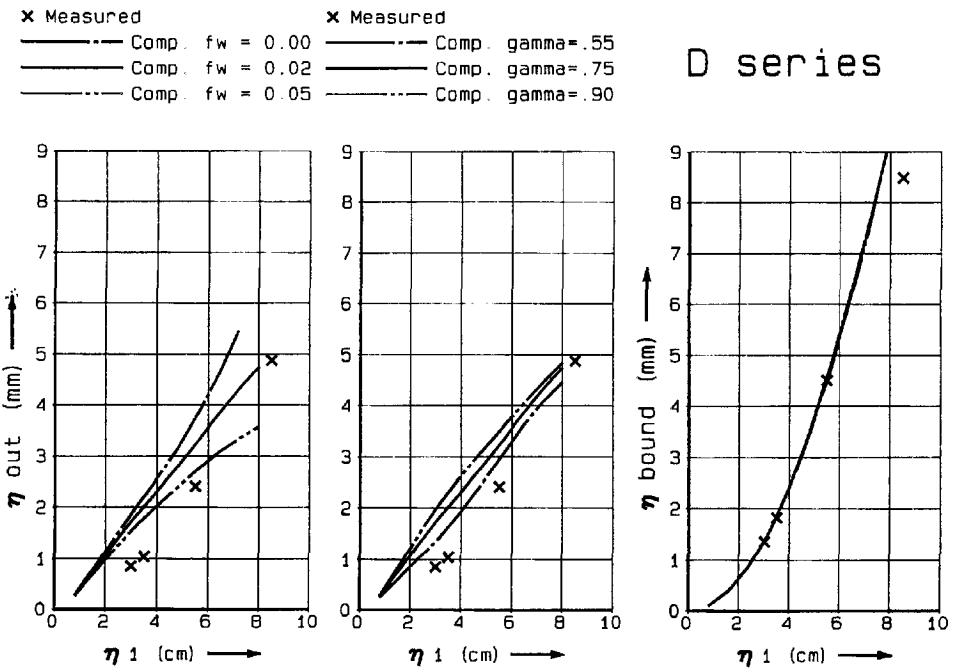

Figure 5.4 *Measured and computed amplitudes of free reflected and bound long wave elevation against primary wave amplitude $\hat{\eta}_1$; series D*

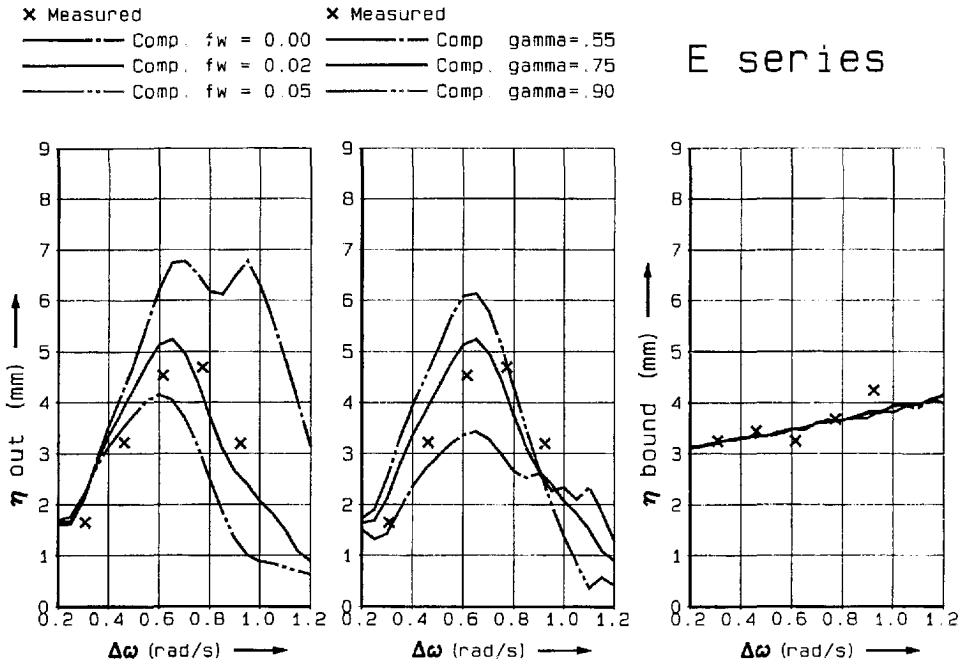

Figure 5.5 *Measured and computed amplitudes of free reflected and bound long wave elevation against difference frequency $\Delta\omega$; series E*

The model results are not extremely sensitive to variations in the breaker parameter γ. A reasonable value of 0.75 for these bichromatic waves gives acceptable results for all series.

The prediction of the reflected free wave amplitude for highly modulated waves in series E is quite accurate; no previous model results on this case have been presented in literature.

A disadvantage of this numerical model is, that it is not possible to separate different mechanisms of long wave generation, viz. the reflection of bound long waves, the break point mechanism or the shoreline set-up mechanism. Probably all of these mechanisms are important at times; the results indicate that no serious errors in the representation of any mechanism have been made.

5.1.5 Conclusions

The numerical model SURFBEAT appears to contain the necessary physics to predict long wave generation in the nearshore zone. Since it can be run with arbitrary boundary conditions over an arbitrary profile, it can be used to model realistic situations where cross-shore processes are dominant.

5.2 Random waves

5.2.1 Introduction

The one-dimensional model SURFBEAT is validated against flume data of random waves on a horizontal bed which ends in a plane 1:25 beach. Methods to derive correct boundary conditions from measurements are discussed. Good agreement is found between measured and computed short wave energy and long wave time series, and between measured and computed covariance diagrams of short wave energy and long wave elevation. We conclude that the model can be used to predict wave group related velocity moments with reasonable accuracy.

In the next Section we first describe the experiments carried out by Van Leeuwen (1992) at Delft University of Technology.

In Section 5.2.3, we treat the generation of correct boundary conditions based on measurements of the surface elevation in the case of unidirectional random waves. The choice of a representative short wave frequency is discussed, based on measurements and theoretical considerations.

Once the boundary conditions and the representative frequency have been established, an integral model test is performed in Section 5.2.4, where all coefficients are set at standard values. We then compare measured and computed time series of short wave energy and long wave elevation, as well as covariance diagrams of both functions. Conclusions are drawn on the accuracy of velocity moments predicted by this model.

In Section 5.2.5, we investigate whether the covariance diagrams found are strongly dependent on the rather particular spectral shape in the measurements, or on a particular realisation of the spectrum. Some comparisons are shown of covariance diagrams based on random-phase realisations of idealised (JONSWAP) spectra.

Finally, we draw conclusions on the wave generation and on the predictive ability of the SURFBEAT model.

5.2.2 Experiments

The experiment which is analyzed was carried out in a wave flume at Delft University of Technology by Van Leeuwen (1992). It concerns random waves on a horizontal bed which ends in a plane 1:25 beach. The flume has glass walls and a smooth concrete bottom.

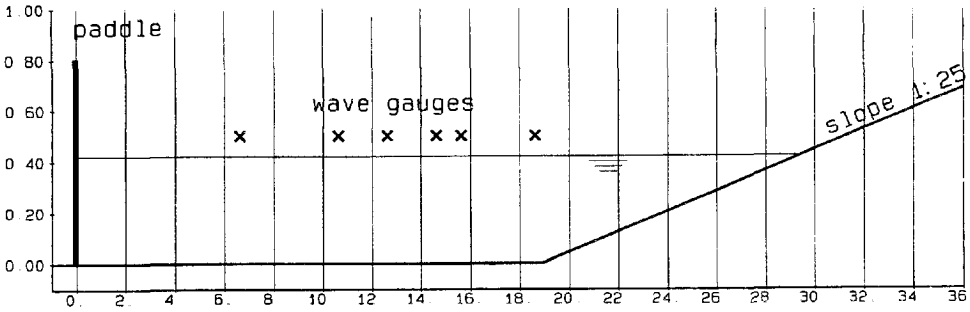

Figure 5.6 *Experimental set-up*

The set-up of the experiment is shown in Figure 5.6. The slope began at 18.89 m from the wave maker; the still water line was at 29.39 m. Waves were generated by a horizontally translating, computer-controlled wave paddle. Second-order wave generation as described in Klopman and Van Leeuwen (1990) was applied. Re-reflection at the paddle of waves reflected from the beach was prevented by the 'active wave absorption' method (Kostense, 1984).

Eight runs were carried out with exactly the same control signal for the wave maker. Six resistance-type wave gauges were used in each run; the locations for each run are given in Table 5.2. The water depth at the horizontal part was 0.42 m.

Code	location gauge 1 (m)	location gauge 2 (m)	location gauge 3 (m)	location gauge 4 (m)	location gauge 5 (m)	location gauge 6 (m)
4j63zoa	18.62	28.99	12.62	6.62	26.72	25.97
4j63zob	18.62	28.99	12.62	6.62	26.88	26.13
4j63zoc	18.62	28.99	12.62	6.62	26.97	n.a.
4j63zod	18.62	28.99	12.62	6.62	27.16	n.a.
4j63zon	18.62	28.99	12.62	6.62	27.30	n.a.
4j63zoh	18.62	28.99	12.62	6.62	26.52	25.72
4j63zoi	18.62	28.99	12.62	6.62	26.82	n.a.
4j63zor	18.62	15.62	12.62	6.62	14.62	10.62

Table 5.2 *Locations of wave gauges for each run*

Waves were generated for approximately 800 s. The peak frequency of the generated spectrum was approximately 0.63 Hz, and the significant wave height was 0.06 m. All six gauges were sampled simultaneously at 20 Hz sampling frequency. Sampling started just before the start of the wave paddle and continued for 810 s.

The dominant breakpoint position was at approximately 26 m. For the first seven runs, two wave gauges were deployed at varying locations near this point, in order to get a good spatial resolution. In these runs, three gauges at 6 m distances were used on the horizontal part, and one very near the still water line.

In the eighth run all gauges were deployed over the horizontal part, in order to enable studying the propagation of short and long waves outside the surf zone in detail.

5.2.3 Input boundary conditions for model

The SURFBEAT model requires as boundary conditions:

a. a time series of the short wave energy E;
b. time series of the incoming long wave elevation and velocity.
c. a representative short wave frequency

Below, we shall discuss how these boundary conditions can be obtained from surface elevation measurements in a single point.

Short wave energy

The short wave energy E is defined as:

$$E = \rho g \overline{\eta_{hi}^2} \tag{5.4}$$

where ρ is the density of water, g the acceleration of gravity and η_{hi} is the short wave surface elevation. The overbar denotes averaging over the short wave time scale.

We now consider the evolution of $\overline{\eta_{hi}^2}$ in time and space. At a certain location, the time series of the total surface elevation, sampled at intervals of Δt for a period T, can be represented by the Fourier series:

$$\eta(t) = \sum_{n=0}^{N-1} \left(a_n \cos(n\Delta\omega\, t) + b_n \sin(n\Delta\omega\, t) \right) \tag{5.5}$$

where $N = T/(2\Delta t)$ is the number of frequencies, $\Delta\omega = 2\pi/T$ is the frequency increment, t is time and a_n and b_n are the Fourier amplitudes.

The short wave surface elevation over the same time span is then given by:

$$\eta_{hi}(t) = \sum_{n=K}^{N-1} \left(a_n \cos(n\Delta\omega\ t) + b_n \sin(n\Delta\omega\ t) \right) \tag{5.6}$$

where $K\Delta\omega$ is the lowest frequency counted as 'short wave'. This frequency is set at half the peak frequency.

For short waves propagating onto a mildly sloping beach, as is the case here, most short wave energy is dissipated on the beach, and reflection of short waves is negligible. Therefore, we can expect the short waves to behave as purely progressive waves, for which the evolution in time and space over a horizontal bottom is given by:

$$\eta_{hi}(x,t) = \sum_{n=K}^{N-1} \left(a_n \cos(n\Delta\omega\ t - k_n x) + b_n \sin(n\Delta\omega\ t - k_n x) \right) \tag{5.7}$$

where x is the coordinate in horizontal direction, relative to some reference point, and k_n the wave number of the n-th frequency.

We can now obtain an expression for the evolution of the short wave variance (which itself varies on the time scale of wave groups) in the following manner: first, the squared sum of all wavelets is rewritten as the (double) sum over the products of all wave pairs:

$$\overline{\eta_{hi}^2} = \overline{\sum_{n=K}^{N-1} \sum_{m=K}^{N-1}} \left(a_n \cos(n\Delta\omega\ t - k_n x) + b_n \sin(n\Delta\omega\ t - k_n x) \right) \cdot \left(a_m \cos(m\Delta\omega\ t - k_m x) + b_m \sin(m\Delta\omega\ t - k_m x) \right) \tag{5.8}$$

Each product consists of a wavelet with a frequency equal to the difference of the two frequencies, and a wavelet with a frequency equal to the sum of both frequencies. In averaging over the short wave period, the wavelets at sum frequencies disappear, so we get the following expression:

$$\begin{aligned} \overline{\eta_{hi}^2} &= \frac{1}{2} \sum_{n=K}^{N-1} \sum_{m=K}^{N-1} (a_n a_m + b_n b_m) \cos[(n-m)\Delta\omega\ t - \Delta k_{nm} x] + \\ &\qquad (a_m b_n - a_n b_m) \sin[(n-m)\Delta\omega\ t - \Delta k_{nm} x] \\ &= \frac{1}{2} \sum_{n=K}^{N-1} \left(a_n^2 + b_n^2 \right) + \sum_{j=1}^{K-1} \sum_{n=K}^{N-j-1} (a_n a_{n+j} + b_n b_{n+j}) \cos(j\Delta\omega\ t - \Delta k_{n,n+j} x) + \\ &\qquad (a_n b_{n+j} - a_{n+j} b_n) \sin(j\Delta\omega\ t - \Delta k_{n,n+j} x) \end{aligned} \tag{5.9}$$

in which $\Delta k_{nm} = k_n - k_m$. This can be reduced to:

$$\overline{\eta_{hi}^2} = \frac{1}{2}\sum_{n=K}^{N-1}\left(a_n^2 + b_n^2 \right) + \sum_{j=1}^{K-1}\left(A_j \cos(j\Delta\omega\, t) + B_j \sin(j\Delta\omega\, t) \right) \tag{5.10}$$

where

$$A_j = \sum_{n=K}^{N-j-1}\left((a_n a_{n+j} + b_n b_{n+j}) \cos(\Delta k_{n,n+j} x) - (a_n b_{n+j} - a_{n+j} b_n) \sin(\Delta k_{n,n+j} x)\right)$$

$$B_j = \sum_{n=K}^{N-j-1}\left((a_n a_{n+j} + b_n b_{n+j}) \sin(\Delta k_{n,n+j} x) + (a_n b_{n+j} - a_{n+j} b_n) \cos(\Delta k_{n,n+j} x)\right)$$

For $x=0$, the above method of computing $\overline{\eta_{hi}^2}$ is equivalent to a method often used (e.g. Abdelrahman and Thornton, 1987) where we first high-pass filter η to obtain η_{hi}. The latter time series is then squared; in order to average the squared signal over the short wave period we low-pass filter it. The formulations of the method used here explicitly contain the contribution of each pair of wavelets, and can be used to predict the time series of $<\eta_{hi}^2>$ in other locations.

The short wave energy time series so derived can be used to obtain an estimate of the short wave envelope A, since:

$$\overline{\eta_{hi}^2} = \frac{1}{2}A^2 \;\Leftrightarrow\; A = \sqrt{2\overline{\eta_{hi}^2}} \tag{5.11}$$

This allows us to check directly if the method produces a realistic and smooth wave energy time series. A comparison between the short wave surface elevation and the computed envelope as in Figure 5.7 shows that the envelope generally follows the maxima quite well, just as the negative envelope follows the minima. For the larger short waves, minor discrepancies occur due to their vertical asymmetry. Near sudden changes in wave energy, as at the start of the record, slightly negative values may occur as the low-pass filtered time series cannot follow these changes. In general the envelope is described adequately.

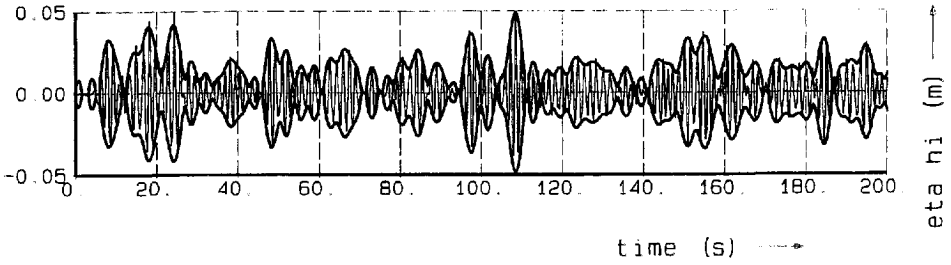

Figure 5.7 *Comparison between short wave record and computed short wave envelope, x=6.62 m; t=0-200 s. T = 1200s, Δt = .05s, N=12000, K = 360*

Short wave energy propagation

A very important aspect of the SURFBEAT model is the description of the propagation of the short wave energy, since this determines not only the speed at which bound waves propagate but also their magnitude. As can be seen in equation (5.10), the mechanism of the energy propagation is that the energy contained in each possible pair of wavelets propagates at a speed $C_{g_{n,n+j}}$ equal to:

$$C_{g_{n,n+j}} = \frac{j\Delta\omega}{k_{n+j}-k_n} \tag{5.12}$$

On a horizontal bed and for small-amplitude waves, the linear dispersion relation holds:

$$(n\Delta\omega)^2 = gk_n \tanh(k_n h) \tag{5.13}$$

from which k_n can be computed for each n. On the other hand, in the SURFBEAT model we assume that the energy propagates at a single group speed, in accordance with the narrow-band approximation. For this approach to be successful, we must find a representative group velocity for which the narrow band approximation yields the smallest errors.

If we consider simultaneous time series of wave energy at two different locations, the narrow band approximation would result in a simple shift of the time series at the inshore location by an amount of Δt, where:

$$\Delta t = \frac{\Delta x}{C_{g,rep}} \tag{5.14}$$

Here, Δx is the distance between the locations and $C_{g,rep}$ the representative group velocity. The mean of the squared errors in the narrow-band prediction of the wave energy at the second location is now smallest if the covariance of the predicted and actual time series at the second location is maximum. For a given value of Δt, we have:

$$E_{x2,pred.}(t+\Delta t) = E_{x1,meas.}(t) \tag{5.15}$$

and so:

$$Cov\left(E_{x2,pred.}(t+\Delta t), E_{x2,meas.}(t+\Delta t)\right) = Cov\left(E_{x1,meas.}(t), E_{x2,meas.}(t+\Delta t)\right) \tag{5.16}$$

From this it follows that the optimum value of Δt equals minus the value τ_{max} at the maximum of the covariance function $C(\tau)$, defined by:

$$C(\tau) = Cov\left(E_{x1}(t), E_{x2}(t-\tau)\right) \tag{5.17}$$

In Figure 5.8, part of the measured time series of E is shown for four locations at equal distances of 4 m, together with the full spectral prediction according to equation (5.10), based on the measured time series at x=6.62 m. The results of run 4j63zor (see Table 5.2) are used for this comparison. Clearly, the group structure remains largely intact while propagating in positive x-direction. The prediction according to the full spectral model is quite accurate in both the propagation and the distortion of the group structure.

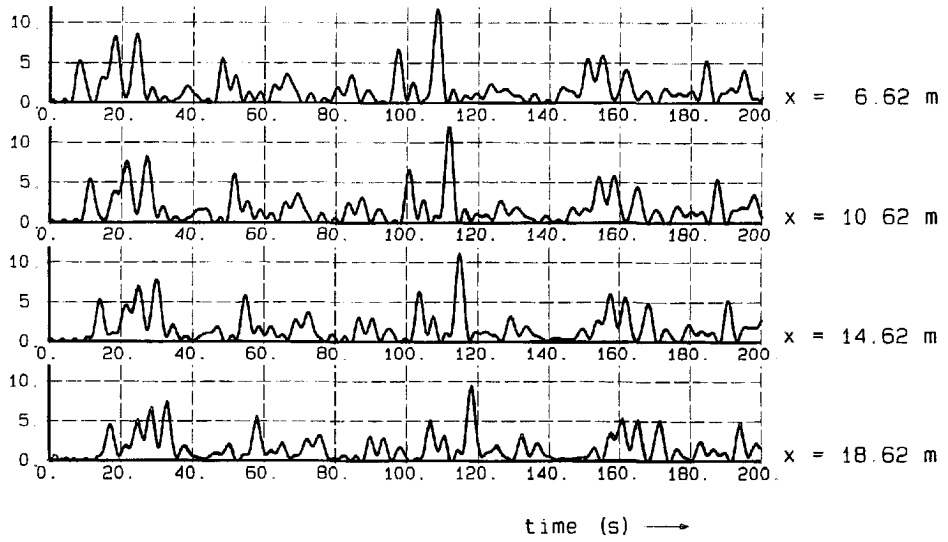

Figure 5.8 *Simultaneous time series of E (J/m^2) at four locations; measurements (thick lines) vs. predictions by full spectral model (thin lines); t=0-200 s.*

In Figure 5.9, the covariance functions of the energy at x = 6.62 m and the energy at x=6.62, 10.62, 14.62 and 18.62 m respectively are shown, for both the measurements and the predictions with the full spectral model. Again, the full spectral model is quite accurate.

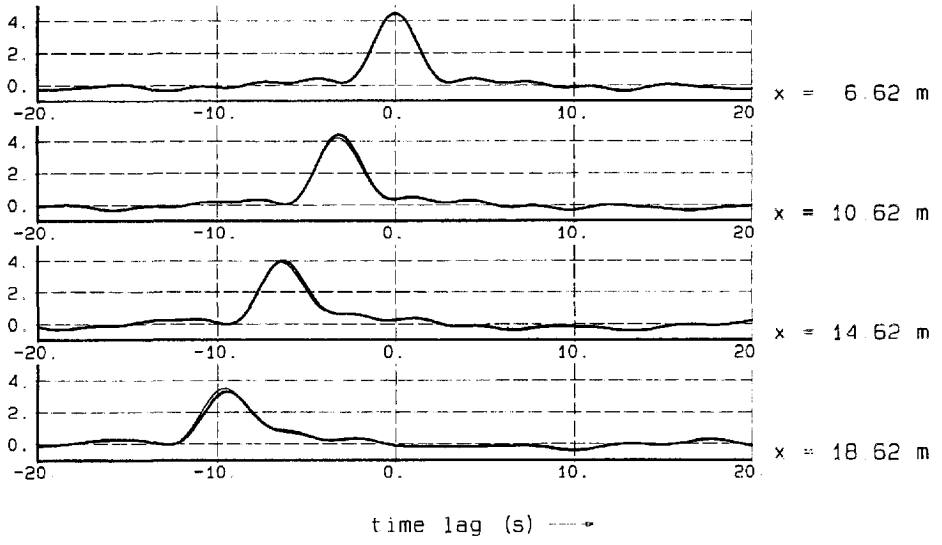

Figure 5.9 *Covariance function (J^2/m^4) of E at x=6.62 m and E at x=6.62, 10.62, 14.62, 18.62 m respectively; measurements (thick lines) vs. predictions by full spectral model (thin lines).*

In Figure 5.10, the time lags at maximum covariance are plotted against the propagation distance. A good linear relationship is found, from which it follows that the representative group velocity is:

$$C_{g,rep} = (1.26 \pm 0.01)\ m/s \tag{5.18}$$

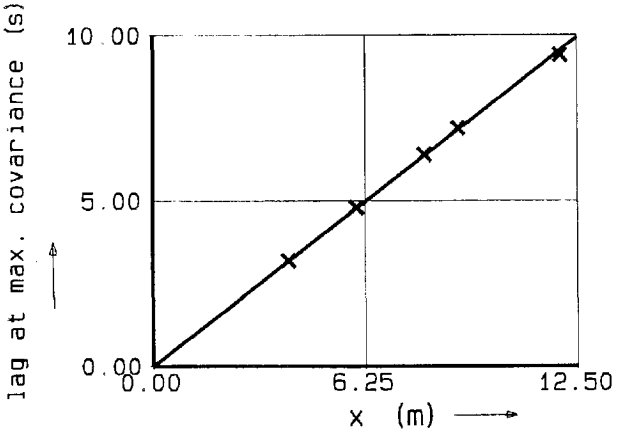

Figure 5.10 *Time lag at maximum covariance vs. horizontal distance for simultaneous time series of E*

Short wave frequency representative for wave energy propagation

In the SURFBEAT model, short wave parameters such as the phase velocity and the group velocity are computed on the basis of a representative short wave frequency, with the help of linear theory. Since we now know the group velocity (at least in deep water) we can iteratively find the frequency that yields the right value. Although there is no proof of this, we may expect that this frequency is also reasonably representative in shallower water.

In the present case, using the result of eq. (5.18), we find a representative frequency f_{rep} of approximately 0.74 Hz, which is considerably higher than the peak frequency of approximately 0.63 Hz. We shall discuss this furtheron.

Evaluation of bound long wave generation in experiment

Full spectral model

The bound long waves generated by the radiation stress gradients accompanying the groups of short waves can be predicted by considering each pair of wavelets described in equation (5.10) to be accompanied by a bound wave as described by Longuet-Higgins and Stewart (1964). We then get:

$$\eta_{bi} = \sum_{j=1}^{K-1} \left(\alpha_j \cos(j\Delta\omega\, t) + \beta_j \sin(j\Delta\omega\, t) \right) \tag{5.19}$$

where

$$\alpha_j = \sum_{n=K}^{N-j} \left((a_n a_{n+j} + b_n b_{n+j}) \cos(\Delta k_{n,n+j} x) - (a_n b_{n+j} - a_{n+j} b_n) \sin(\Delta k_{n,n+j} x) \right) R_{n,n+j}$$

$$\beta_j = \sum_{n=K}^{N-j} \left((a_n a_{n+j} + b_n b_{n+j}) \sin(\Delta k_{n,n+j} x) + (a_n b_{n+j} - a_{n+j} b_n) \cos(\Delta k_{n,n+j} x) \right) R_{n,n+j}$$

Here η_{bi} is the bound incoming long wave elevation and $R_{n,n+j}$ a (dimensional) response function, given by:

$$R_{n,n+j} = g \left[\frac{2\dfrac{C_{g_{n,n+j}}}{C_{n,n+j}} - \dfrac{1}{2}}{C_{g_{n,n+j}}^2 - gh} \right] \tag{5.20}$$

The phase velocity $C_{n,n+j}$ is given by:

$$C_{n,n+j} = \frac{(2n+j)\Delta\omega}{k_n + k_{n+j}} \tag{5.21}$$

Given the accuracy of equation (5.10) in predicting the propagation of energy over the horizontal bed, equation (5.19) can be expected to produce quite accurate results for the bound long waves.

SURFBEAT model

We can compare this full spectral model with the formulation of bound waves in SURFBEAT model, where:

$$\eta_{bi} = \frac{1}{\rho}\left[\frac{2\frac{C_{g,rep}}{C_{rep}} - \frac{1}{2}}{C_{g,rep}^2 - gh}\right]\left(E - \langle E \rangle\right) = \frac{R_{rep}}{\rho g}\left(E - \langle E \rangle\right) \tag{5.22}$$

The value of the R_{rep} can be computed as the linear regression coeffient of η_{bi} according to equation (5.19) as a function of $\overline{\eta_{hi}^2}$ according to equation (5.10). (Note that $E = \rho g \overline{\eta_{hi}^2}$
For the present case we find $R_{rep} = -4.16\ m/m^2$.

The propagation speed of the bound long waves, C_{bi} can be computed by considering the covariance function of η_{bi}, computed by equation (5.19) at $x = 6.62m$, with η_{bi} at other locations, and determining the regression for the time lag at maximum covariance as a function of propagation distance, similar to what is shown in Figures 5.9 and 5.10 for the short wave energy. Here, we find $C_{bi} = 1.31\ m/s$, which is different from the measured group velocity. However, it turns out that a single representative frequency that produces approximately correct values of both C_{bi} and R_{rep} can be found, and is approximately 0.71 Hz.

Wave generation model

The bound long waves generated by the wave paddle in the experiment are according to the predictions by a model (Klopman and Van Leeuwen, 1990) that is very similar to the SURFBEAT model, in that it also uses the narrow band approximation, where the propagation of the short wave energy is represented by a single representative group velocity. This group frequency is computed based on the peak frequency of the spectrum, which in the present case is approximately 0.63 Hz. The value of R_{rep} in that

case is $-5.30\ m/m^2$, which is 25%-30% higher than the prediction by the full spectral model. The long waves generated at the wave maker are described by:

$$\eta_{incoming}\ |_{x=0} = R_{f_p} \sum_{j=1}^{K-1} \left(A_j \cos(j\Delta\omega\ t) + B_j \sin(j\Delta\omega\ t) \right) \tag{5.23}$$

where

$$A_j = \sum_{n=K}^{N-j-1} \left((a_n a_{n+j} + b_n b_{n+j}) \cos(\Delta k_{n,n+j}(-x_0)) - (a_n b_{n+j} - a_{n+j} b_n) \sin(\Delta k_{n,n+j}(-x_0)) \right)$$

$$B_j = \sum_{n=K}^{N-j-1} \left((a_n a_{n+j} + b_n b_{n+j}) \sin(\Delta k_{n,n+j}(-x_0)) + (a_n b_{n+j} - a_{n+j} b_n) \cos(\Delta k_{n,n+j}(-x_0)) \right)$$

Because of the mismatch in group velocity, these long waves cannot be fully carried along as bound waves; the difference between $\eta_{incoming}$ and η_{bi} will propagate as free waves, at a propagation speed equal to $\sqrt{gh}$. In the measurements, we will therefore have incoming free waves η_{fi}, described by:

$$\eta_{fi} = \sum_{j=1}^{K-1} \left[\gamma_j \cos(j\Delta\omega\ (t - \frac{x}{\sqrt{gh}})) + \delta_j \sin(j\Delta\omega\ (t - \frac{x}{\sqrt{gh}})) \right] \tag{5.24}$$

where

$$\gamma_j = \sum_{n=K}^{N-j-1} \left((a_n a_{n+j} + b_n b_{n+j}) \cos(\Delta k_{n,n+j}(-x_0)) - (a_n b_{n+j} - a_{n+j} b_n) \sin(\Delta k_{n,n+j}(-x_0)) \right) (R_{f_p} - R_{n,n+j})$$

$$\delta_j = \sum_{n=K}^{N-j-1} \left((a_n a_{n+j} + b_n b_{n+j}) \sin(\Delta k_{n,n+j}(-x_0)) + (a_n b_{n+j} - a_{n+j} b_n) \cos(\Delta k_{n,n+j}(-x_0)) \right) (R_{f_p} - R_{n,n+j})$$

Here, $x_0 = 6.62\ m$ is the distance of the first wave gauge from the wave paddle. These free waves are in phase with the bound waves at the wave paddle, but will run ahead of the bound waves furtheron in the flume.

The fact that this is actually happening in the flume can be shown in covariance diagrams of E at a certain location and the total long wave η_{lo} at the same location; these are given in Figure 5.11 for x = 6.62, 10.62, 12.62, 14.62, 15.62 and 18.62 m respectively. At x=6.62 m we still see a single negative peak at slightly positive time lag, whereas for increasing x we see a second peak developing to the right. This indicates free long waves coming in before the wave groups, as we expect. The influence of reflected free waves shows up on the left side of the lower figures. This will

be dealt with furtheron. The reflected free waves have no significant influence on the part of the covariance diagram between -10 s and 10 s.

In Figure 5.11 we have also drawn covariance diagrams as predicted by the full spectral model, including the incoming free waves. The agreement with the measurements is quite good and can serve as proof of the validity of the full spectral model.

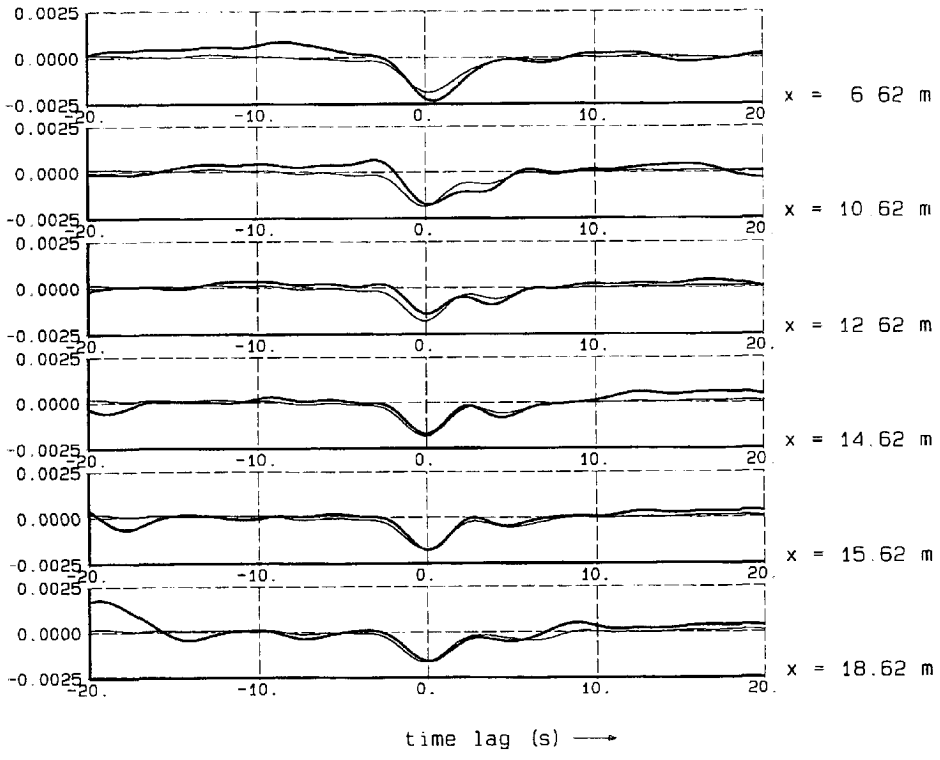

Figure 5.11 *Covariance function (mJ/m^2) of E and total long wave elevation at six measurement locations; measurements (thick lines) and prediction by full spectral model (incoming waves only)*

Conclusions on boundary conditions

For the present case the narrow-band model of bound long waves leads to an overestimation of these bound waves by approximately 25 - 30% if the peak frequency is used as a representative frequency. If this model is used to generate a second order control signal for the wave paddle, spurious free waves are generated.

Both the bound long waves and the spurious free waves can be predicted accurately by a full spectral model. This model can therefore be used to compute a representative frequency to be used in the narrow-band approach. This frequency depends on the phenomenon one wants to describe. There is a small but significant difference in the 'best-fit' propagation speed of the wave energy and that of the bound long waves. Since our interest is focused on the generation, propagation and reflection of long waves, the frequency is chosen that best represents that process. For the present case this amounts to 0.71 Hz, which is significantly higher than the peak frequency of 0.63 Hz.

The time series of the short wave energy at the wave paddle can be derived from the short wave spectrum at the nearest wave gauge, with the help of equation (5.10).

In order to reproduce the long waves generated in these measurements, the boundary condition for the incoming long waves in the SURFBEAT model must be similar to that at the wave paddle, which means that it is based on equation (5.22) with R_{rep} computed from the peak frequency.

5.2.4 Integral model test

Parameter settings

Since we have now derived optimum boundary conditions for the SURFBEAT model, we can perform an integral model test. The internal coefficients in the model are set at their standard values, as derived in the calibration phase. These settings are repeated here.

For the short wave dissipation we have the following settings, in accordance with the findings in Chapter 4:

$\alpha = 1.0$
$\gamma = 0.55$
$n = 10$

The bottom friction coefficient f_w is set at 0.02, which was found to be a reasonable value for the Kostense (1984) case.

A non-equidistant grid of 100 computational points is used, and a time step of 0.1 s. This ensures that numerical errors in propagation speeds are generally less than 1%. Results of computations over a period of 800 s are shown here.

Comparison of time series over horizontal bottom

First, we show a direct comparison between measured and computed time series of the short wave energy (Fig. 5.12 a-d) and the total long wave elevation (Fig. 5.13 a-d) in four points at 4 m spacing. The measurements were taken from run 4j63zor (see Table 5.2).

The time series of the short wave energy are generally reproduced reasonably well. Since in the model the energy propagates undisturbed over the horizontal bed, whereas in reality the groups are gradually deformed, the errors in the prediction increase with increasing distance from the wave paddle. This is expressed by the coefficient of correlation between measured and computed short wave energy, which decreases from 0.95 at x=6.62 m to 0.70 at x=18.62 m. As was shown in Section 5.2.3, this is almost entirely due to the narrow-band approximation used in SURFBEAT, where the slow variation in time of the group velocity is neglected.

The phase errors in the prediction of the short wave energy are transferred to phase errors both in the incoming bound waves and in the reflected free waves, and thus in the total long wave elevations. The phase errors in the bound waves increase with increasing distance from the wave paddle because of the increasing errors in the short wave energy. On the other hand, the phase errors in the reflected free waves are the result of the errors in the propagation of the short wave energy throughout the flume, and can be expected not to increase on the way back. Because of this, the total errors are smallest at the point nearest to the wave paddle, as can be seen in Fig. 5.13 a-d. Here, the coefficient of correlation between measured and computed total long wave elevation is still 0.70, whereas it decreases to 0.51 at x=18.62 m.

From Fig. 5.13 a-d we see that qualitatively the agreement between measured and computed long wave elevations is quite reasonable, given the relative simplicity of the model.

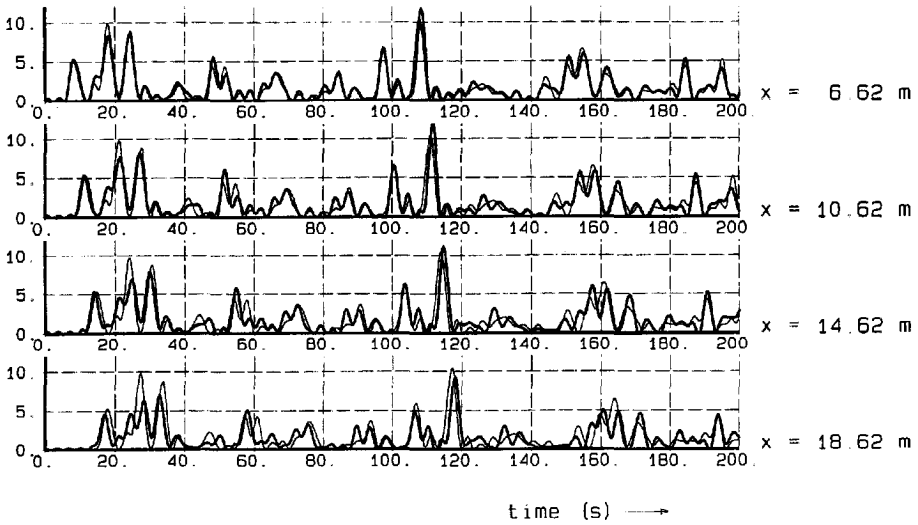

Figure 5.12a *Time series of short wave energy (J/m^2) in 4 points at 4 m spacing; measured (thick lines) and computed by SURFBEAT model (thin lines); 0-200 s.*

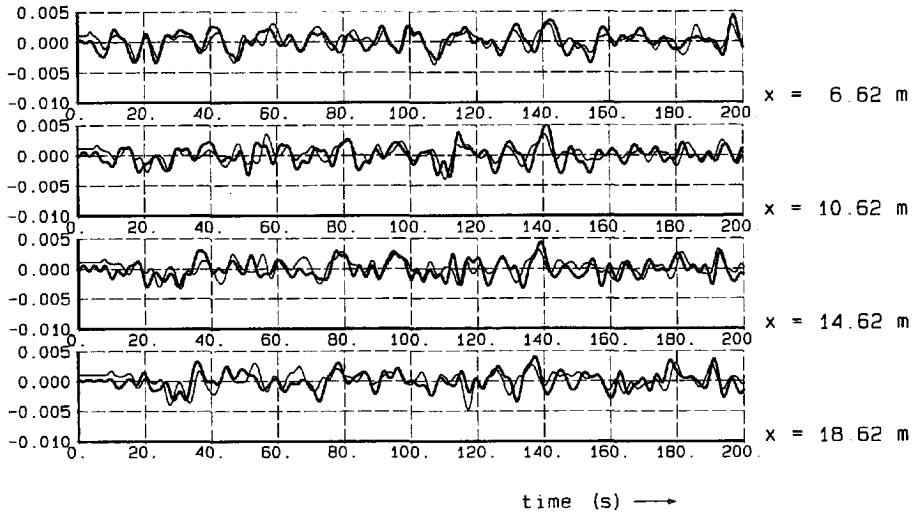

Figure 5.13a *Time series of total long wave elevation (m) at 4 points at 4 m spacing; measured (thick lines) and computed by SURFBEAT model (thin lines); 0-200 s.*

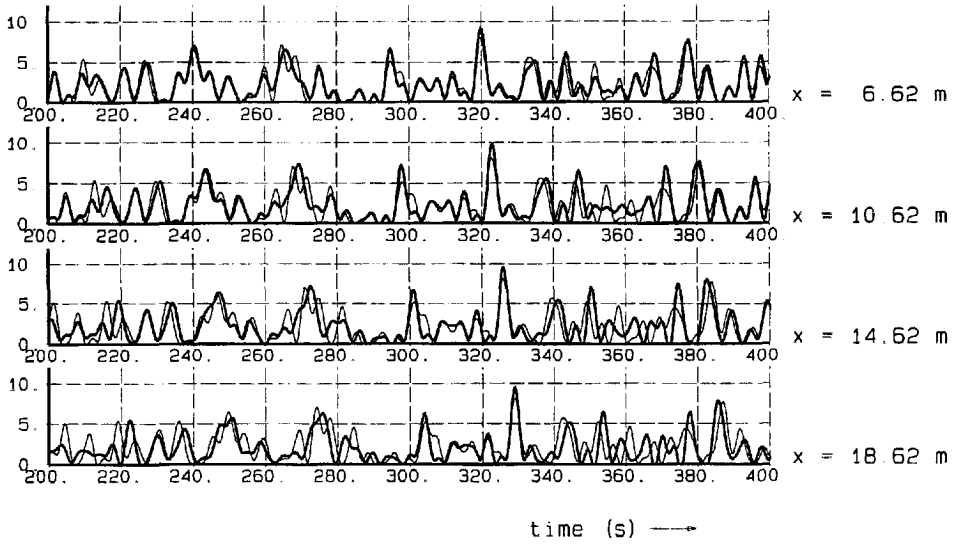

Figure 5.12b *Time series of short wave energy (J/m^2) in 4 points at 4 m spacing; measured (thick lines) and computed by SURFBEAT model (thin lines); 200-400 s.*

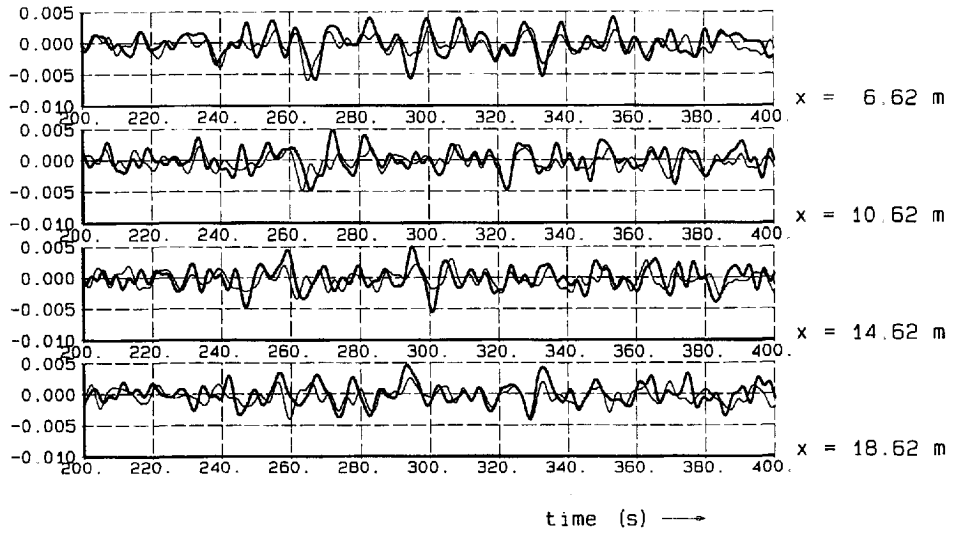

Figure 5.13b *Time series of total long wave elevation (m) at 4 points at 4 m spacing; measured (thick lines) and computed by SURFBEAT model (thin lines); 200-400 s.*

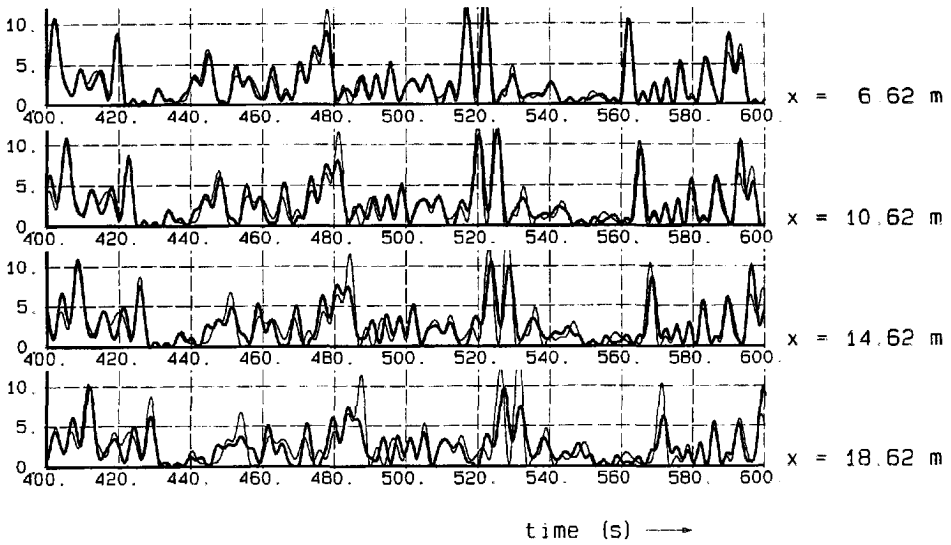

Figure 5.12c *Time series of short wave energy (J/m^2) in 4 points at 4 m spacing; measured (thick lines) and computed by SURFBEAT model (thin lines); 400-600 s.*

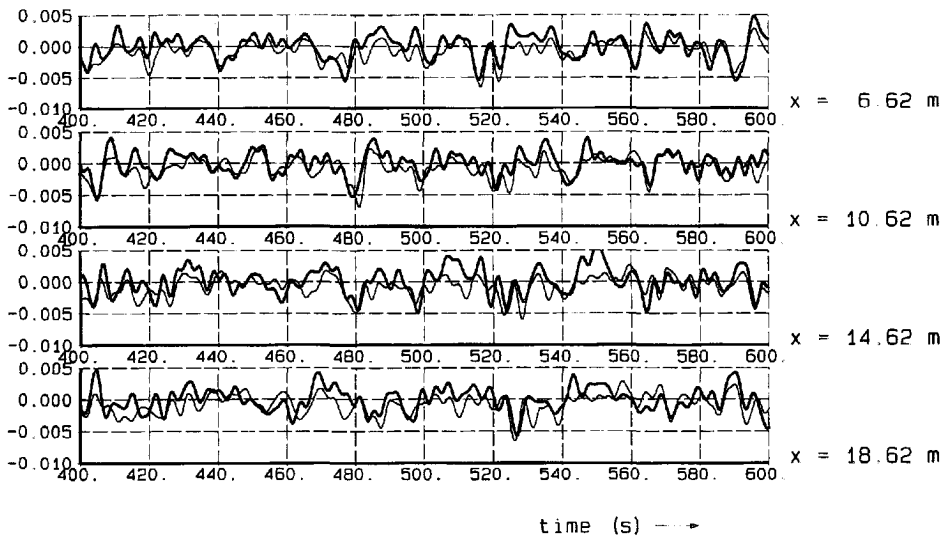

Figure 5.13c *Time series of total long wave elevation (m) at 4 points at 4 m spacing; measured (thick lines) and computed by SURFBEAT model (thin lines); 400-600 s.*

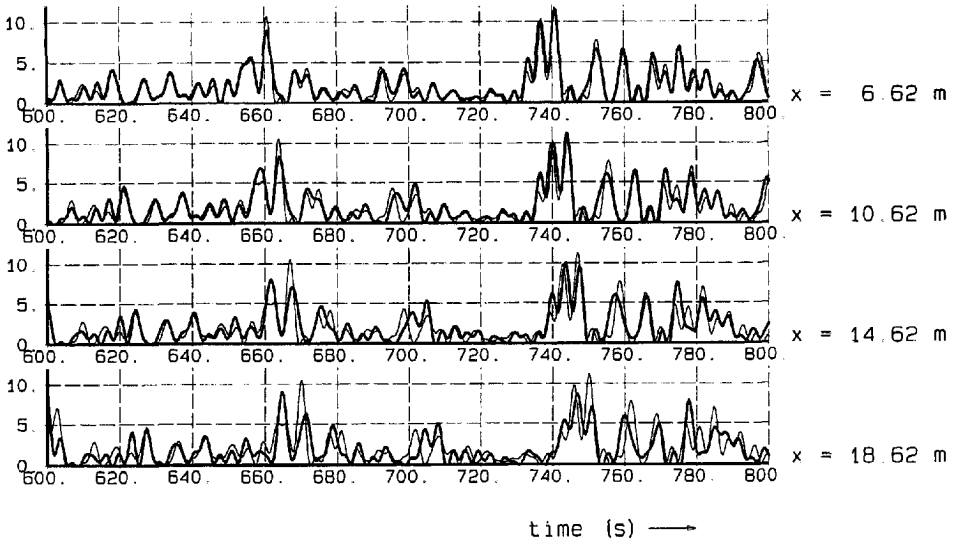

Figure 5.12d *Time series of short wave energy (J/m^2) in 4 points at 4 m spacing; measured (thick lines) and computed by SURFBEAT model (thin lines); 600-800 s.*

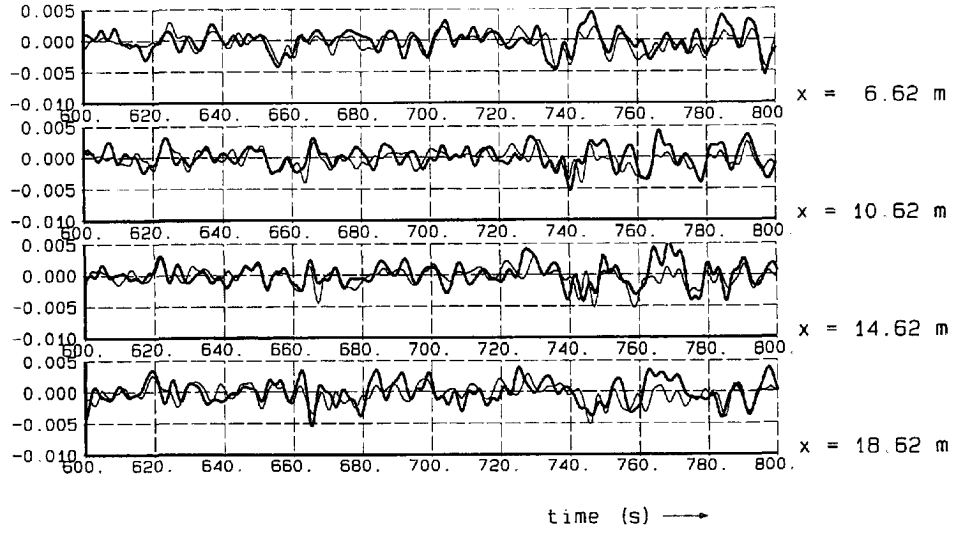

Figure 5.13d *Time series of total long wave elevation (m) at 4 points at 4 m spacing; measured (thick lines) and computed by SURFBEAT model (thin lines); 600-800 s.*

Comparison of covariance functions over horizontal bottom

In Figure 5.14, we have plotted the measured and computed covariance function of short wave energy and total long wave elevation in all six measurement locations. Here we find that all basic features of the measured covariance diagrams are reproduced by the model: the minimum at zero time lag due to the bound waves, the smaller minimum at positive time lag due to the (spurious) incoming free waves and the feature at decreasing negative time lag due to the reflected free waves. Quantitatively, the agreement is good for the bound waves and the incoming free waves, and for the reflected free waves it is good at the points nearest to the paddle and still reasonable for the shoreward points. The plots are given in absolute values of the covariance function.

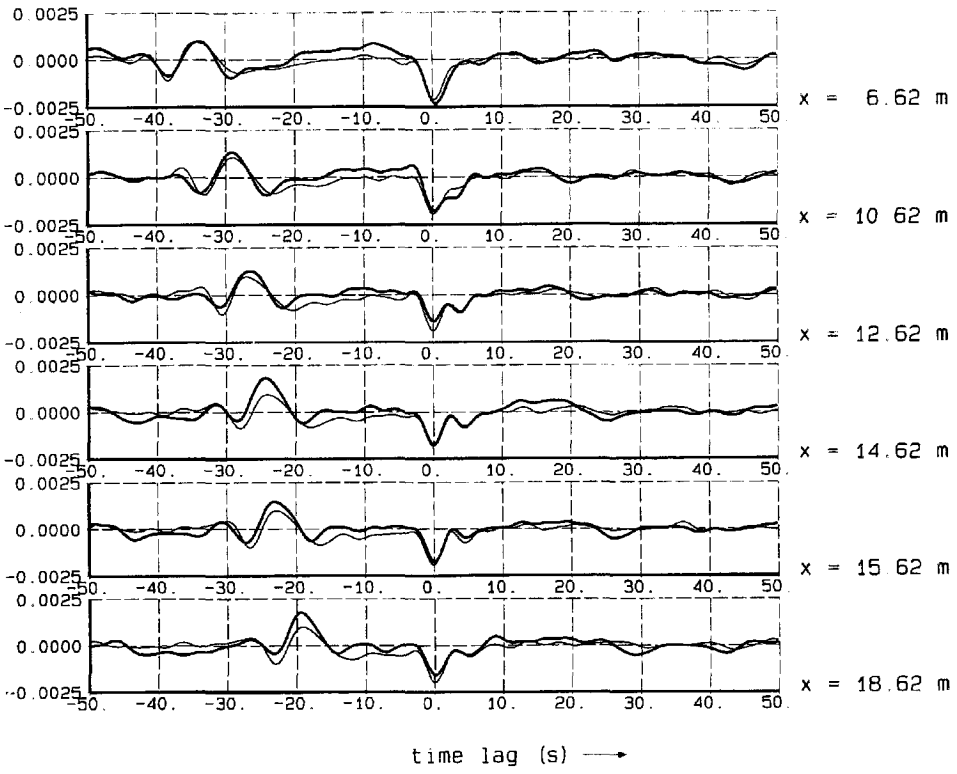

Figure 5.14 *Covariance functions (mJ/m^2) of short wave energy and long wave elevation; measured (thick lines) and predicted by SURFBEAT model (thin lines); all measurement points, run 4j63zor*

In evaluating the relevance of this result, we must consider that for application of the model to morphological problems, the main interest is in predicting contributions of the interaction of long waves and short waves to velocity moments like:

$$< u_{lo} \overline{u_{hi}^2} > \tag{5.25}$$

where u_{lo} is the long wave particle velocity and u_{hi} is the short wave particle velocity. For the case of propagating bound long waves, we have:

$$u_{lo} \approx \frac{C_{g,rep}}{h} \eta_{lo} \tag{5.26}$$

and

$$\overline{u_{hi}^2} \approx \left[\frac{2\pi f_{rep}}{\sinh(k_{rep} h)} \right]^2 \frac{E}{\rho g} \tag{5.27}$$

we find:

$$< u_{lo} \overline{u_{hi}^2} > \approx \frac{1}{\rho g} \left[\frac{2\pi f_{rep}}{\sinh(k_{rep} h)} \right]^2 \frac{C_{g,rep}}{h} < E \, \eta_{lo} > \tag{5.28}$$

where the term $< E \, \eta_{lo} >$ is equal to the covariance between E and η_{lo} at zero time lag. This means that the prediction of the velocity moments is of almost the same accuracy as that of the covariance at zero time lag, and that given the result of Figure 5.14, the SURFBEAT model seems to be accurate enough in that respect.

This is valid for the points on the horizontal part of the flume, where the covariance at zero time lag is dominated by the bound waves. Inside the surf zone, we can expect that the part of the covariance function that is dominated by the bound waves will overlap with the part that is dominated by the reflected free waves. Comparisons between model predictions and measurements for this case are discussed in the next paragraphs.

Decay of short wave energy in the surf zone

The relative importance of several long wave generation mechanisms inside the surf zone has been studied by some authors (Schäffer and Jonsson, 1990; List, 1992) The description of the propagation and decay of short wave groups in the shoaling and breaking regions is essential in predicting the release of bound long waves and the generation of free long waves due to other mechanisms. Important aspects to consider are the decay of mean energy, the average breakpoint location and the decrease (if any) of the groupiness.

In Figure 5.15, a comparison between measured and computed average short wave energy is given. Results from all measurement runs are combined here. There seems to be some scatter in the measurements, even on the horizontal part. Generally, the errors in the prediction of the energy are less than 10 %. The location of the average breakpoint and the decay inside the surf zone are predicted accurately. Since the dissipation model was calibrated against similar data on mean energy decay (see Chapter 4) this should not be surprising.

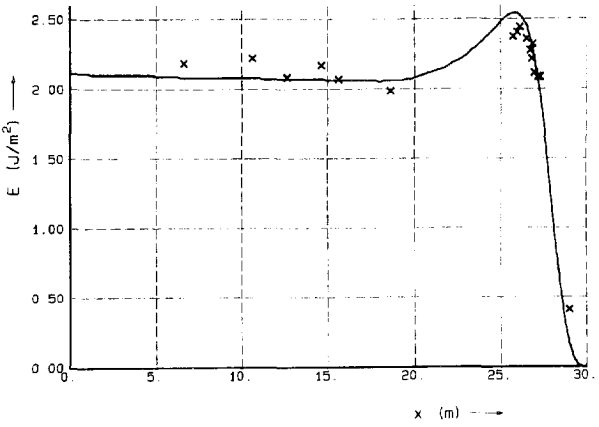

Figure 5.15 *Average short wave energy as function of distance from wave maker. Measurements from all runs (crosses) vs. computation (drawn line)*

In Figures 5.16 a-d, the measured and computed time series of short wave energy are shown for five locations during run 4j63zob (see Table 5.2); a point near the wave maker, one near the start of the slope, two points just shoreward of the average break point and one point very near the still water line. For the points just after breaking, there still is a reasonable agreement between measured and computed time series. Discrepancies seem to be in the same order of magnitude as near the start of the slope (x = **18.89** m), and can be ascribed mainly to the partial desintegration of the wave groups over the horizontal part. Contrary to the wide-spread concept of a 'saturated zone', where the wave height becomes more constant in time, the group structure remains largely intact both in the measurements and in the model. At the point near the still water line, the model underpredicts the variability in wave energy. The effect of the long wave velocity on the short wave modulation must be important here (see Abdelrahman and Thornton, 1987). This has not been taken into account. The model results do show some modulation of wave energy in this point, which is due to the water level variation.

Long waves inside the surf zone

For the same five points as above the measured and predicted long wave elevations are given in Figures 5.17 a-d. Both in the measurements and in the computations the long wave amplitudes inside the surf zone are much higher than at the horizontal part. Qualitatively, the agreement between measured and computed long wave elevations is quite good even up to the point near the still water line, in a still water depth of 1.6 *cm*. The variations in water level are in the right order of magnitude, although there are discrepancies. These are due partly to phase errors related to the narrow band approximation, as discussed before.

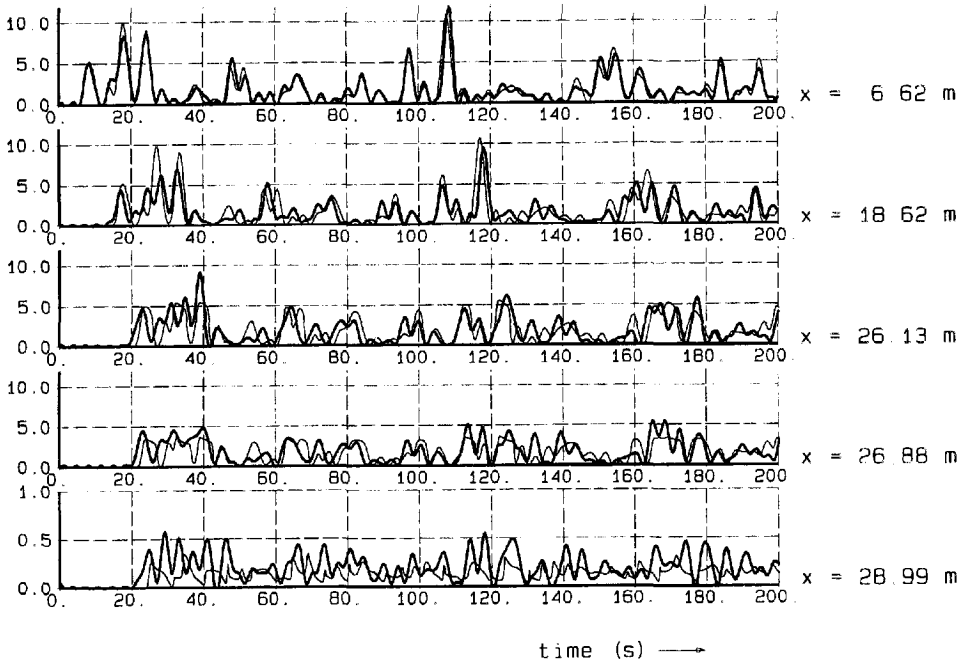

Figure 5.16a *Measured (thick lines) and computed (thin lines) time series of short wave energy (J/m^2); 5 locations, run 4j63zob; 0-200 s*

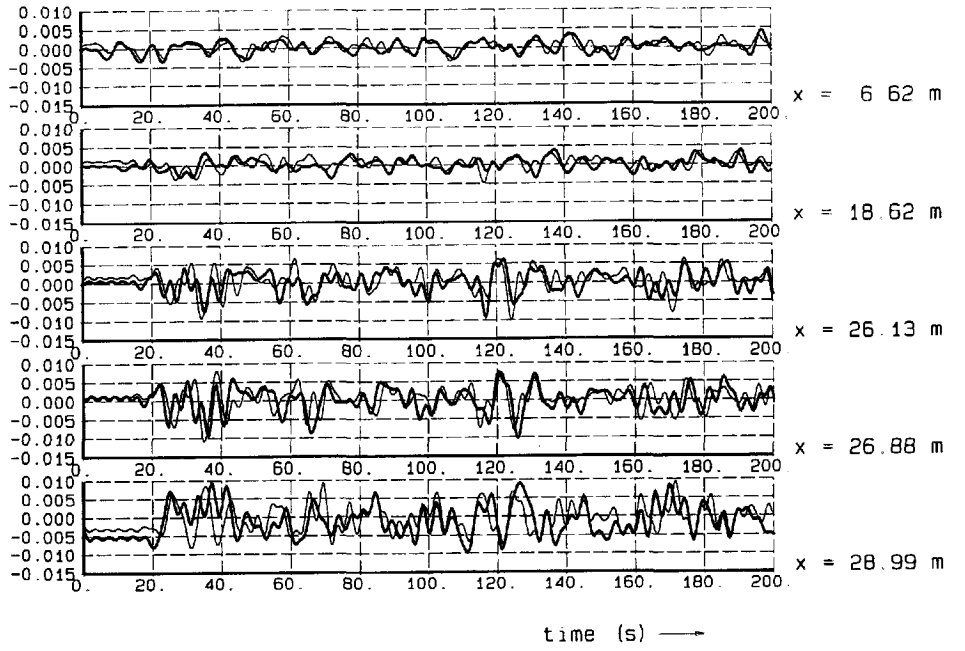

Figure 5.17a *Measured (thick lines) and computed (thin lines) time series of total long wave elevation (m); 5 locations, run 4j63zob; 0-200 s*

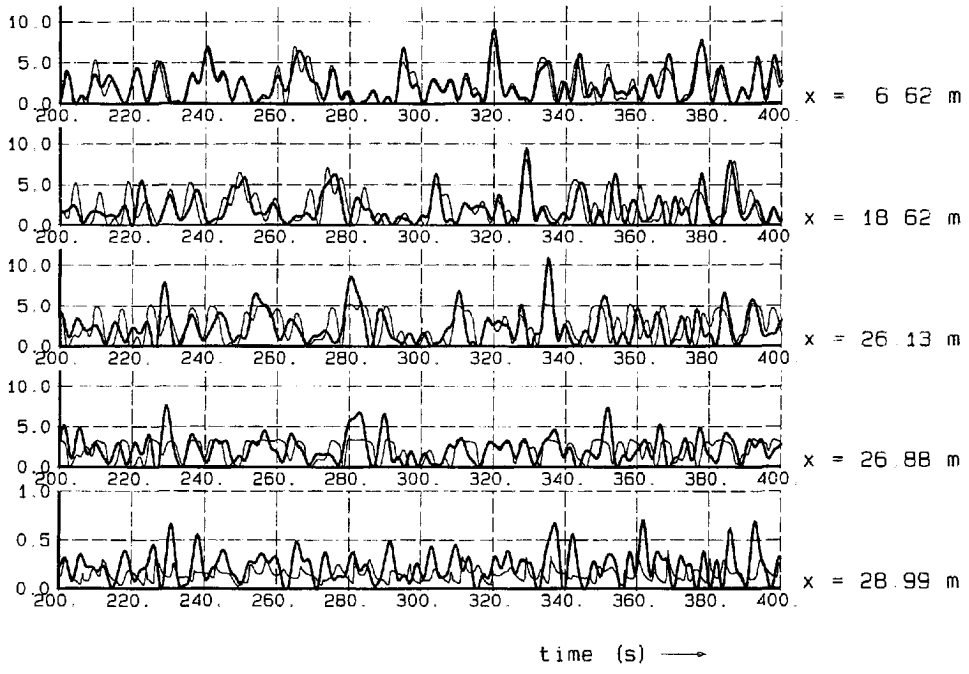

Figure 5.16b *Measured (thick lines) and computed (thin lines) time series of short wave energy (J/m^2); 5 locations, run 4j63zob; 200-400 s*

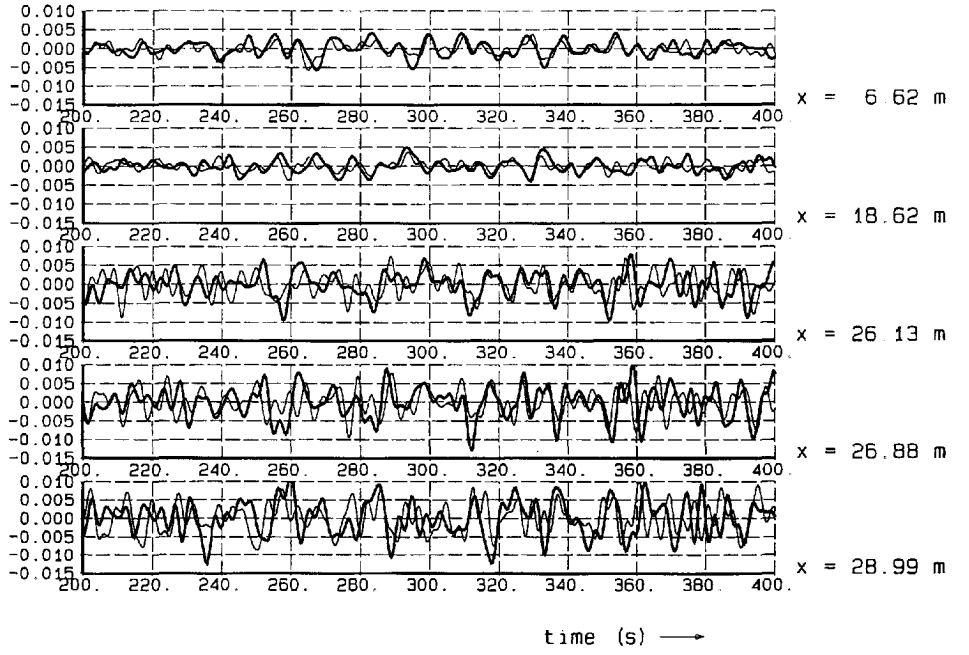

Figure 5.17b *Measured (thick lines) and computed (thin lines) time series of total long wave elevation (m); 5 locations, run 4j63zob; 200-400 s*

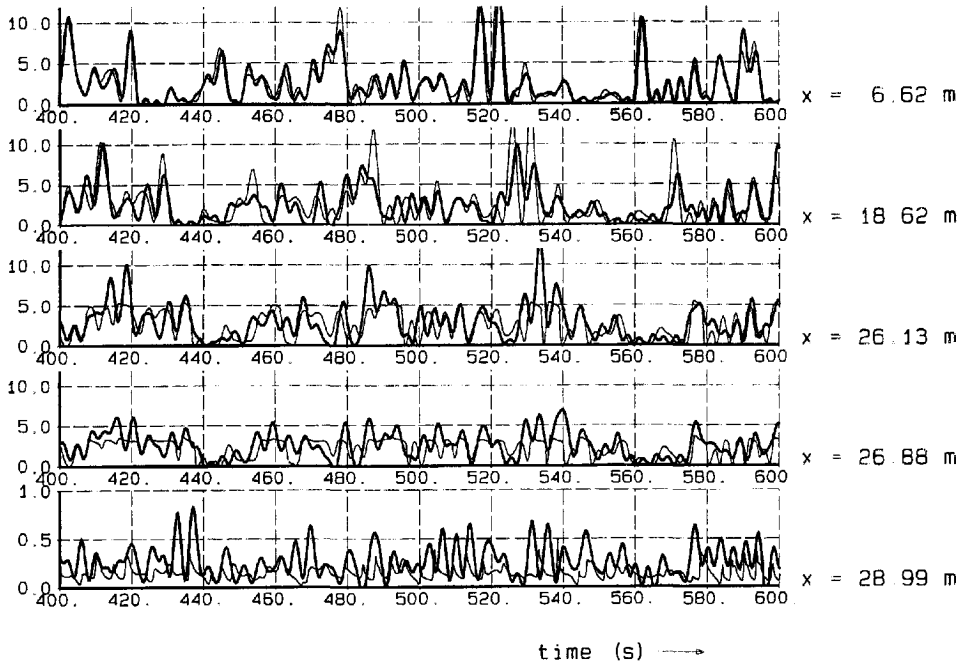

Figure 5.16c *Measured (thick lines) and computed (thin lines) time series of short wave energy (J/m^2); 5 locations, run 4j63zob; 400-600 s*

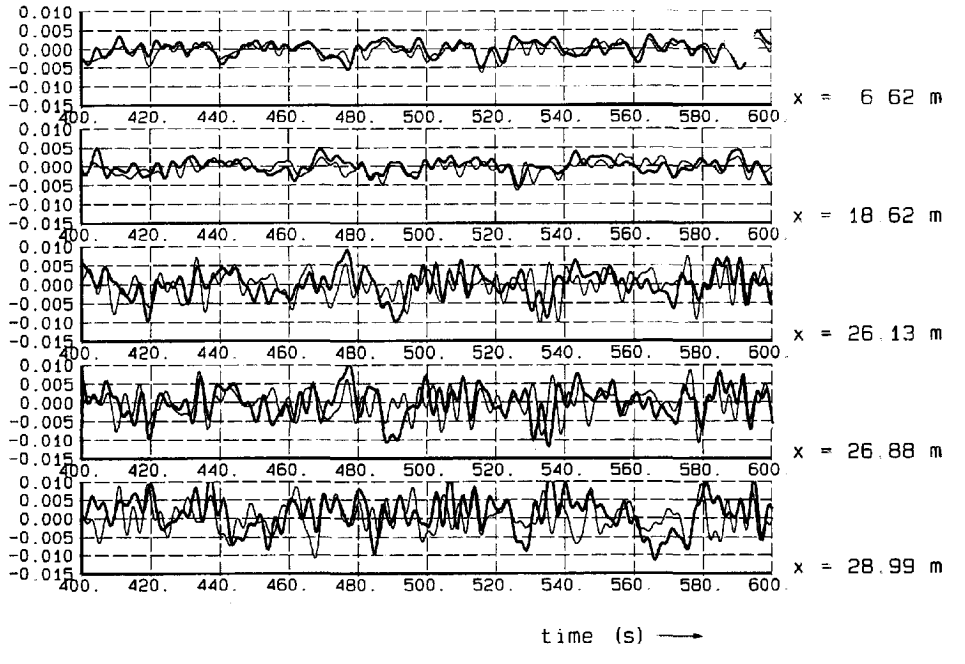

Figure 5.17c *Measured (thick lines) and computed (thin lines) time series of total long wave elevation (m); 5 locations, run 4j63zob 400-600 s*

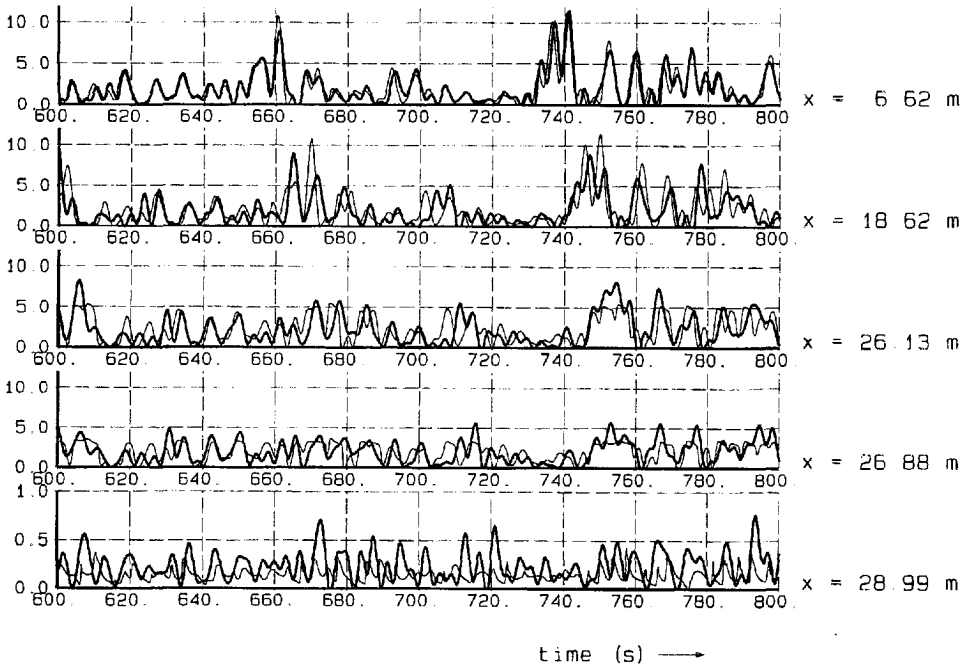

Figure 5.16d *Measured (thick lines) and computed (thin lines) time series of short wave energy (J/m^2); 5 locations, run 4j63zob; 600-800 s*

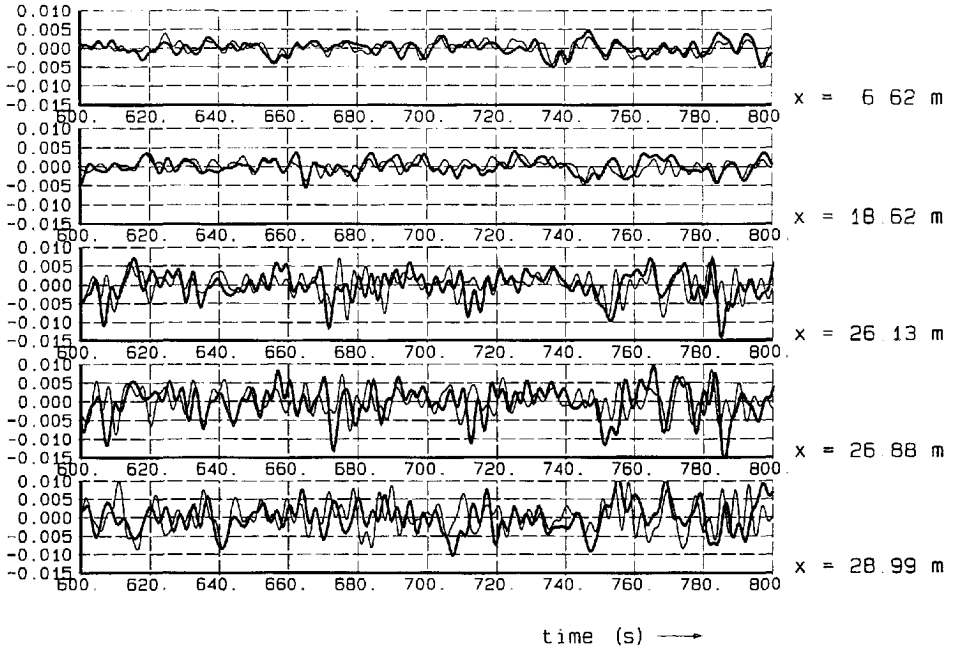

Figure 5.17d *Measured (thick lines) and computed (thin lines) time series of total long wave elevation (m); 5 locations, run 4j63zob; 600-800 s*

Another part of the discrepancies arises from re-reflections of very long waves in the measurements. Because of leakage of water past the wave maker, the performance of the wave absorption system drops sharply for waves with frequencies lower than .1 *Hz*, as is evident from Figure 5.18, where the coefficient of reflection measured at the wave maker is given as a function of the frequency.

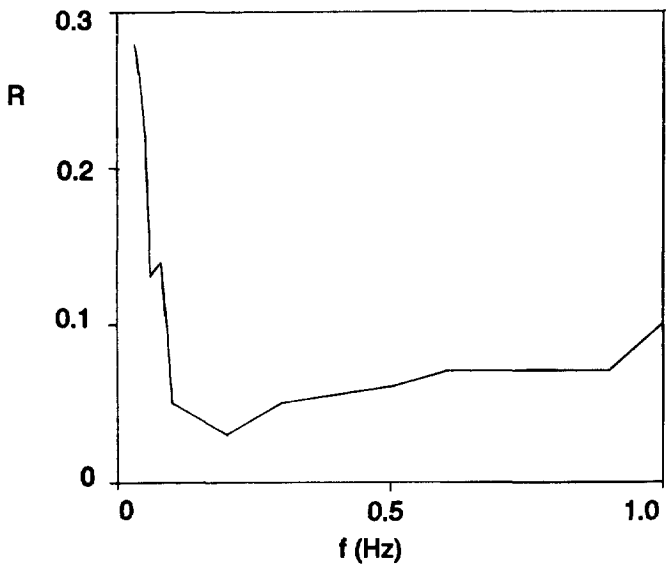

Figure 5.18 *Reflection coefficient R of the wave board with active absorption versus frequency f. From: Van Leeuwen, (1992)*

The effect of this clearly shows up in comparisons between measured and predicted long wave spectra, given in Figures 5.19 a-f. In the range of 0.1 Hz to 0.3 Hz the agreement between measured and predicted spectra is quite reasonable. For the frequencies below 0.1 Hz, there are discrepancies between model and measurements, due to the imperfect absorption of long waves at the wave board. The measurements show a peak at approximately 0.04 Hz, which is close to the lowest resonance frequency of the flume.

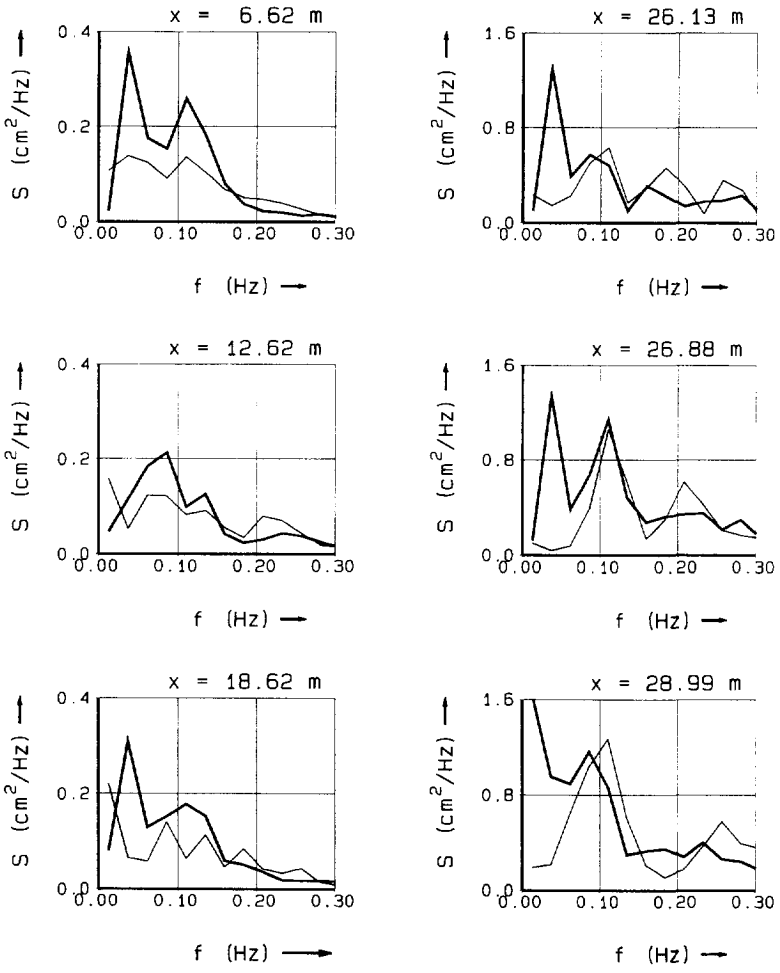

Figure 5.19 *Measured (thick lines) vs. computed (thin lines) long wave spectra, averaged over 20 frequency bins; all points in run 4j63zob*

Covariance functions inside the surf zone

As was discussed above, the covariance function between short wave energy and long wave elevation is closely related to velocity moments, which are important for sediment transport. We derived this for propagating rather than standing long waves, which is valid outside the surf zone, where reflected free waves have no influence on the covariance function near zero time lag. Inside the surf zone, this does no longer hold, so there is no direct relationship between the covariance at zero time lag and the velocity moments. Still, we may assume that the quality of the prediction of the covariance function is a good indication of our ability to predict the velociity moments

here. In Figure 5.20, the measured and computed covariance functions for all points in run 4j63zob are shown. Note the different scales on the vertical axes. The agreement is quite good for the points just inside the breaker zone ($x > 26\ m$), and is still reasonable for the point near the still water line, where the covariance function is an order of magnitude smaller. The phenomenon, noted in literature (e.g. Abdelrahman and Thornton, 1987; Roelvink and Stive, 1989) that the correlation at zero time lag becomes positive close to the shore, is reproduced by the model.

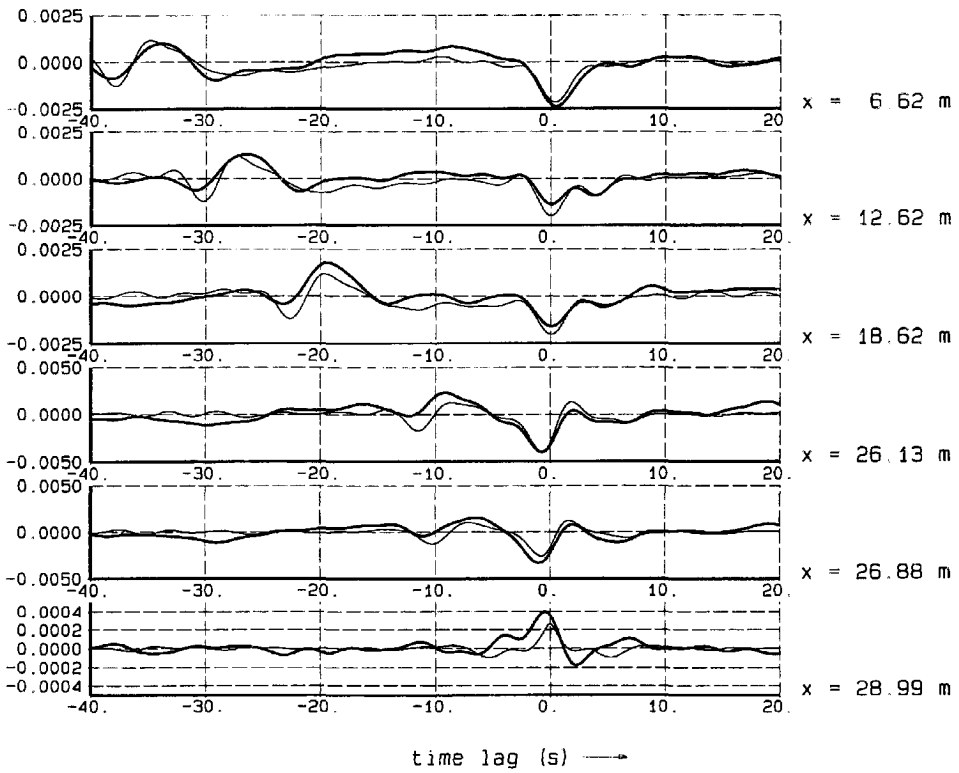

Figure 5.20 *Covariance function (mJ/m^2) of E and total long wave at six measurement locations, run 4j63zob; measurements (thick lines) and prediction by SURFBEAT (thin lines)*

5.2.5 Generalisation of results

In order to establish whether the covariance diagrams found are strongly dependent on the particular spectral shape in the measurements, or even on a particular realisation of a given spectrum, some test computations were carried out. As a reference, we take the computed covariance diagram at x=6.62 m. This is shown in the top graph of Figure 5.21. In the graph below this, we show the result for the case where no spurious

free waves are excited at the paddle, in other words for 'ideal' boundary conditions. There is a clear influence on the covariance at zero time lag, and also some influence on the part dominated by the reflected waves.

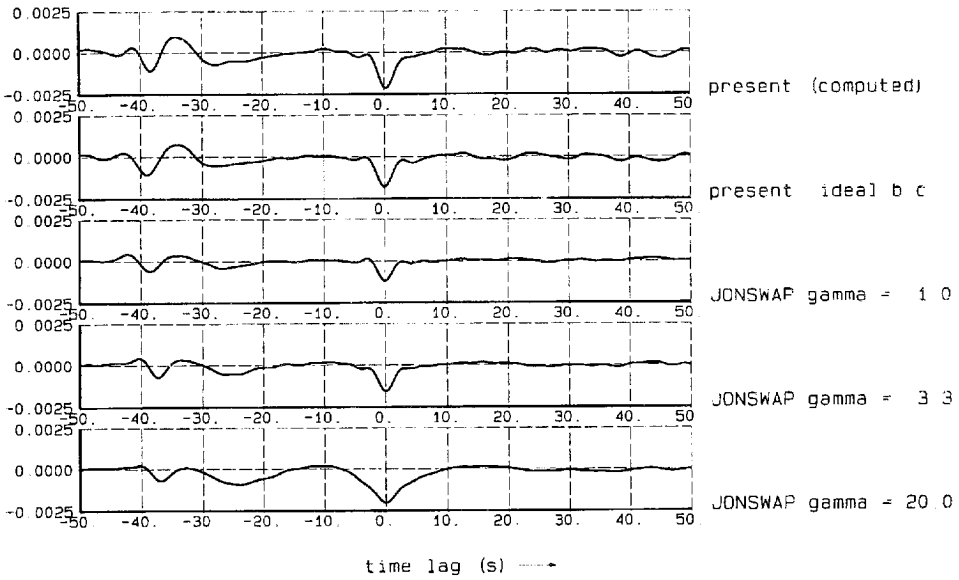

Figure 5.21 *Covariance diagrams of short wave energy and long wave elevation, based on experiment hindcast; hindcast for ideal boundary conditions; and based on realisations of idealised JONSWAP spectra with gamma = 1.0, 3.3 and 20, respectively.*

In the bottom three graphs computed covariance diagrams at the same location are shown, based on random-phase realisations of a JONSWAP spectrum with spectral peakedness parameter γ = 1.0, 3.3, 20.0 respectively (see Figures 5.22 a and b for a comparison of the measured spectrum and the numerically generated spectra for γ = 1.0 and 3.3). Clearly, the overall shape and magnitude of the covariance function is reproduced quite well, especially for γ = 1.0. The width of the negative 'hump' at zero time lag is related to the group length, which increases for increasing γ. The representative frequencies for these three γ-values are 0.68, 0.65 and 0.63 (close to f_p), respectively, which explains why the magnitude of the minimum at zero time lag increases for increasing γ. We may conclude that the shape and magnitude of the covariance diagrams are not extremely sensitive to the spectral shape; the effect of the profile shape has to be a point of further study.

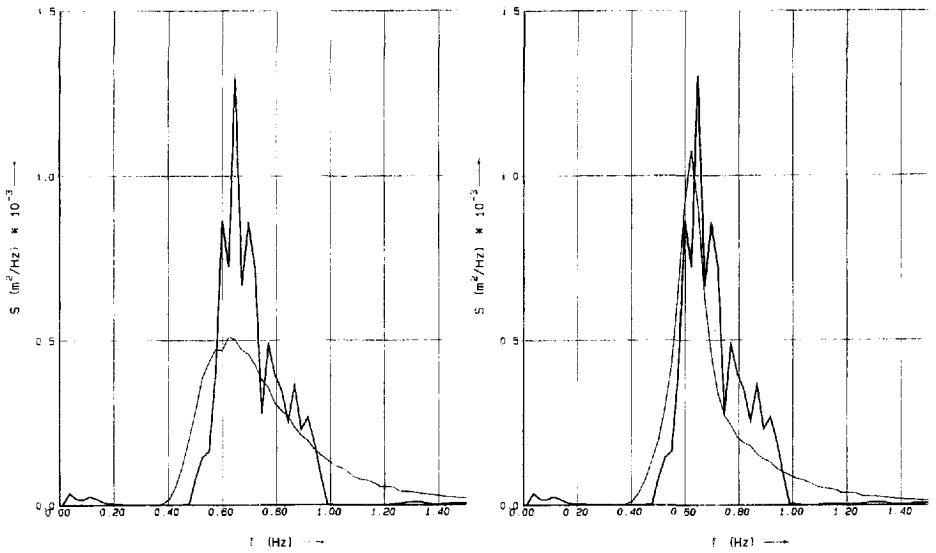

Figure 5.22 *Variance density spectrum at x = 6.62 m, averaged over 20 frequency bins; measured (thick line) and generated by random phase method (thin line); JONSWAP gamma = 1.0 (left) and gamma = 3.3 (right)*

5.2.6 Conclusions

An accurate method to generate correct boundary conditions for the SURFBEAT model, based on water elevation time series in a single point, has been developed and tested. Also, a single representative frequency can be derived for use in models like SURFBEAT that use the narrow-band approximation. This frequency is close to the peak frequency for idealised spectra like the JONSWAP spectrum, but can differ considerably for spectra with a different shape, as is the case in the set of measurements discussed in this Chapter.

When applied with accurate boundary conditions, the SURFBEAT model reproduces time series of short wave energy and total long wave elevation qualitatively. The main factor reducing the accuracy of these time series is the slow variation of the group velocity, which is neglected in the narrow-band approach.

The covariance diagrams of short wave energy and long wave elevation are reproduced accurately by the model, both outside and inside the surf zone. The velocity moments due to long wave - short wave interaction are predicted with the same accuracy.

The resulting covariance diagrams are not extremely sensitive to the spectral shape or to individual realisations of a spectrum. This means that for instance velocity moments can be predicted given simple parameters such as a significant wave height, a peak frequency and spectral shape parameters.

6. EFFECT OF SURF BEAT ON MORPHOLOGY

6.1 Introduction

The mechanism of cross-shore transport under a combination of net flow, long wave flow and the orbital velocity related to the short wave motion is extremely complex, and at this moment no universal formulation of sufficient accuracy is available. Still, reasonable results appear to be obtained by a simple concept first applied in this context by Bowen (1980), which is based on a model by Bagnold (1966). In this formulation, it is assumed that the total sediment transport responds instantaneously to fluctuations in the velocity above the bed boundary layer. The rate of sediment transport is assumed to be proportional to the dissipation of energy near the bed; this rate can then be expressed as a linear combination of terms containing powers of the instantaneous velocity. The time-averaged transport rate can then be expressed as (see Bailard, 1981):

$$<i(t)> = <i_B(t)> + <i_S(t)> = \rho c_f \frac{\epsilon_B}{\tan\phi}\left(<|u(t)|^2 u(t)> - \frac{\tan\beta}{\tan\phi}<|u(t)|^3>\right) \qquad (6.1)$$

$$+\rho c_f \frac{\epsilon_S}{w}\left(<|u(t)|^3 u(t)> - \frac{\epsilon_S}{w}\tan\beta <|u(t)|^5>\right)$$

where i is the total cross-shore immersed weight sediment transport rate, c_f is the drag coefficient for the bed, $u(t)$ is the instantaneous near-bed velocity, ϕ is the internal angle of friction of the sediment, $\tan\beta$ is the bottom slope, w is the sediment fall velocity, and ϵ_B and ϵ_S are bed load and suspended load "efficiency factors". The $< >$ indicate time-averaging over the short wave and wave group scale. The terms with $\tan\beta$, containing even velocity moments, are directed downslope. Their effect is generally small. In the following, we shall focus on the terms containing the odd velocity moments $<|u(t)|^2 u(t)>$ and $<|u(t)|^3 u(t)>$, which are usually an order of magnitude larger.

Roelvink and Stive (1989), whom we shall further refer to as "R+S", analysed the role of several mechanisms in determining the magnitude and direction of these terms based on three experiments in a wave flume with a sandy beach, and concluded that the most important contributions were given by:

$$<|u|^2 u> = 3<|u_{hi}|^2 \bar{u}> + <|u_{hi}|^2 u_{hi}> + 3<|u_{hi}|^2 u_{lo}> + \ldots \qquad (6.2)$$

$$<|u|^3 u> = 4<|u_{hi}|^3 \bar{u}> + <|u_{hi}|^3 u_{hi}> + 4<|u_{hi}|^3 u_{lo}> + \ldots \qquad (6.3)$$

where the velocity u is assumed to consist of a wave group averaged component $\bar{u}$, a short wave averaged oscillatory component u_{lo} and a short wave component u_{hi}; generally $\bar{u} \ll u_{hi}$ and $u_{lo} \ll u_{hi}$.

The terms in equations (6.3) and (6.4) were shown to be of the same order of magnitude. The first terms in equations (6.2) and (6.3) are related to the return flow under breaking waves, but in principle also cover any net drift velocity effect associated with standing long waves. Since the latter effect is a fourth order effect if it is related to long waves generated by wave groups, as compared to the return flow which is a second order effect, the net drift due to standing long waves can be expected to be negligible compared to the return flow. R+S found reasonable agreement between measurements of the net velocity and a model which only incorporates return flow effects.

The term associated with the asymmetry of the short waves was found by R+S to be accurately predicted by a non-linear, monochromatic wave theory, based on the stream function method (Rienecker and Fenton, 1981).

The interaction term between long wave velocity and the slowly varying short wave velocity variance was shown to be of similar magnitude as the short wave asymmetry term. Since a predictive model of this term was lacking, R+S chose a simple, mainly empirical approach which clarified the behaviour of the term in the experiments they described, and which allowed a reasonably accurate description of the total velocity moments needed in morphological simulations of these tests.

The approach adopted by R+S consisted of schematising the random wave field to a representative bichromatic wave train with its associated long wave. The amplitude of the long wave was estimated using Sand's (1981) solution for bound long waves. This produced reasonable, if not very accurate results, even inside the surf zone. For bound long waves, the modulation of the long wave velocity and the modulation of the short wave velocity variance would be 180 degrees out of phase, so would have a correlation coefficient of -1. From the tests however, the correlation coefficient was shown to vary from negative values outside the surf zone to positive values near the shore; a simple relationship was fitted to these values and was used to reproduce the long wave - short wave interaction term.

The fact that this simple empirical model of the long wave - short wave interaction term is not generally applicable has been an important motivation for the present study. A logical first step in assessing the effect of the long waves on cross-shore profiles is therefore to check to which extent we can now predict the same measurements with the present model. This is discussed in Section 6.2.

In the rest of this Chapter we address the question: "What is the effect of surf beat on cross-shore profiles?" in a more general sense.

Two approaches to this question are possible. In the first approach, adopted by R+S, the (in their case very simple) model of the long wave - short wave interaction term is incorporated in a cross-shore morphological model. In such a model, the evolution of the profile is computed by solving the conservation equation for bottom material:

$$\frac{\partial z_b}{\partial t} + \frac{\partial S}{\partial x} = 0 \tag{6.4}$$

where S is the bulk volume transport of sediment, averaged over a time period that is long compared to the short wave and wave group time scales, but short compared to the morphological time scale. The effect of the bottom changes on the transport is taken into account by computing the transport distribution over the modified profile after each morphological time step.

By comparing results of computations in R+S where all mechanisms were included with computations where the long wave - short wave interaction term was left out, we see (Figure 6.1) that the long waves have an important effect, and that for the case presented the effect was to reduce the bar amplitude and to move the bar in seaward direction. This conclusion does not necessarily hold in general; a method to investigate in general the effect of surf beat on profiles could be to incorporate our present model in a dynamic morphological model, and to compute the behaviour for a range of initial profiles and boundary conditions. Since this would be prohibitively expensive, a different approach is chosen, which is outlined below.

An important factor governing the morphodynamic behaviour of the profile is, to what extent the sediment transport distribution over the profile is sensitive to profile changes. We will clarify this in two schematic examples.

As a first extreme example, we assume that the transport pattern due to the interaction of long waves and short waves is not sensitive to bottom changes, and that the typical length scales and position of the pattern are determined by external factors; an example may be the transport pattern associated with a standing wave pattern of constant period. For a sediment transport pattern of the form:

$$S = \hat{S}\cos(kx) \tag{6.5}$$

where $\hat{S}$ is the amplitude of the pattern and k its typical wave number, the bottom evolution directly follows from the continuity equation (6.4) and is given by:

$$z_b(t) = z_{b,t=0} + \hat{S}k\sin(kx)\,t \tag{6.6}$$

The solution is a bar system at a fixed location, with an amplitude that grows linearly in time.

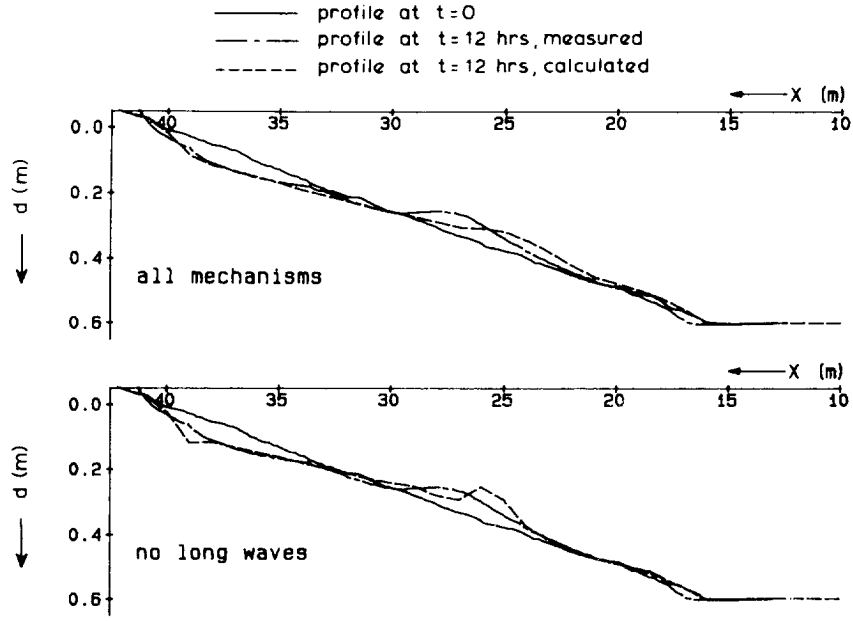

Figure 6.1 Profile deformation and bar formation on an initially 1 in 40 slope (test 1); observations and predictions with and without the effect of long waves. From: Roelvink and Stive (1989)

A very different behaviour is found if we assume that the transport pattern is mostly dependent on the profile shape, and that modulations in the profile shape immediately lead to modulations of the transport pattern. This is shown in the second example, where a modulation in the profile of the form:

$$z_b = z_{b,t=0} + \hat{z}_b\, e^{pt}\cos(kx - \omega t) \tag{6.7}$$

leads to a transport modulation of the form:

$$S = A\,\hat{z}_b\, e^{pt}\cos(kx - \omega t - \phi) \tag{6.8}$$

where A is the (positive) ratio of the sediment transport amplitude over the amplitude of the bottom modulation, and ϕ is the phase shift between the bottom modulation and the transport modulation. Solutions of equation (6.4) are found in this case for:

$$p = -Ak\sin(\phi) \text{ and } \omega/k = A\cos(\phi) \tag{6.9}$$

The modulation of the bottom profile propagates in positive x-direction for $-\frac{1}{2}\pi < \phi < \frac{1}{2}\pi$, and in negative direction for $\frac{1}{2}\pi < \phi < \frac{3}{2}\pi$; the bar amplitude grows exponentially for $\pi < \phi < 2\pi$ and decays exponentially for $0 < \phi < \pi$.

Both the propagation speed and the growth rate depend on the sensitivity of the transport to bottom changes, represented in this example by the coefficient A; the location of the transport maxima relative to the bar crests determines whether bars will grow or decay.

It is clear from these two examples that the dynamic morphological behaviour of a coastal profile is determined partly by the initial transport pattern on the undisturbed profile, and partly by the sensitivity of the transport pattern to profile changes. Both these aspects can be studied without actually computing the time-dependent dynamic behaviour in a complete morphological model.

The sensitivity of the transport pattern due to the interaction between short and long waves to changes in the bar topography will be established by schematizing the profile shape to a realistic, parametric form of which the parameters can be varied in a systematic way. By means of numerical simulations the sensitivity of the long wave - short wave interaction term to the spacing, position and amplitude of longshore bars is studied, in relation to the basic pattern on an unbarred "equilibrium" profile.

This is carried out for two typical wave conditions. Separately, the sensitivity of the result for a typical barred profile to incident wave conditions is investigated, in order to verify that the conclusions are generally valid, and to identify the most important parameters of the incident wave field.

The profiles and wave conditions chosen are based on typical conditions on the Dutch coast; however, the analysis could be easily extended to other coasts. In order to be able to cover a wide range of existing profile shapes in a systematic way, we first schematize the profile to a shape that can be described analytically and where the main features are captured by a limited number of parameters; this is described in Section 6.3. A similar approach is taken for the input wave conditions, where the wave climate is assumed to be represented by a number of stationary wave systems. These are characterised by a spectrum that can be described by a limited number of parameters. This is discussed in Section 6.4. In Section 6.5 we describe the input parameters for the simulation runs. Results are presented in Section 6.6, and the conclusions in Section 6.7.

6.2 Oscillatory velocity moments

6.2.1 Test case

In this section we compare results from the SURFBEAT model with the data presented in R+S, where the general set-up of the tests can be found. The main points are highlighted here. The tests were carried out in the "Schelde flume" at DELFT HYDRAULICS, which has a length of 55 m, a width of 1 m and a height of 1 m. The beach consisted of sand of 100 μm median grain diameter. The characteristics of the three cases are outlined in Table 6.1 below.

Test	Initial profile	$H_{rms,\,incident}$ (cm)	f_p (Hz)	Duration (hrs)
1	plane	12.3	0.50	12
2a	single bar	8.1	0.50	12
2b	single bar	13.3	0.50	12

Table 6.1 *Laboratory test cases*

The random wave fields generated were of the JONSWAP type with a peak enhancement factor of 3.3. No second order wave generation was available at the time, which is important when considering the boundary conditions for the SURFBEAT model. The method of active wave absorption (Kostense, 1984) was applied to remove free waves reflected from the beach. The water depth at the toe of the profile was 0.60 m.

The three tests lasted for 12 hours, during which period the beach changed considerably. The velocity was measured at 5 cm above the bottom at various locations, one at a time; sample duration was 30 minutes in most cases. Surface elevations were measured in two points at a time.

6.2.2 Simulation procedure

Since the measurements were not taken simultaneously, but in different points at different times during the tests, the simulations were performed both on the initial profile for each test and on the final profile. Since the profile adjustments are usually the most rapid at the start of a test, computations on the final profile can be expected to yield slightly better comparisons.

For each test, a time series of the short wave surface elevation was generated using a random-phase approach. From this series, a time series of the short wave energy was then generated and the representative frequency determined using the method outlined in Chapter 5. This frequency was approximately 0.53 Hz. The incoming bound waves were set to zero in the computations, in accordance with the first-order wave generation in the experiments. The weakly reflective boundary condition was maintained in the computations, since this has the same effect as active wave absorption.

The model was run for 12 minutes, of which the last 10 minutes were used for analysis. The time step was 0.1 s, and the number of grid points 100. After each run, a number of time-averaged parameters were computed for comparison with the measurements:

the rms wave height:

$$H_{rms} = \sqrt{\frac{8<E>}{\rho g}} \tag{6.10}$$

the correlation coefficient between long wave elevation z_s and short wave energy:

$$C_r = \frac{Cov(E, z_s)}{\sigma_E \sigma_{z_s}} \tag{6.11}$$

the standard deviation of the long wave velocity:

$$\sigma_{u_{lo}} = \sigma_U \tag{6.12}$$

the slowly-varying short wave velocity variance:

$$Var(u_{hi}) = \left(\frac{2\pi f_{rep}}{\sinh(k_{rep} h)} \right)^2 \frac{E}{\rho g} \tag{6.13}$$

the correlation coefficient between long wave velocity and short wave velocity variance:

$$C_{r,u} = \frac{Cov(Var(u_{hi}), U)}{\sigma_{Var(u_{hi})} \sigma_U} \tag{6.14}$$

the time-averaged short wave velocity variance:

$$<u_{hi}^2> = <Var(u_{hi})> \tag{6.15}$$

the long wave contribution to the third-order odd velocity moment:

$$3 \langle |u_{hi}|^2 u_{lo} \rangle = 3\, Cov\left(Var(u_{hi}), U \right) \tag{6.16}$$

and the long wave contribution to the fourth-order odd velocity moment:

$$4 \langle |u_{hi}|^3 u_{lo} \rangle = 4\, Cov\left(Var^{3/2}(u_{hi}), U \right) \tag{6.17}$$

All coefficients were set at standard values: $\alpha = 1.0$, $\gamma = 0.55$, $n = 10$ and $f_w = 0.02$; no in situ calibration was performed.

6.2.3 Results

In Figures 6.2 a through c, the computed wave height H_{rms} and correlation coefficient C_r over the initial and final profile are compared with the measurements. The wave height decay is predicted accurately for all tests; for the correlation coefficient, the trends are predicted correctly, and except for the part outside the surf zone the quantitative agreement is quite satisfactory. The relatively low absolute magnitude of the correlation outside the surf zone must be ascribed mainly to the first order wave generation, which leads to spurious free waves that are in anti-phase with the bound waves at the wave maker. This was accounted for in our model computations. Differences between model and measurements in this region may perhaps be explained by wave adjustments in the measurements, especially for relatively steep waves.

In Figures 6.3 a through c, the standard deviations of the long wave velocity and the mean short wave velocity variance are shown as computed and measured. The agreement is good for both parameters. Especially in tests 1 and 2b, there is a significant effect of the profile deformation on both parameters. In test 2b, the peaks in the long wave velocity over the bar crests are somewhat underpredicted.

The computed and measured long wave contributions to the velocity moments are shown in Figures 6.4 a through c. For comparison the measured short wave asymmetry contributions are also drawn in these Figures, together with the computed results from R+S; these were obtained for the average profile only. We see that the trends and order of magnitude in the long wave contributions to the moments are predicted correctly; quantitatively, discrepancies up to 50 % of the maximum values occur for tests 1 and 2b, whereas very good agreement is found for test 2a. The main cause for the discrepancies is probably the description of the propagation of the wave groups, where effects of variations of the group velocity and the effect of the long wave velocity on the short wave propagation are not accounted for; especially the latter can be expected to be more important for the cases with higher waves.

It is important to note that the correlation coefficient based on surface elevations, C_r, is not the same as that based on velocities, $C_{r,u}$. In Figure 6.5 the two parameters are compared for the three tests.

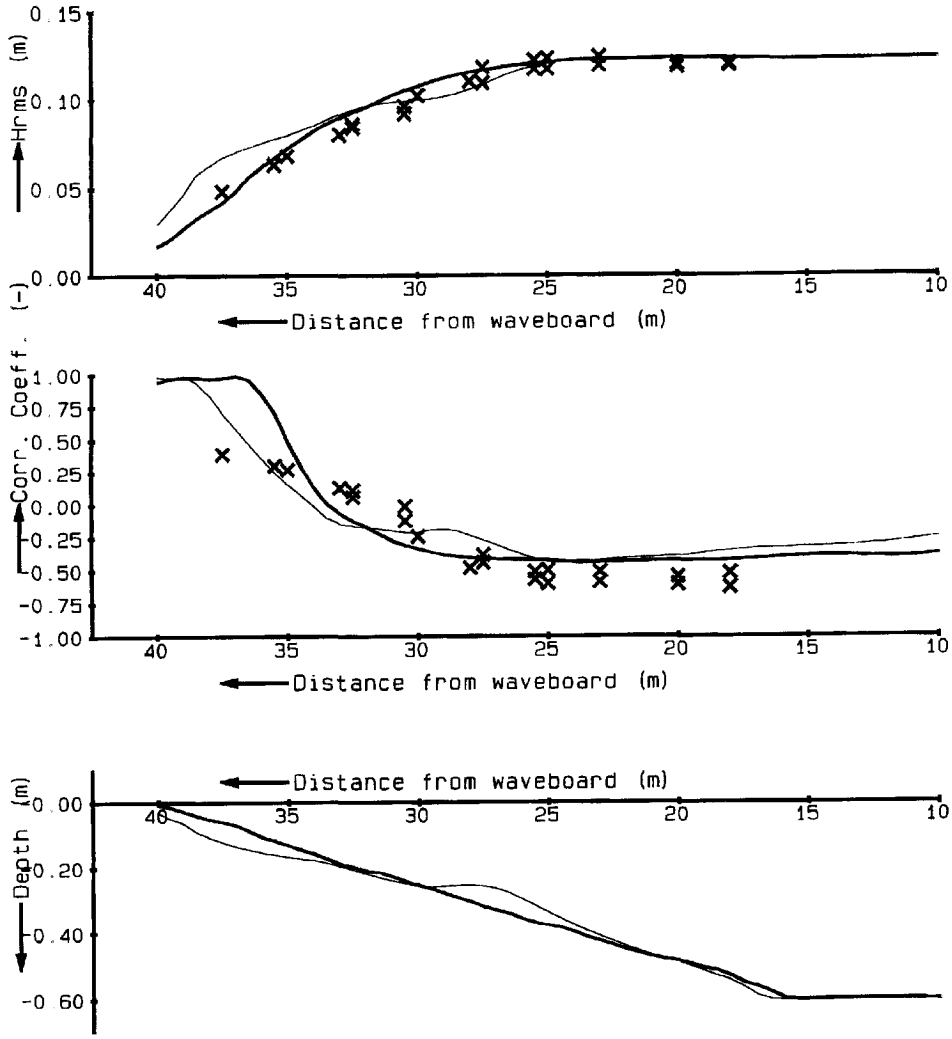

Figure 6.2a *Initial (thick line) and final (thin line) bottom profile, computed correlation coefficient C_r and H_{rms} wave height over initial profile (thick line) and final profile (thin line) and measured values (crosses); Test 1*

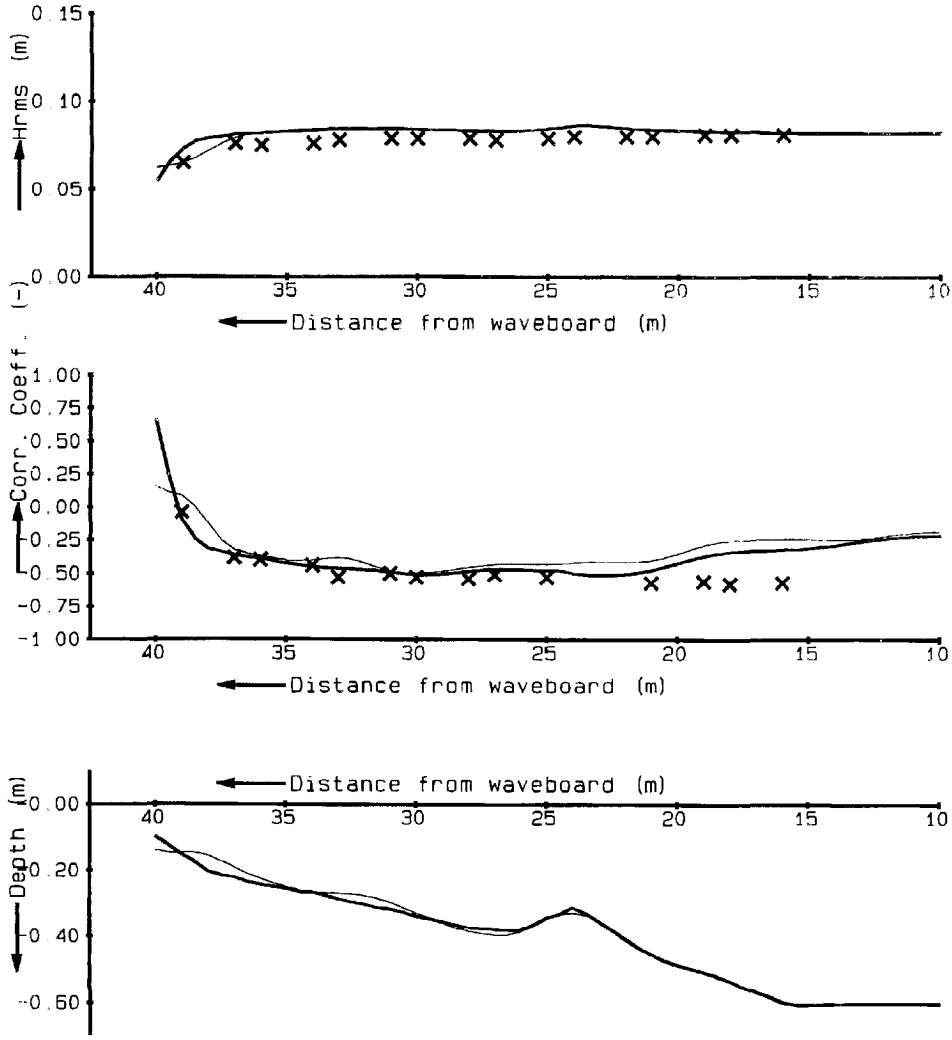

Figure 6.2b *Initial (thick line) and final (thin line) bottom profile, computed correlation coefficient C_r and H_{rms} wave height over initial profile (thick line) and final profile (thin line) and measured values (crosses); Test 2a*

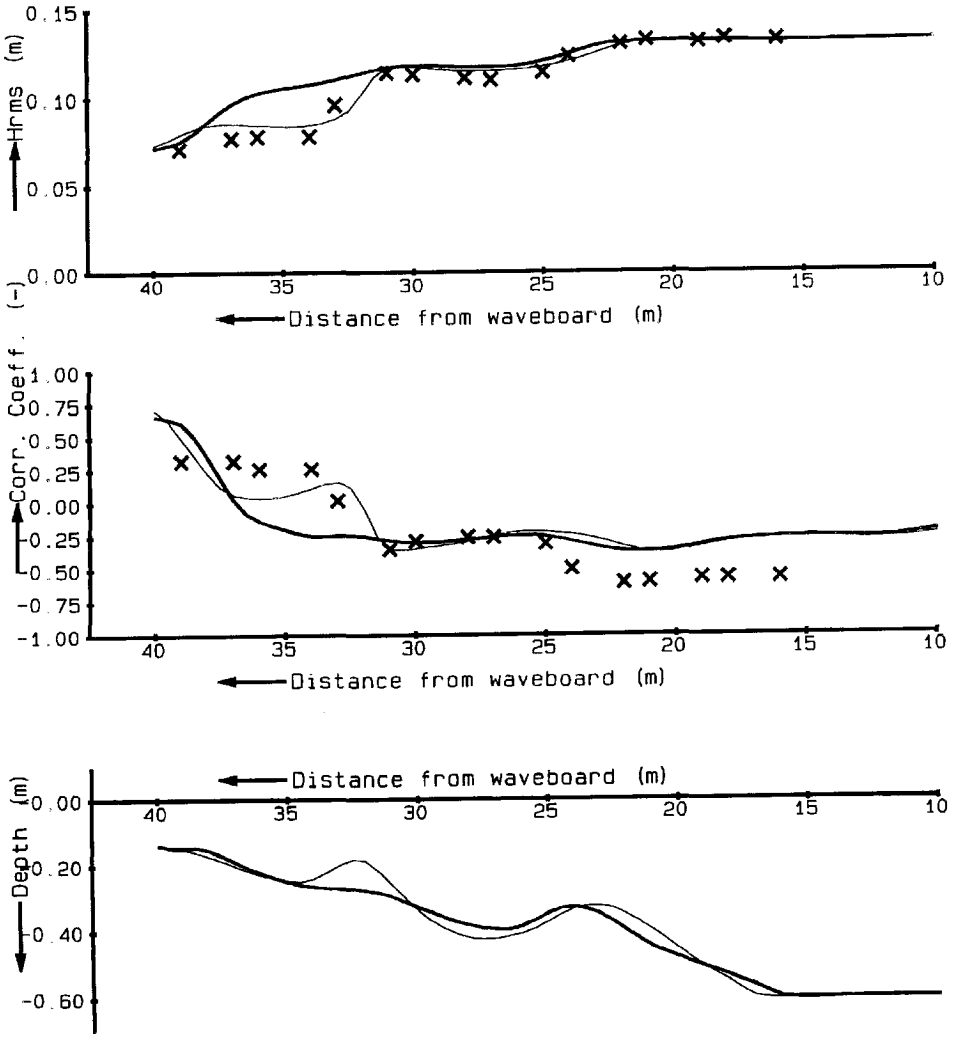

Figure 6.2c *Initial (thick line) and final (thin line) bottom profile, computed correlation coefficient C_r and H_{rms} wave height over initial profile (thick line) and final profile (thin line) and measured values (crosses); Test 2b*

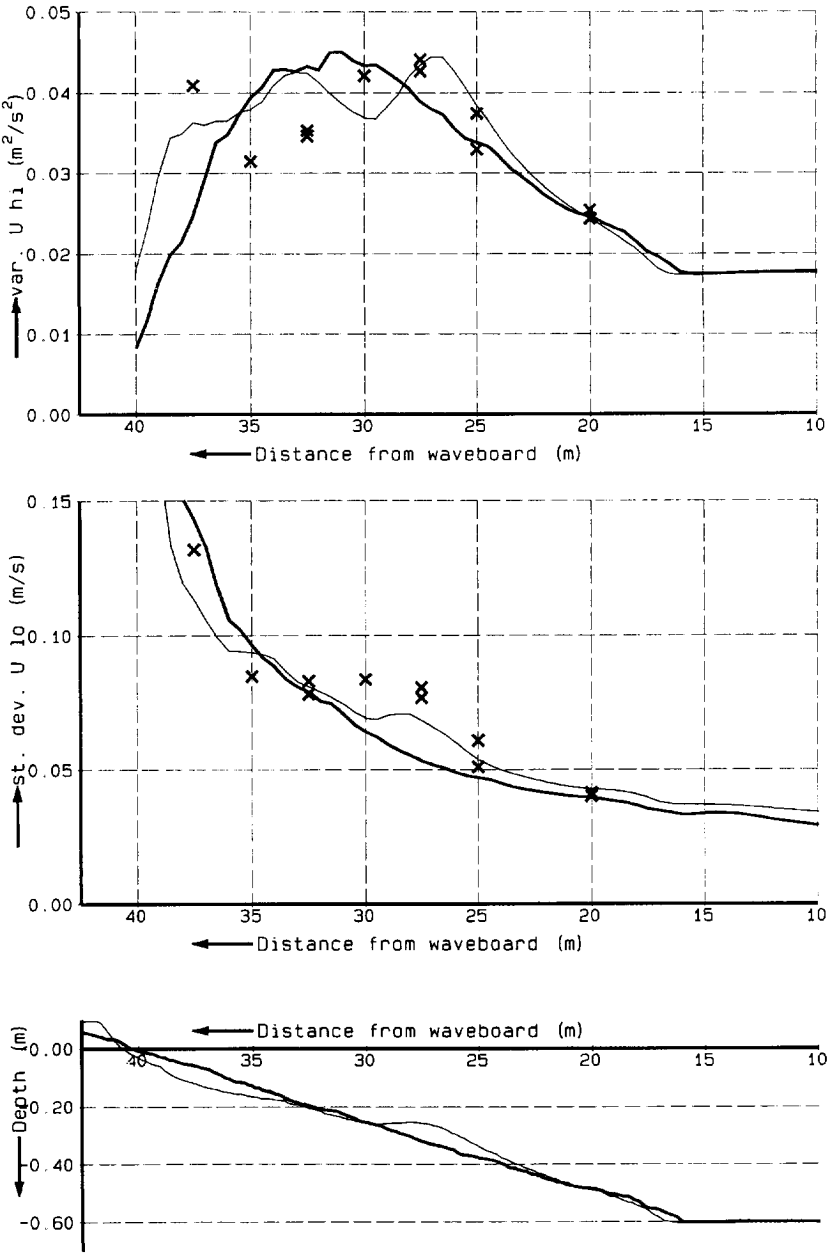

Figure 6.3a *Initial (thick line) and final (thin line) bottom profile, computed standard deviation of long wave velocity and mean variance of short wave velocity over initial profile (thick line) and final profile (thin line) and measured values (crosses); Test 1*

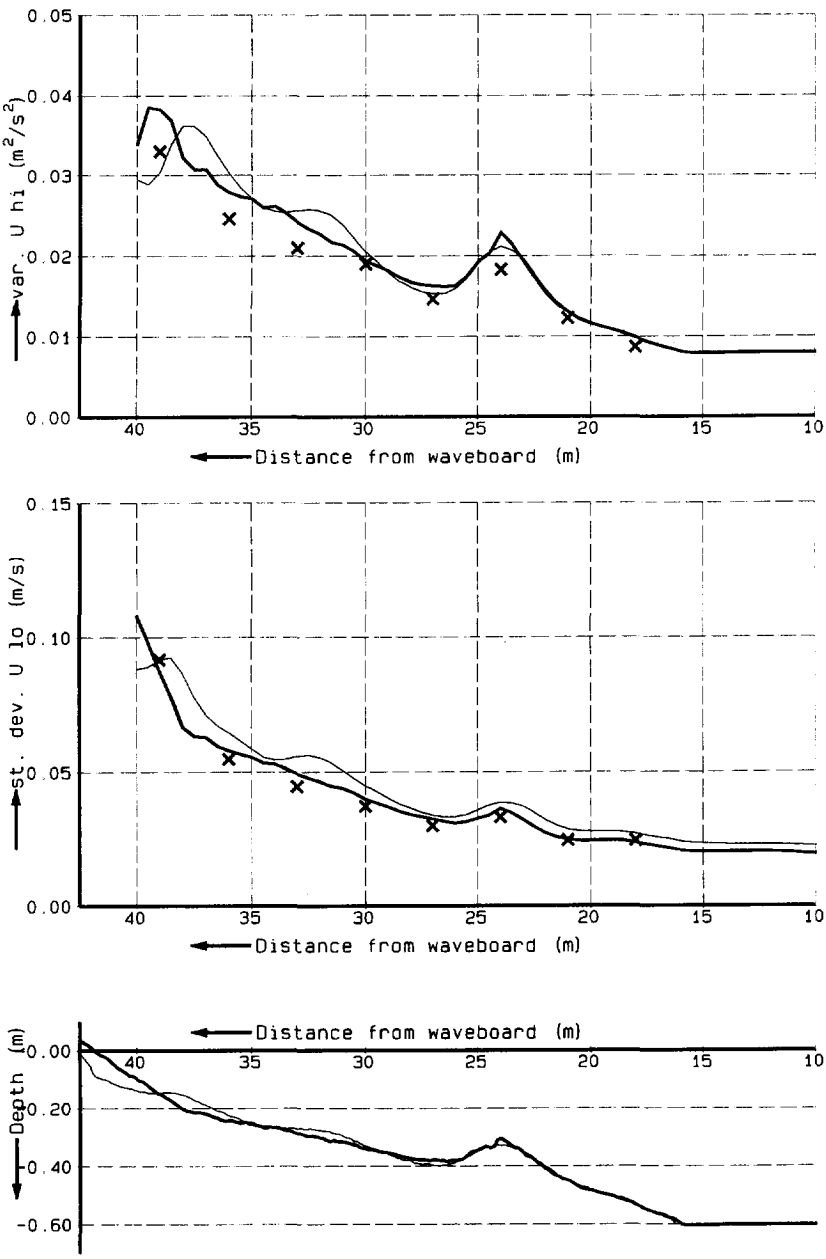

Figure 6.3b *Initial (thick line) and final (thin line) bottom profile, computed standard deviation of long wave velocity and mean variance of short wave velocity over initial profile (thick line) and final profile (thin line) and measured values (crosses); Test 2a*

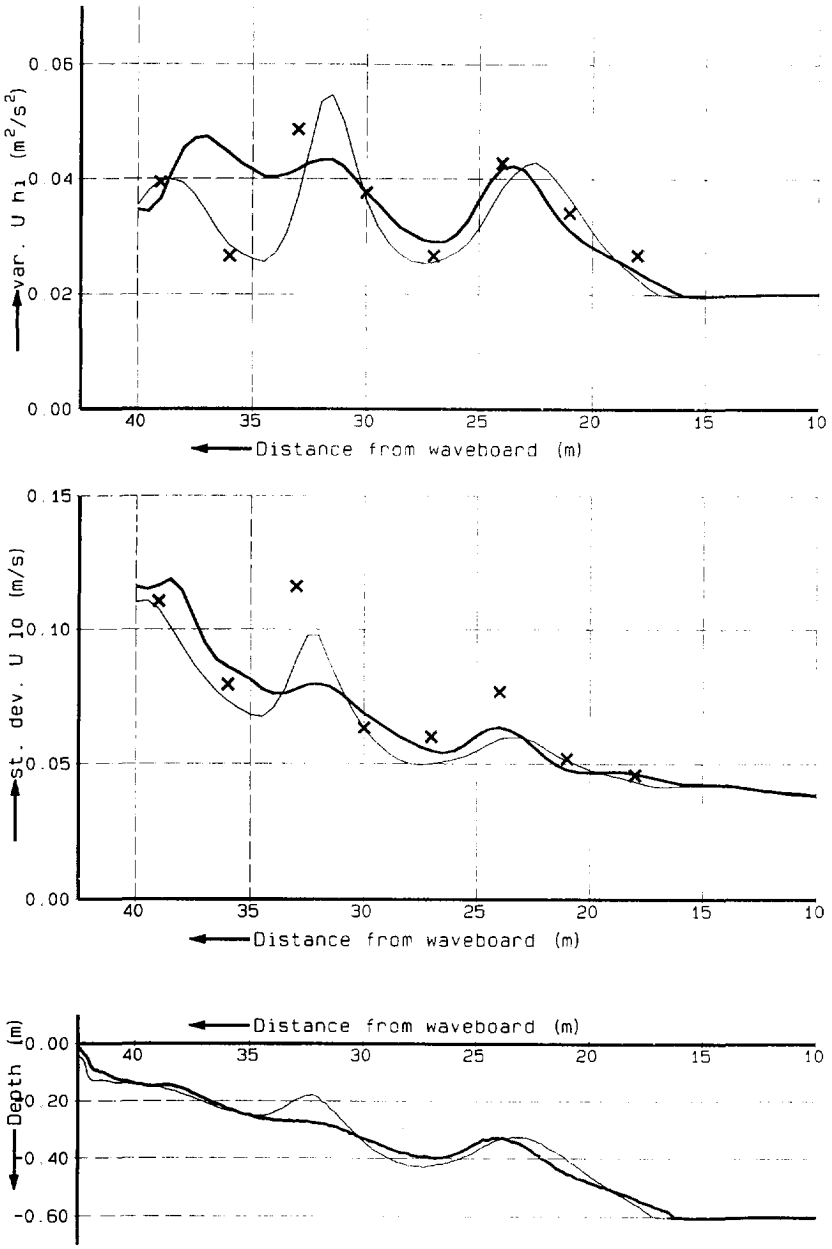

Figure 6.3c *Initial (thick line) and final (thin line) bottom profile, computed standard deviation of long wave velocity and mean variance of short wave velocity over initial profile (thick line) and final profile (thin line) and measured values (crosses); Test 2b*

In deep water, the absolute magnitude of the correlation based on velocities is higher than that based on surface elevations. This is due to the fact, that the reverse shoaling of the reflected free waves is proportional with $\sqrt{h}$ for the surface elevation, but with h for the velocity. As a result, the ratio of bound wave amplitude to reflected free wave amplitude is higher for the velocity, and thus the absolute magnitude of the correlation coefficient is also higher for the velocity.

In shallow water, the modulation of the short wave envelope of the surface elevation is due to modulation of the surface elevation because of the long waves; hence the positive correlation coefficient is found. Since the long waves are partially standing near the shore, the correlation coefficient based on velocities is much smaller than that based on surface elevations.

In the empirical approach used by R+S this difference was not accounted for.

6.2.4 Conclusions

The most important time-averaged properties of long waves, short waves and their interaction are predicted with reasonable accuracy by the SURFBEAT model with standard parameter settings. The quantitative agreement between predictions and measurements of the long wave contribution to the odd velocity moments is good for relatively low short waves, and still reasonable for higher incident waves. The order of magnitude of the long wave contribution to the velocity moments is similar to that of the short wave asymmetry in these tests. There are significant differences between the correlation coefficient based on surface elevations and that based on velocities.

In terms of morphological effect, the long wave - short wave interaction term has an order of magnitude similar to the effect of short wave asymmetry and generally the opposite direction. The beach-building effect of the short waves is therefore greatly reduced. In the tests considered, the effect of the long wave - short wave interaction term appears to reduce the growth of sand bars, and to move them in seaward direction.

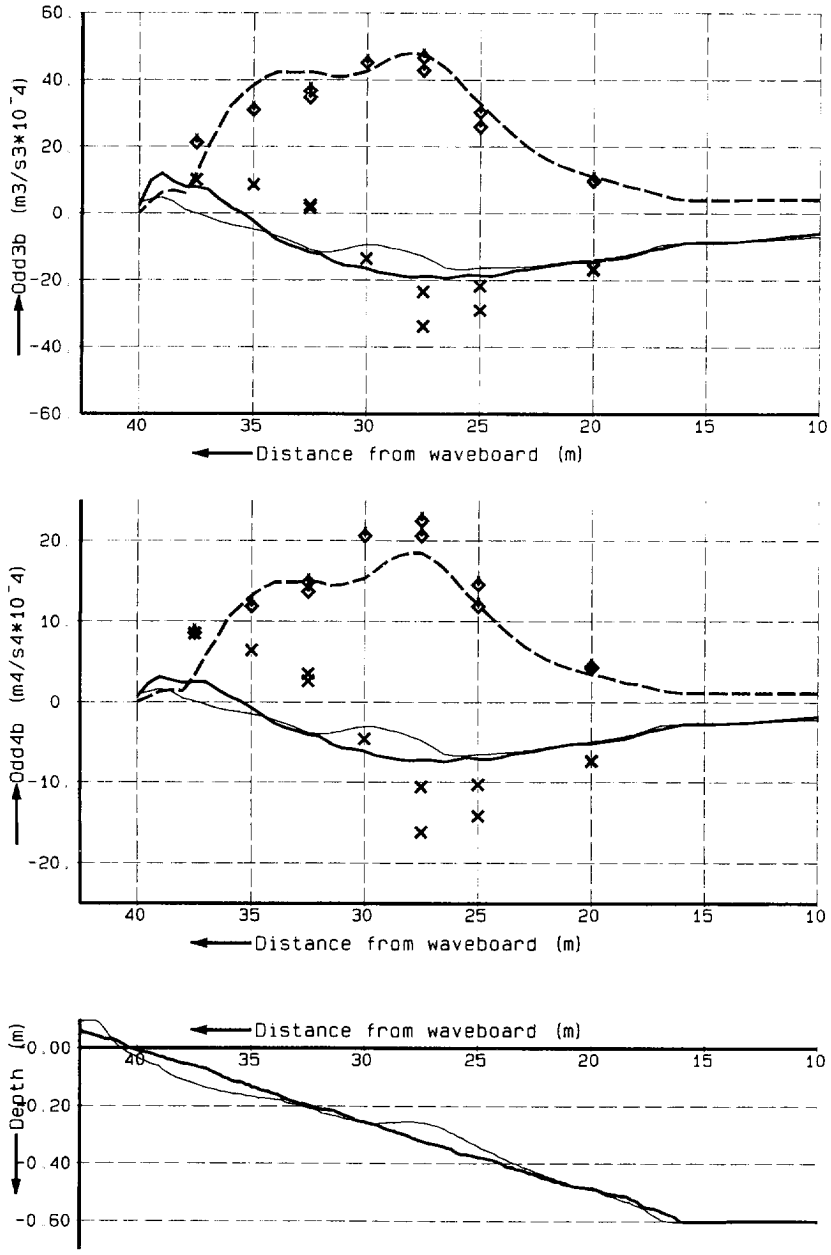

Figure 6.4a *Initial (thick line) and final (thin line) bottom profile, computed contributions to third order and fourth order odd velocity moments over initial profile (thick line) and final profile (thin line) and measured values (long wave contribution: crosses; short wave contribution: diamonds); Test 1*

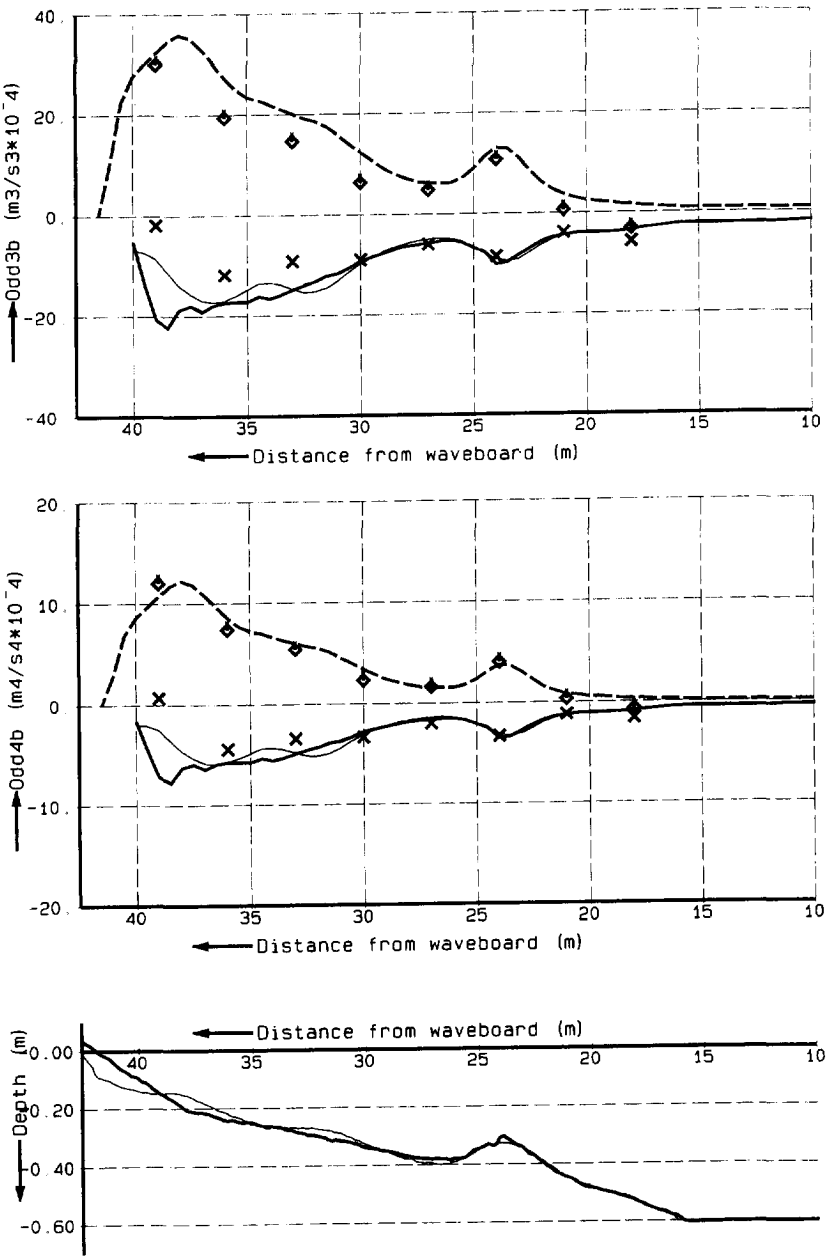

Figure 6.4b *Initial (thick line) and final (thin line) bottom profile, computed contributions to third order and fourth order odd velocity moments over initial profile (thick line) and final profile (thin line) and measured values (long wave contribution: crosses; short wave contribution: diamonds); Test 2a*

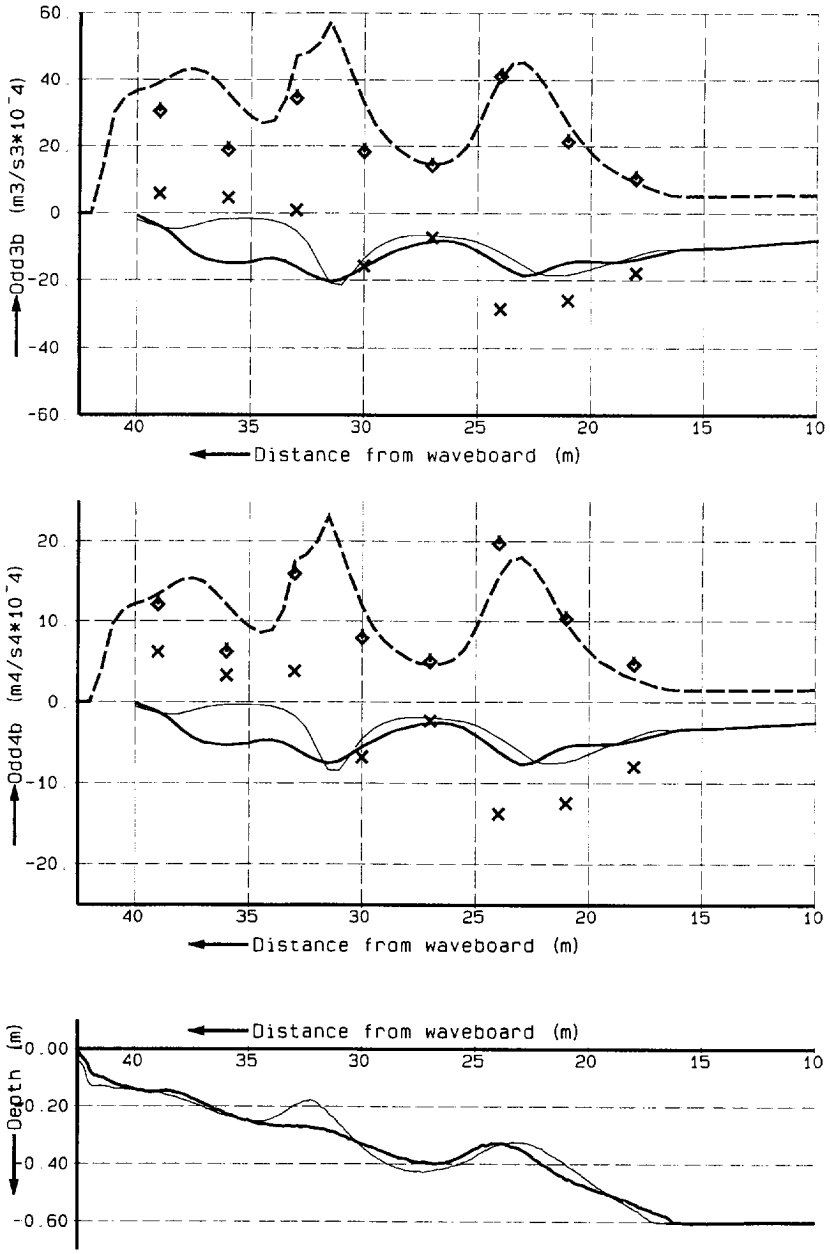

Figure 6.4c *Initial (thick line) and final (thin line) bottom profile, computed contributions to third order and fourth order odd velocity moments over initial profile (thick line) and final profile (thin line) and measured values (long wave contribution: crosses; short wave contribution: diamonds); Test 2b*

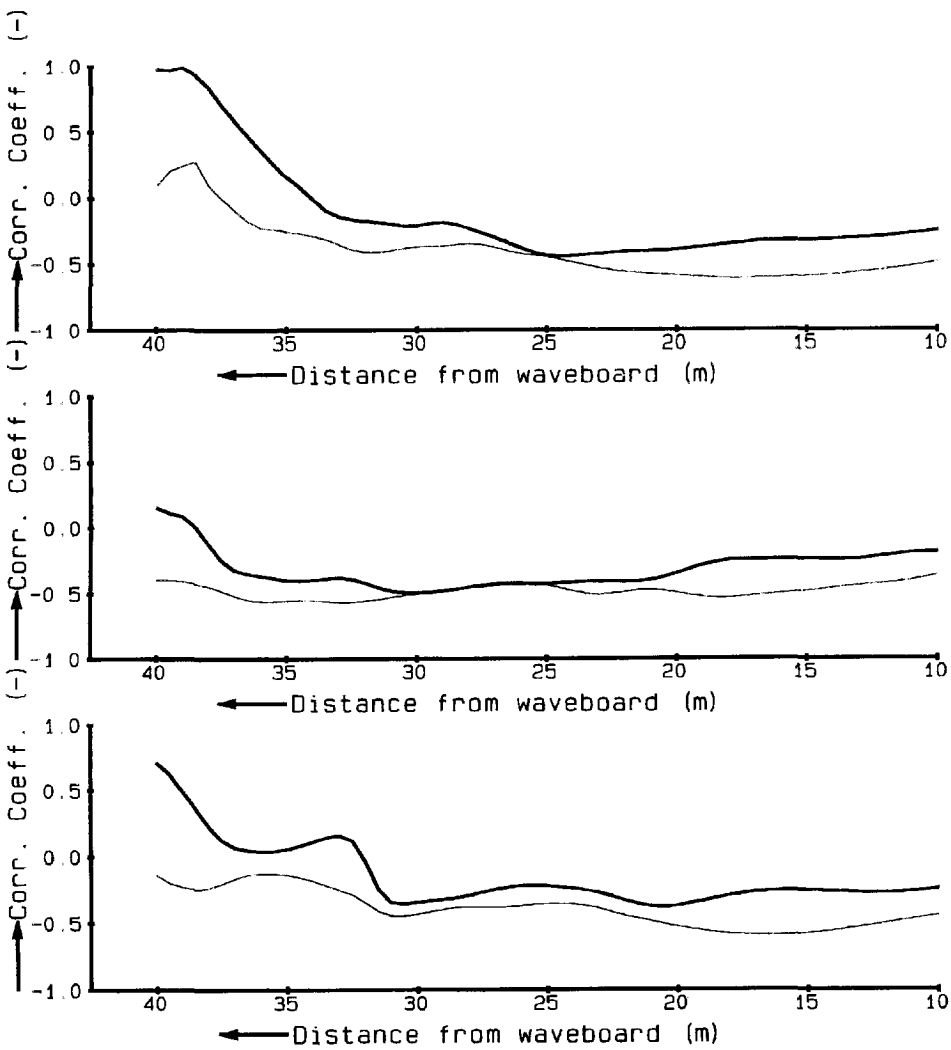

Figure 6.5 *Comparison between correlation coefficient between long wave surface elevation and short wave envelope of surface elevation (thick lines) and correlation coefficient between long wave velocity and short wave velocity variance (thin lines); Test 1 (upper), Test 2a (middle) and Test 2b (lower); computed over final profiles*

6.3 Beach profile for simulation runs

6.3.1 Mean profile

For most sandy beaches, a reasonable description of the average beach profile is given by a simple power curve such as:

$$z_{b,mean} - z_r = -A\left(x - x_r\right)^b \tag{6.18}$$

where $z_{b,mean}$ is the height of the average profile above mean water level, z_r is a reference height, x is the horizontal coordinate, positive in seaward direction, x_r is the location where $z_{b,mean} = z_r$, b is an exponent and A a dimensional constant (e.g. Bruun, 1954; Dean, 1977). Dean (1977) finds theoretical support for a 2/3 power curve, arguing that nature aims at a uniform energy dissipation per unit volume of water. Although the basis for this assumption is not very solid, especially for varying wave conditions, a good fit is obtained for many US coastal profiles using this curve.

For Dutch profiles, W.T. Bakker (priv. comm.) recommends the following values:

$z_r = 6m$
$b = 0.323$
$A = 1.4\,m^{1-b}$

This curve generally gives a reasonable description of the time-averaged profiles of the Holland coast. A very similar result for the underwater profile is obtained by taking $A = 0.08\,m^{1/3}$, $b = 2/3$ and requiring the same bottom slope at $x=0$.

6.3.2 Variations around mean profile

Bakker and De Vroeg (1988) have studied the systematic behaviour of sand bars on Dutch profiles and has found tendencies that are described qualitatively by the following form:

$$z_b = z_{b,mean} - A_b e^{-\left(\frac{x-x_b}{R_b}\right)^2} \cos\left(2\pi\frac{x-x_b}{L_b} - \phi_b\right) \tag{6.19}$$

where A_b is the maximum bar amplitude, x_b is the location of the maximum bar amplitude, R_b is a measure of the width of the barred part of the profile, L_b is the bar spacing and ϕ_b is the phase of the bar system.

This formulation is useful as a basis for systematic study of the influence of the bar topography on long waves, since it describes the main bar features with only a limited number of parameters.

6.4 Wave conditions

As was shown in Chapter 5, individual realisations of a wave system characte-rised by a given spectrum do not influence time-averaged parameters of the com-bined short wave and long wave motion. This means that the input wave condi-tions are sufficiently specified by the surface elevation spectrum. In order to systematically investigate the effect of the spectrum on parameters relevant for the morphology, we use a paramete-rised spectral shape, viz. the JONSWAP spectrum:

$$S(f) = \frac{\beta H_{rms}^2}{f_p}\left(\frac{f}{f_p}\right)^{-5}\exp\left(-\frac{5}{4}\left(\frac{f}{f_p}\right)^{-4}\right)\gamma_p^{\exp\left(-\frac{1}{2}\left(\frac{f-f_p}{\sigma f_p}\right)^2\right)} \tag{6.20}$$

where $\sigma = 0.07$ for $f<f_p$ and $\sigma = 0.09$ for $f\geq f_p$. The coefficient β is defined such that:

$$\int_0^\infty S(f)\,df = \frac{1}{8}H_{rms}^2 \tag{6.21}$$

This spectrum is defined by three parameters: the wave height H_{rms}, the peak frequency f_p or its inverse, the peak period T_p, and the spectral peak enhancement factor γ_p.

6.5 Model runs

6.5.1 Input parameters

The most important parameters in describing the bar topography are the maximum amplitude A_b,the bar spacing L_b and the relative phase ϕ_b of the bar. The width and location of the barred area do not vary much along the Dutch coast, and will be kept constant. The mean profile will be kept constant for all simulations.

The most important parameters describing the wave conditions are the root-mean-square wave height H_{rms}, the peak period f_p and the spectral peak enhancement factor γ_p.

These six input parameters can all attain a range of values. Obviously, it is impossible to compute the effects of every possible combination; moreover, it is doubtful if much insight would be gained from that. The approach we take is therefore to choose a "base case", meaning a fixed set of input values, and to systematically vary the input parameters one at a time. In this way we hope to isolate the effects of each individual input parameter. In order to check if the resulting trends depend much on the base case that is chosen, the process is repeated for a second base case.

Base cases

Two base cases were chosen, where the only difference is in the input wave height. We thus obtain results for relatively high energy and relatively low energy. The base case bar topography was chosen to be similar to profiles found at Egmond aan Zee on the Holland coast, which is a field study site in the Coastal Genesis Programme. The choice of the distance of the seaward boundary from the shore is a compromise between the wish to limit computational cost and the wish to start at a sufficient water depth. The depth at the chosen distance is approximately 8 m, which is generally seen as the limit of the active zone in a morphological sense. The profile parameters are listed in Table 6.2.

Parameter	Symbol	Value	Unit
Maximum bar amplitude	A_b	1.00	m
Bar spacing	L_b	200	m
Size of barred area	R_b	200	m
Location of maximum bar amplitude	x_b	300	m
Phase of bar at maximum amplitude	ϕ_b	180	deg.
Start distance from shoreline	x_L	1200	m
Step size	Δx	10	m

Table 6.2 *Input parameters for generation of bottom profile; base case. Program module: GENPRO*

The resulting bottom profile is drawn in Figure 6.6.

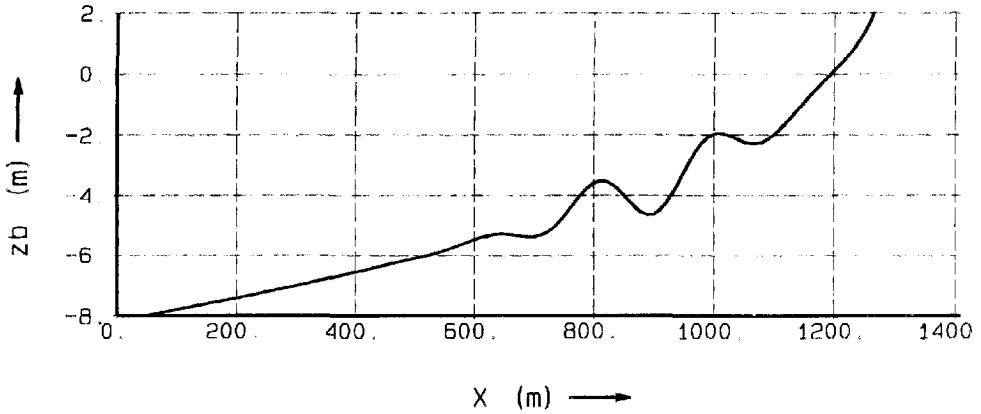

Figure 6.6 *Bottom profile; base case*

For given spectral parameters, a time series of the short wave surface elevation is generated by assigning random phases to the spectral components, and applying a Fast Fourier Transform to these components. Since the focus of this study is on time-averaged parameters rather than detailed analyses of long wave spectra, the duration of a run can be limited to approximately 20 minutes after the initial conditions have propagated out of the model area. The base case parameters for the generation of time series are given in Table 6.3.

Parameter	Symbol	Value	Unit
Length of generated time series	T_{max}	1500	s
Time step to generate time series	Δt	.5	s
Peak period	T_p	6.25	s
Peak enhancement factor	γ_p	3.3	-
Wave height	H_{rms}	0.5 / 1.0	m

Table 6.3 *Input parameters for random-phase generation of short wave elevation time series; base cases. Program module: GENSER*

The surface elevation time series that is generated can be treated as a measured time series. From this time series, a time series of the short wave energy is generated, and the representative frequency is determined using the procedures outlined in Chapter 5.

The separating frequency between long and short wave motions is set at half the peak frequency. Base case parameter values are listed in Table 6.4.

Parameter	Symbol	Value	Unit
Number of data points to be analysed	N_t	3000	-
Time step	Δt	.5	s
Separating frequency long/short waves	f_{split}	0.08	Hz
Lowest frequency allowed	f_{lo}	0.00	Hz
Nyqvist frequency	f_{Nyq}	2.00	Hz
Density of water	ρ	1025	kg/m^3
Acceleration of gravity	g	9.81	m/s^2
Water depth at seaward boundary	h_0	8.163	m

Table 6.4 *Input parameters for computation of short wave envelope and bound long waves at seaward boundary; base case. Program module: ENVELO*

The input parameters and coefficients for the SURFBEAT model are shown in Table 6.5. These are the same for all runs. Results are written after the first 200 s, when most of the effect of the initial conditions has propagated out of the model area. The number of grid points was determined by some trial computations; 120 grid points appeared to be sufficiently accurate. In this case, the physical grid size varies from approximately 13 m at the seaward end to approximately 5 m near the shore. With a time step of 1.0 s, Courant numbers are less than 0.7 throughout the model. All coefficients are set at standard values for random waves.

Parameter	Symbol	Value	Unit
Reference level for grid transformation	ϵ	1	m
Number of grid points	N_s	120	-
Time step	Δt	1.0	s
Number of time steps	N_t	1400	-
Start time step for writing output	N_{start}	200	-
Initial water level	$z_{s,0}$	0	m
Breaker dissipation coefficient	α	1.00	-
Coefficient probability of breaking	γ	0.55	-
Exponent breaking probability function	n	10	-
Acceleration of gravity	g	9.81	m/s^2
Density of water	ρ	1025	kg/m^3
Water depth at landward boundary	δ	0.05	m

Table 6.5 *Input parameters for SURFBEAT computation; base case. Program module: SURF2*

Sensitivity series

The six basic input variables were assigned a series of values around their base case values, in a realistic range. The coefficient f_w was added to the list of variables, since its value is uncertain. By varying the input variables one at a time, we hope to obtain more insight into the behaviour of time-averaged parameters of the long wave motion, and of parameters that indicate the effect of the long wave motion on the cross-shore morphology. The input values of the different series are listed in Table 6.6.

Series	H_{rms}	Variable	Range	Increment	Unit
1	Varying	H_{rms}	0.25 - 1.50	0.25	m
2	1.0	γ_p	1.0 - 20.0	1.0	-
3	1.0	T_p	4.0 - 9.5	0.5	s
4	1.0	L_b	100 - 300	50	m
5	1.0	A_b	0.00 - 2.00	0.25	m
6	1.0	ϕ_b	0 - 180	30	deg.
7	1.0	f_w	0.00 - 0.05	0.01	-
8	0.5	γ_p	1.0 - 20.0	1.0	-
9	0.5	T_p	4.0 - 9.5	0.5	s
10	0.5	L_b	100 - 300	50	m
11	0.5	A_b	0.00 - 2.00	0.25	m
12	0.5	ϕ_b	0 - 180	30	deg.
13	0.5	f_w	0.00 - 0.05	0.01	-

Table 6.6 *Overview of model run series*

6.5.2 Output parameters

During each model run, the basic variables were stored for each grid point and time step. After completion of the run, a number of time-averaged parameters was computed in 120 equidistant points at 10 m spacing. Only these results were kept for further analysis.

The most important parameters that we shall discuss below are the wind wave height $H_{rms,hi}$, the low-frequency wave height $H_{rms,lo}$, defined by:

$$H_{rms,lo} = \sqrt{8}\,\sigma_{z_s}; \tag{6.22}$$

where σ_{z_s} is the standard deviation of the low-frequency surface elevation; the standard deviation of the low-frequency velocity, σ_U, the interaction term between long wave velocity and short wave velocity variance:

$$\langle |u_{hi}|^2 u_{lo} \rangle = Cov\left(Var(u_{hi}), u_{lo}\right) \tag{6.23}$$

and the coefficient of correlation between long wave velocity and short wave velocity variance:

$$C_{r,u} = \frac{Cov\left(Var(u_{hi}), u_{lo}\right)}{\sigma_{Var(u_{hi})}\,\sigma_{u_{lo}}} \tag{6.24}$$

6.6 Results

In Section 6.1 we discussed how the morphological behaviour of a profile is determined by the transport distribution over the profile and by the sensitivity of this tranport pattern to bottom changes. Here we consider only the contribution of the long wave - short wave interaction term to the third velocity moment, and thus to the bottom transport part of the cross-shore transport according to equation 6.1.

First we shall briefly discuss some characteristics of the behaviour of the long waves themselves. We then examine the shape of the transport term due to long wave - short wave interaction and its sensitivity to bottom changes, since these aspects determine the morphological effect of the long wave - short wave interaction. After this we check to what extent these results are sensitive to the incident wave conditions.

6.6.1 Long wave parameters

Variation of incident wave height

The incident wave height has a strong influence on the long wave height and velocity (Figure 6.7). At the deeper end, the increase of the velocities is approximately proportional to the wave height squared, which indicates that bound wave effects are dominant.

This is explained by the reverse shoaling of reflected free waves, which is felt strongly in the velocities. This effect is less strong in the heights of the long waves, where for low incident wave heights the reflected free waves are dominant in deep water. Near the shore, after an initially strong increase, both low-frequency wave heights and velocities reach a limiting magnitude, which is probably due to suppression of bound wave growth due to a reduction in groupiness of the short waves; for high incident wave heights, the higher short waves are topped off far away from the beach.

Variation of peak period

The influence of the peak period is very strong (Figure 6.8). Long wave amplitudes increase by a factor of four when the peak period increases from 4 s to 9 s. Since the effect of the peak period on the short wave propagation is limited, this is a strong indicator of the importance of bound waves. The occurrence of peaks in the amplitudes of both the velocity and the wave height of the long waves over the bar crests also points to this fact. The increase in amplitudes is quite monotonic, which again indicates that resonance conditions do not occur or are averaged out.

Variation of spectral peak enhancement factor

The spectral peak enhancement factor has a very limited effect on these time-averaged long wave parameters.

Conclusions

The main conclusions are that the most important incident wave parameters are wave height and period. Long wave amplitudes increase strongly near the shore, as opposed to short wave amplitudes. Long wave amplitudes keep increasing for increasing short wave period, as opposed to what happens with increasing wave height for the same period. However, since generally the wave period increases with increasing wave height, the long wave amplitudes on the beach will keep growing with increasing wave height.

Over this wide range of wave characteristics, we find no evidence of resonance conditions.

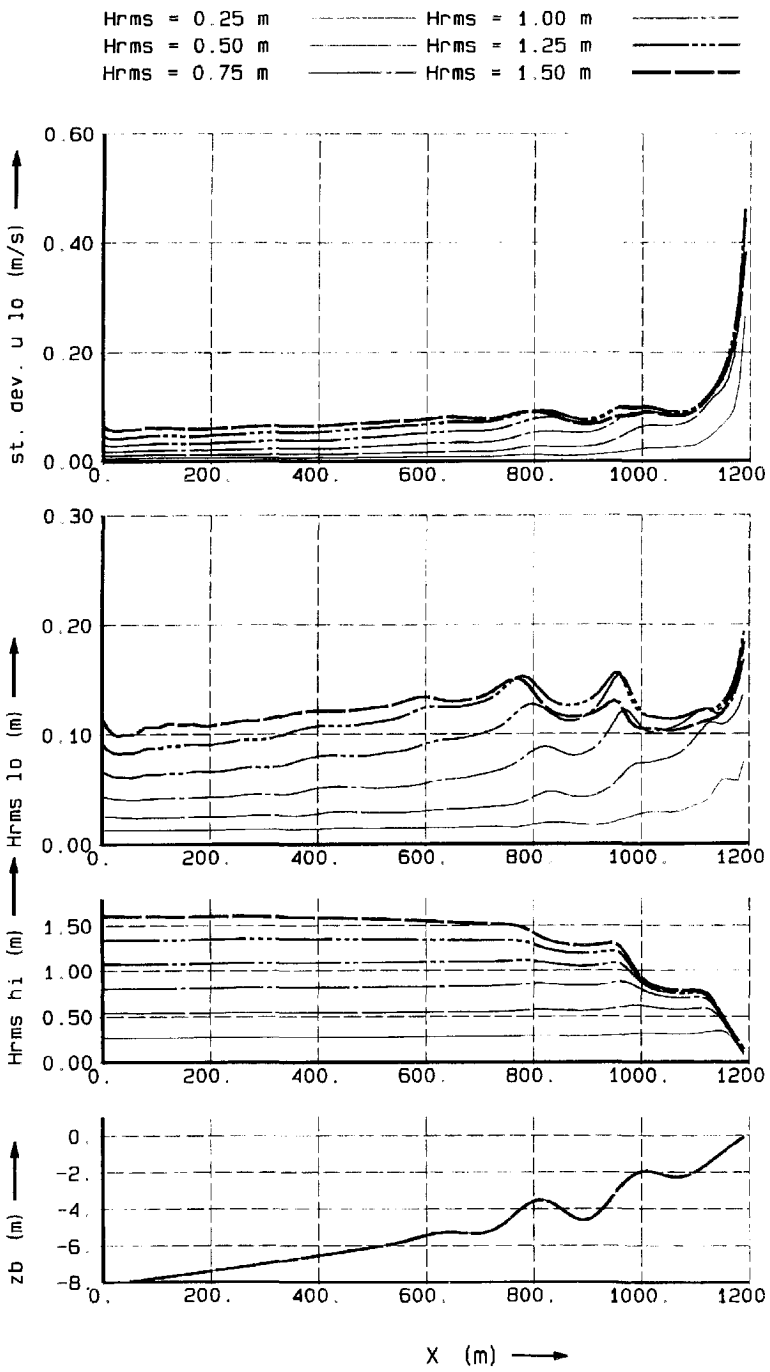

Figure 6.7 *Sensitivity of wind wave height $H_{rms,hi}$, low-frequency wave height $H_{rms,lo}$ and standard deviation of the long wave velocity $\sigma_{u_{lo}}$ to variation of the incident wave height H_{rms}*

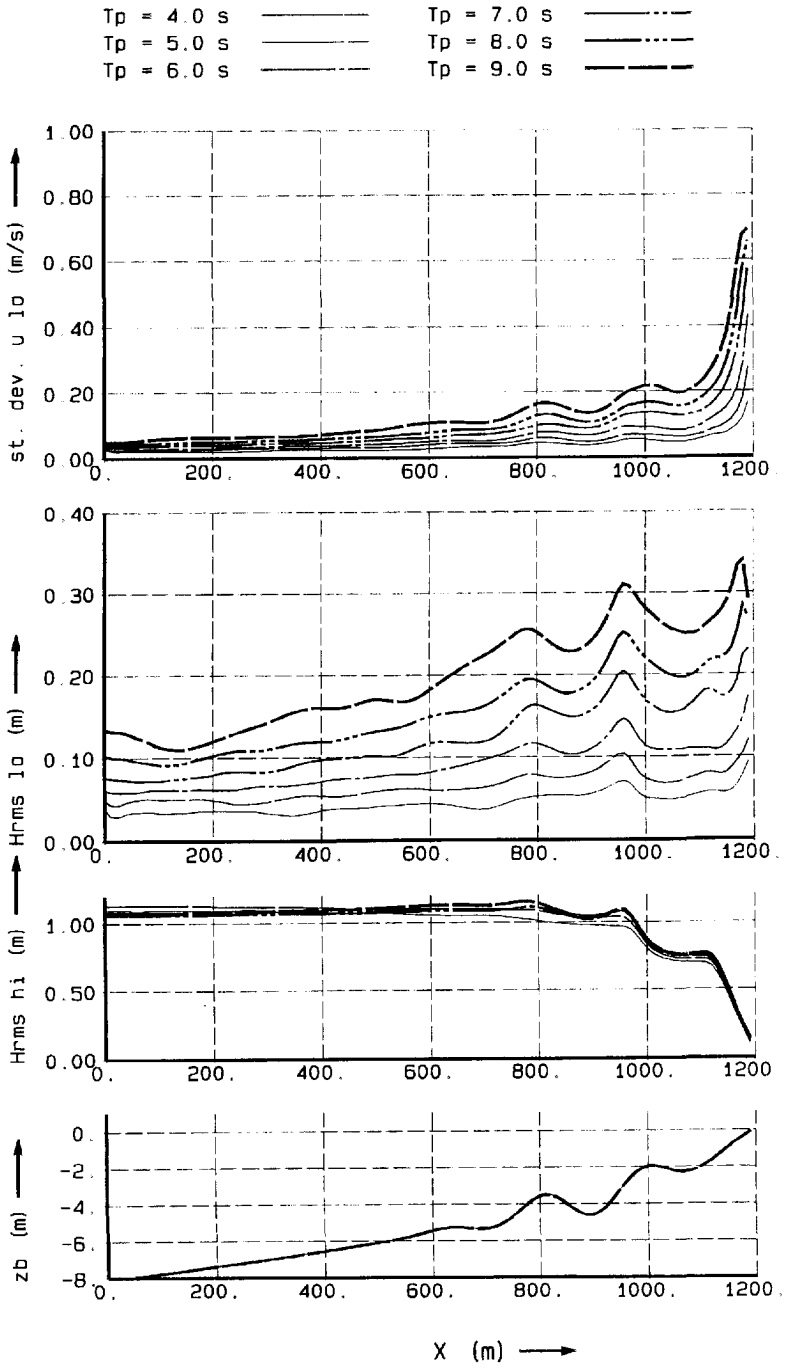

Figure 6.8 *Sensitivity of wind wave height $H_{rms,hi}$, low-frequency wave height $H_{rms,lo}$ and standard deviation of the long wave velocity $\sigma_{u_{lo}}$ to variation of the peak period T_p; H_{rms} = 1.0 m*

6.6.2 Sensitivity of transport term to bottom changes

Effect of bar amplitude

In Figure 6.9, the bottom profile, distribution of short wave height, correlation coefficient $C_{r,u}$ and the long wave - short wave interaction term are shown for varying bar amplitude and an incident wave height $H_{rms} = 1.0m$; in Figure 6.10, the same is given for $H_{rms} = 0.5m$. Clearly, the scale of the transport pattern on the average profile is closely related to the scale of the surf zone. The transport term is directed seaward, except very close to the shore. In a profile free of bars, bar formation due to this pattern would start in the area with a negative transport gradient, and would be strongest for the lower wave height, since the transport gradients are higher in absolute terms. However, we see that for increasing amplitude of the sand bar, the transport pattern reacts strongly to these changes. Negative peaks in the transport occur just seaward of the bar crests, indicating a tendency to move the bars seaward and to reduce their amplitude.

Beside a local influence on the transport pattern the bars influence the transport in the area shoreward of them; the seaward transport is generally reduced by increasing bar amplitude. Mechanisms to explain this are a reduction in short wave orbital velocity due to short wave dissipation, and a strong increase in the (negative) correlation coefficient which occurs simultaneously with the dissipation of short waves by breaking.

Effect of bar spacing

The effect of the bar spacing is shown in Figures 6.11 and 6.12. Regardless of the spacing of the bars, the transport pattern is dominated by the variations directly related to the bottom modulation. Again, the negative peaks in transport are located just seaward of the bar crests. The water depth at the crest location appears to be important in determining the magnitude of these transport peaks.

Effect of phase of the bar

In Figures 6.13 and 6.14 we clearly see that the sensitivity of transport due to long wave - short wave interaction to bottom changes is similar to the description given by equation 6.8; the transport modulation follows the bottom modulation at a constant phase lag. Since the negative peaks are consistently located just seaward of the bar crests, the effect of this term will be to move the bars in seaward direction while reducing their amplitude; apparently, this tendency is present regardless of the location of the bar.

6.6.3 Sensitivity to incident wave parameters

Variation of wave height

In deeper water, the long wave velocity moment increases very strongly with wave height (Figure 6.15). For higher wave heights, a saturation effect is evident inside the surf zone. The magnitude of the correlation coefficient $C_{r,u}$ in deeper water is small for small wave heights, indicating that reflected free waves are dominant for small incident waves. The correlation coefficient increases towards the shore in much the same way as the wave height decreases, a fact which was also found by Roelvink and Stive (1989) in their experiments. Apart from the region very near the shore, the velocity moment is negative, indicating an offshore directed contribution to cross-shore transport. Negative peaks in the moment occur just seaward of the bar crest locations.

Variation of spectral peak enhancement factor

The effect of the spectral shape is relatively small (Figure 6.16). The peak enhancement factor influences the average length of wave groups. If resonance effects in the low-frequency waves on the barred profile would be important, this would be an important parameter. The small influence of the peak enhancement factor on the velocity moment indicates that strong resonance effects are absent.

Variation of peak period

The influence of the peak period is very strong, both in the velocity moments and in the correlation coefficient near the shore (Figure 6.17). The increase in the positive correlation near the shore for increasing peak period may indicate that the long waves have a propagating rather than a standing character, due to breaking of the higher long waves which reduces their reflection from the beach. In all cases, the negative peaks occur over or just seaward of the bar crest.

Variation of the friction coefficient

The velocity moment due to long waves is insensitive to the bottom friction coefficient, so the uncertainty in this coefficient does not affect our conclusions.

6.7 Conclusions of sensitivity study

Due to the absence of strong resonance effects on time-averaged long wave parameters on the barred profiles considered here, and due to the broad-bandedness of the low-frequency spectrum, phase coupling between the short wave envelope and the **reflected** long waves is generally very weak. As a result, the velocity moments are dominated by the phase coupling between **incoming** long waves and the short wave envelope. This phase coupling results in a seaward directed effect, except very near the shoreline. Since both long wave velocity and short wave velocity variance have a maximum just seaward of the bar crests, the velocity moments are strongest on or just seaward of the bar crests. This effect increases for increasing bar amplitudes, and is found irrespective of bar spacing and location.

The morphological effect of cross-shore long waves is therefore generally to increase offshore transport, except very near the shoreline, and to move bars in seaward direction, while reducing their amplitude.

The most important incident wave parameters governing these processes are the wave height, and to an even greater extent, the wave period, while the spectral shape has a very limited effect.

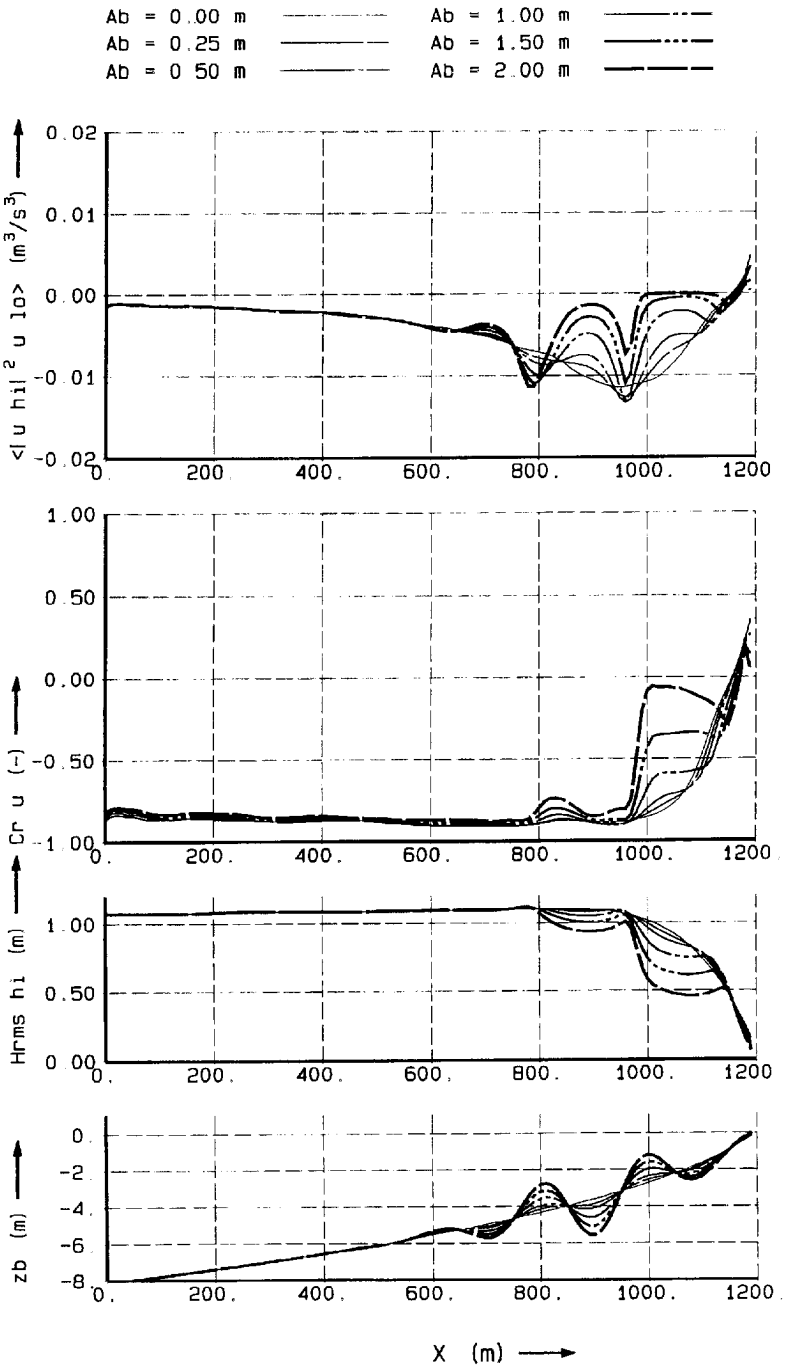

Figure 6.9 *Sensitivity of wind wave height $H_{rms,hi}$, correlation coefficient $C_{r,u}$ and long wave - short wave interaction term $\langle |u_{hi}|^2 u_{lo} \rangle$ to variation of the bar amplitude A_b; H_{rms} = 1.0 m*

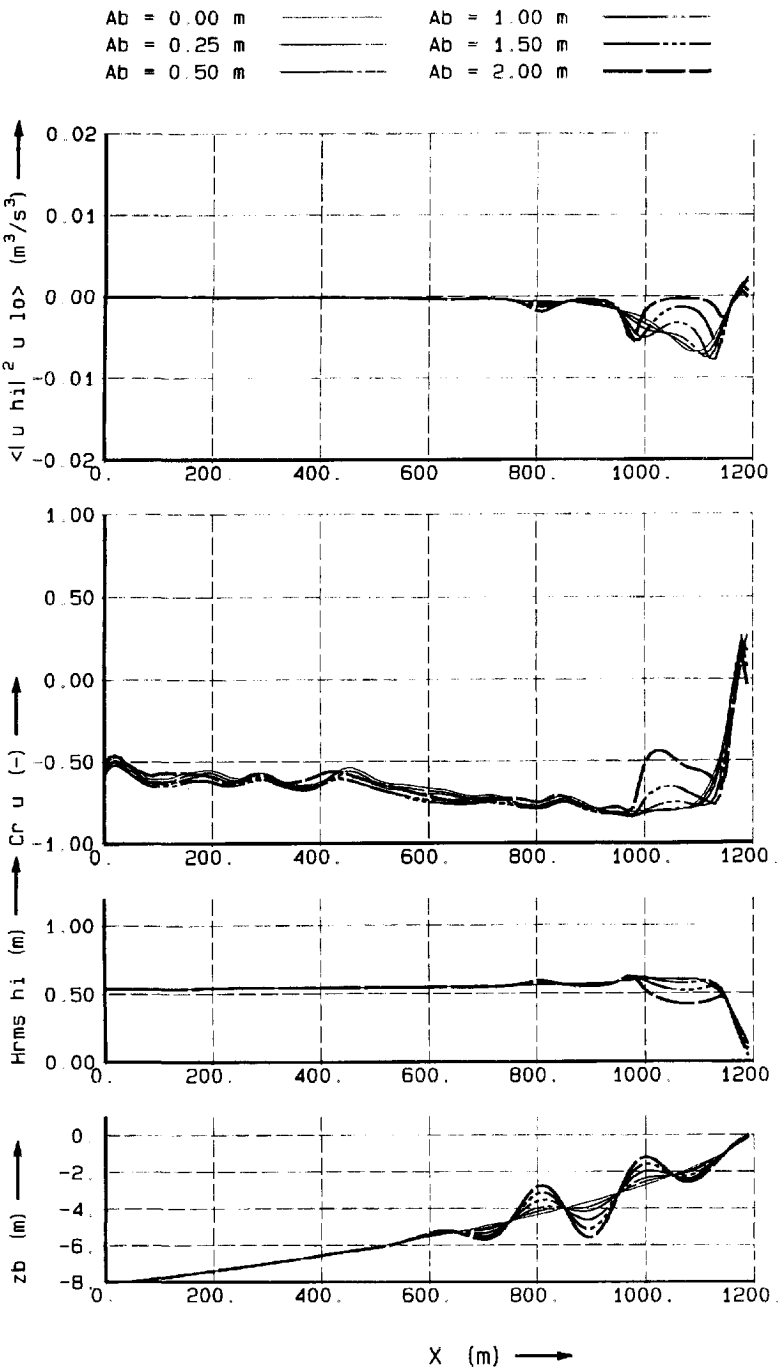

Figure 6.10 *Sensitivity of wind wave height $H_{rms,hi}$, correlation coefficient $C_{r,u}$ and long wave - short wave interaction term $\langle |u_{hi}|^2 u_{lo} \rangle$ to variation of the bar amplitude A_b; H_{rms} = 0.5 m*

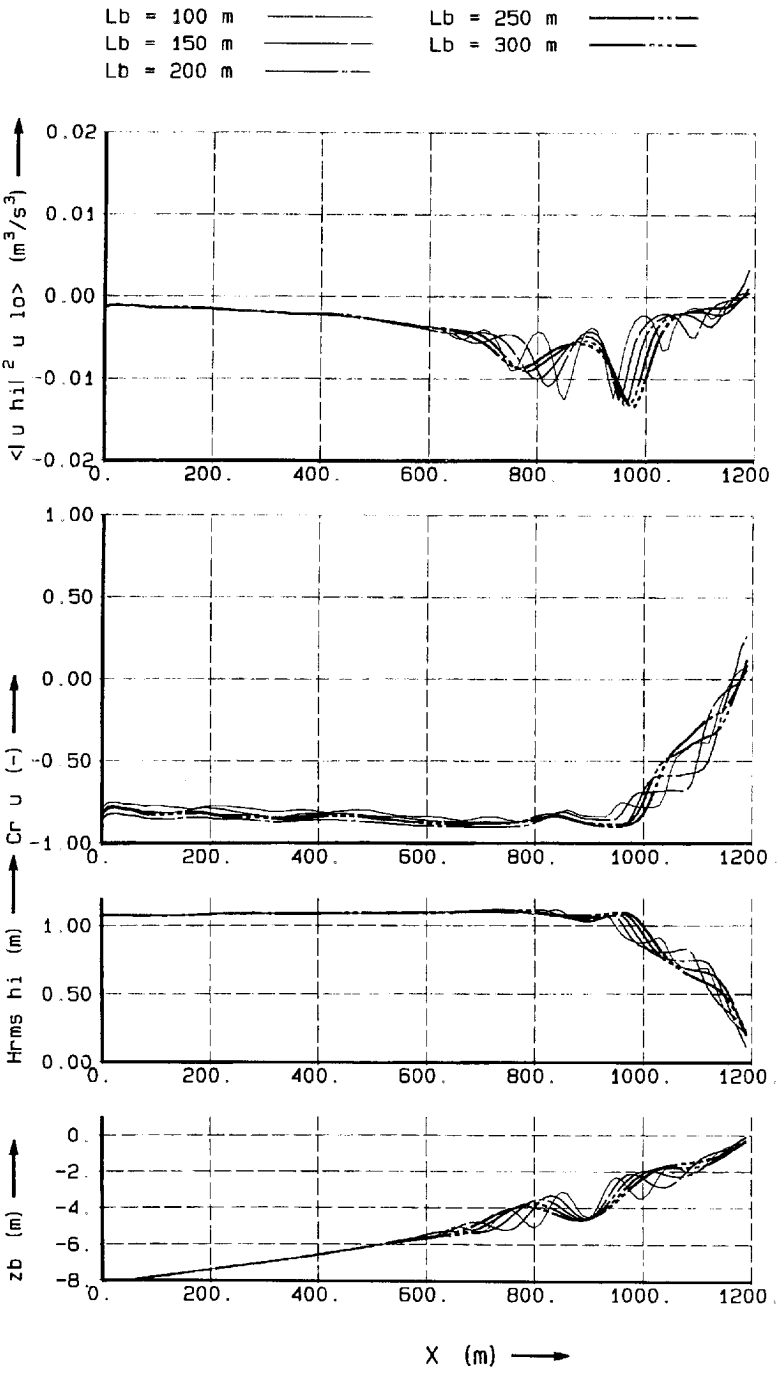

Figure 6.11 *Sensitivity of wind wave height $H_{rms,hi}$, correlation coefficient $C_{r,u}$ and long wave - short wave interaction term $\langle |u_{hi}|^2 u_{lo} \rangle$ to variation of the bar spacing L_b; H_{rms} = 1.0 m*

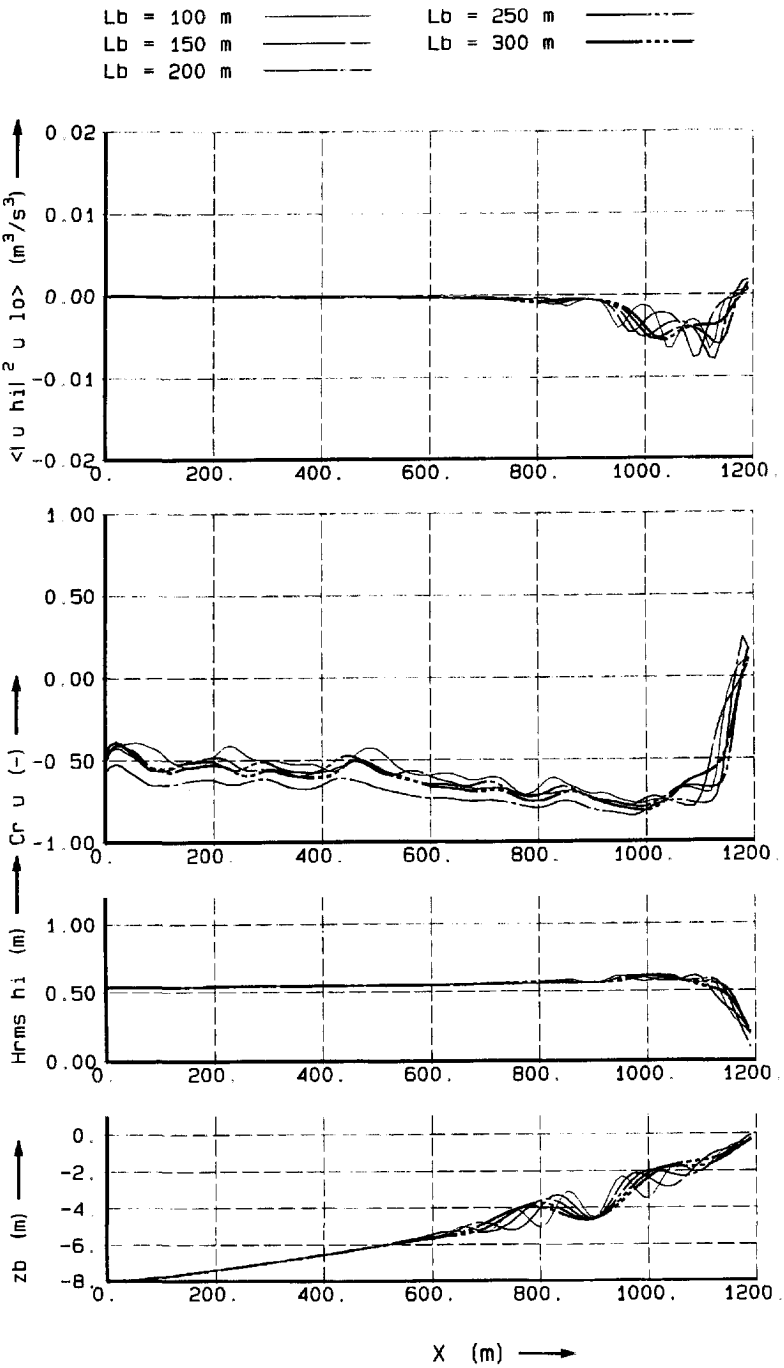

Figure 6.12 *Sensitivity of wind wave height $H_{rms,hi}$, correlation coefficient $C_{r,u}$ and long wave - short wave interaction term $\langle |u_{hi}|^2 u_{lo} \rangle$ to variation of the bar spacing L_b; H_{rms} = 0.5 m*

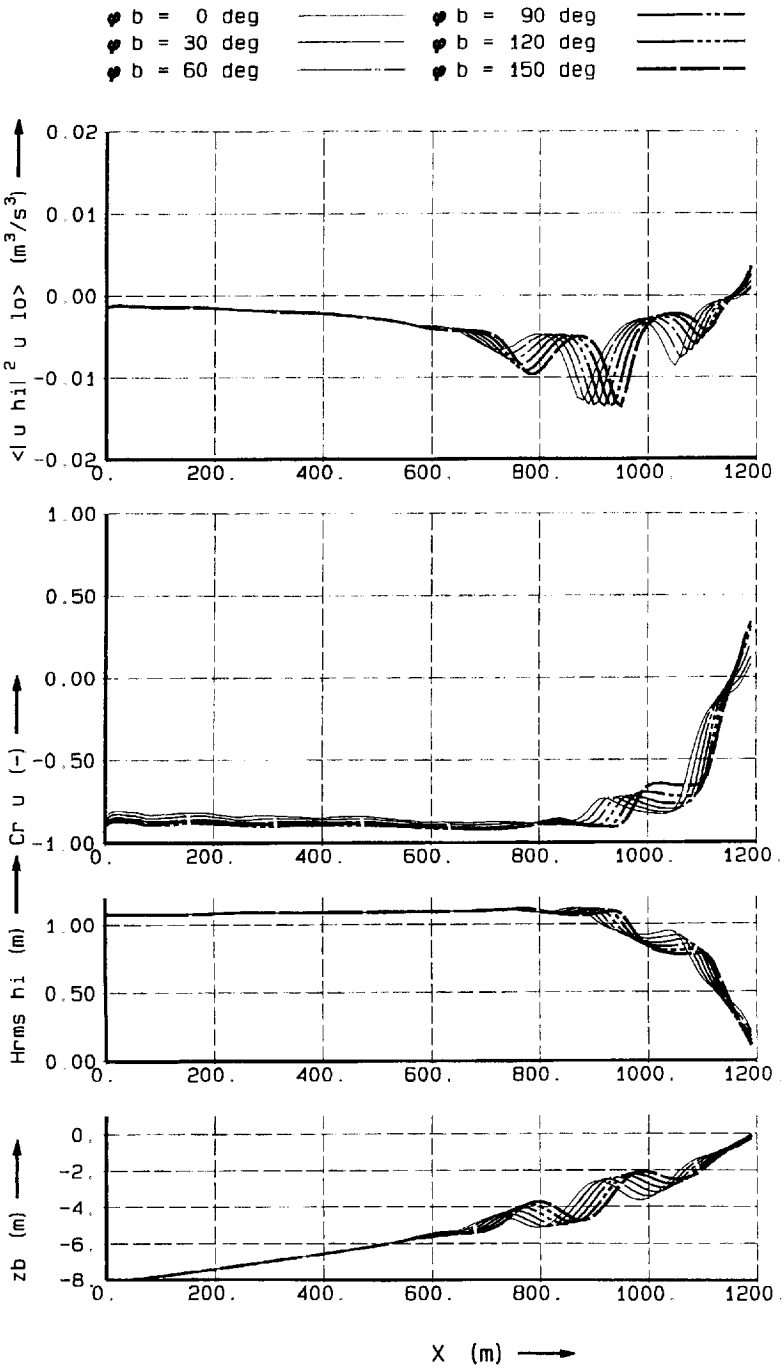

Figure 6.13 *Sensitivity of wind wave height $H_{rms,hi}$, correlation coefficient $C_{r,u}$ and long wave - short wave interaction term $\langle |u_{hi}|^2 u_{lo} \rangle$ to variation of the bar phase ϕ_b; H_{rms} = 1.0 m*

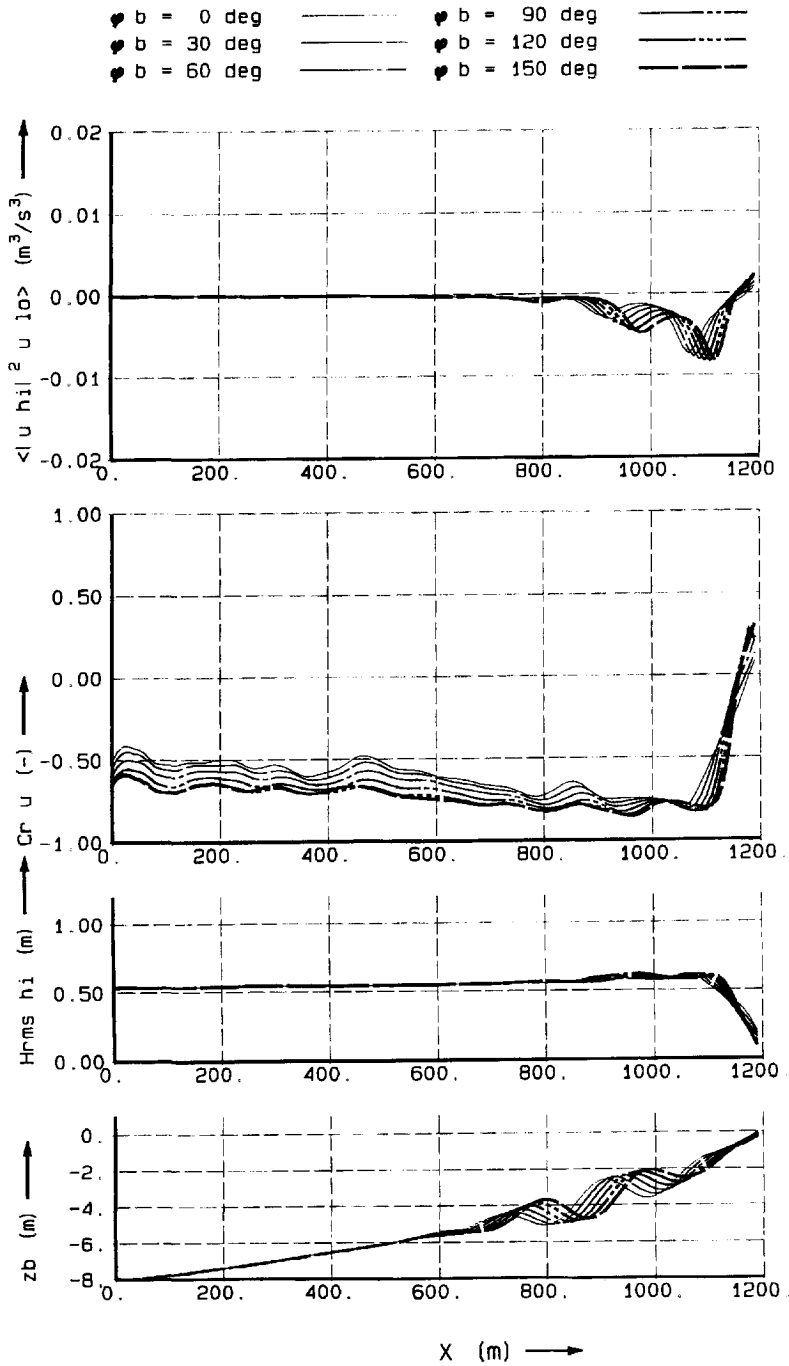

Figure 6.14 *Sensitivity of wind wave height $H_{rms,hi}$, correlation coefficient $C_{r,u}$ and long wave - short wave interaction term $\langle |u_{hi}|^2 u_{lo} \rangle$ to variation of the bar phase ϕ_b; H_{rms} = 0.5 m*

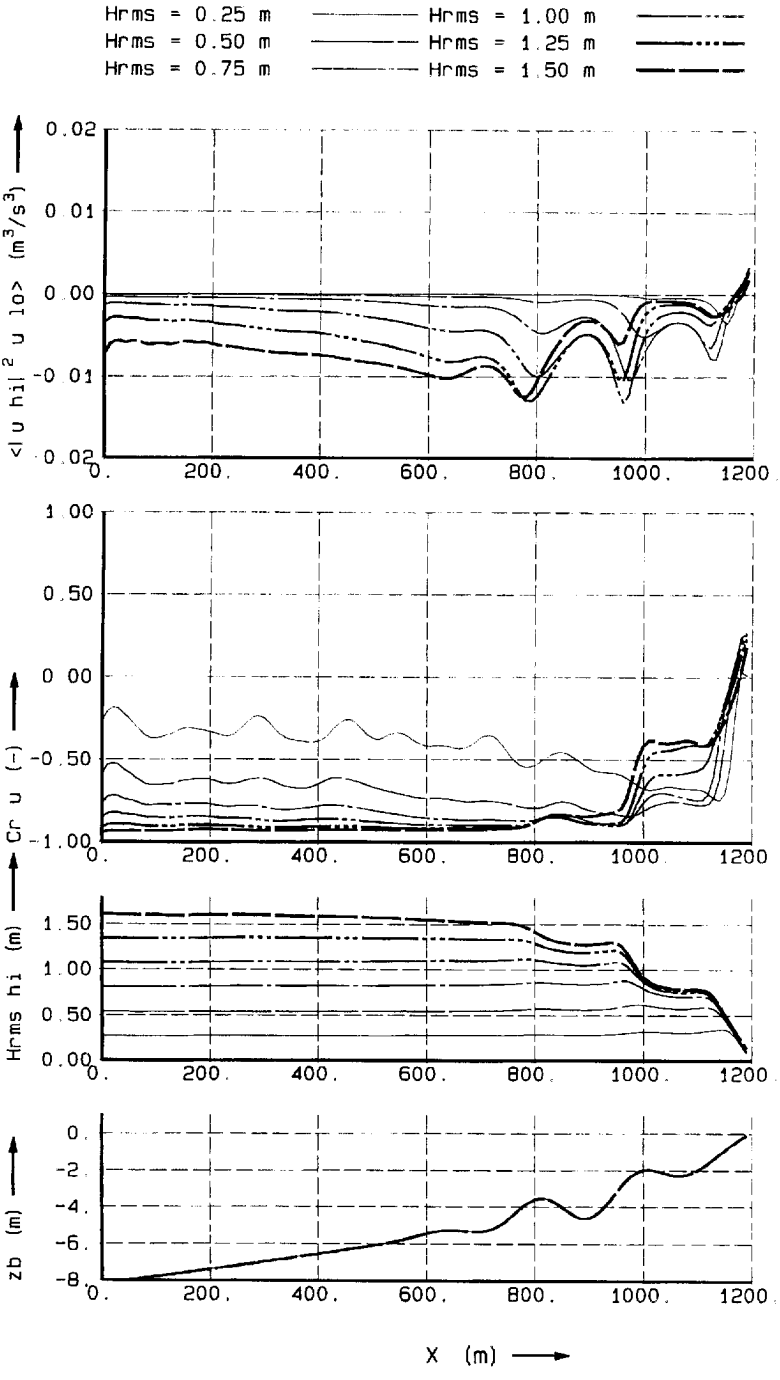

Figure 6.15 *Sensitivity of wind wave height $H_{rms,hi}$, correlation coefficient $C_{r,u}$ and long wave - short wave interaction term $\langle |u_{hi}|^2 u_{lo} \rangle$ to variation of the incident wave height H_{rms}*

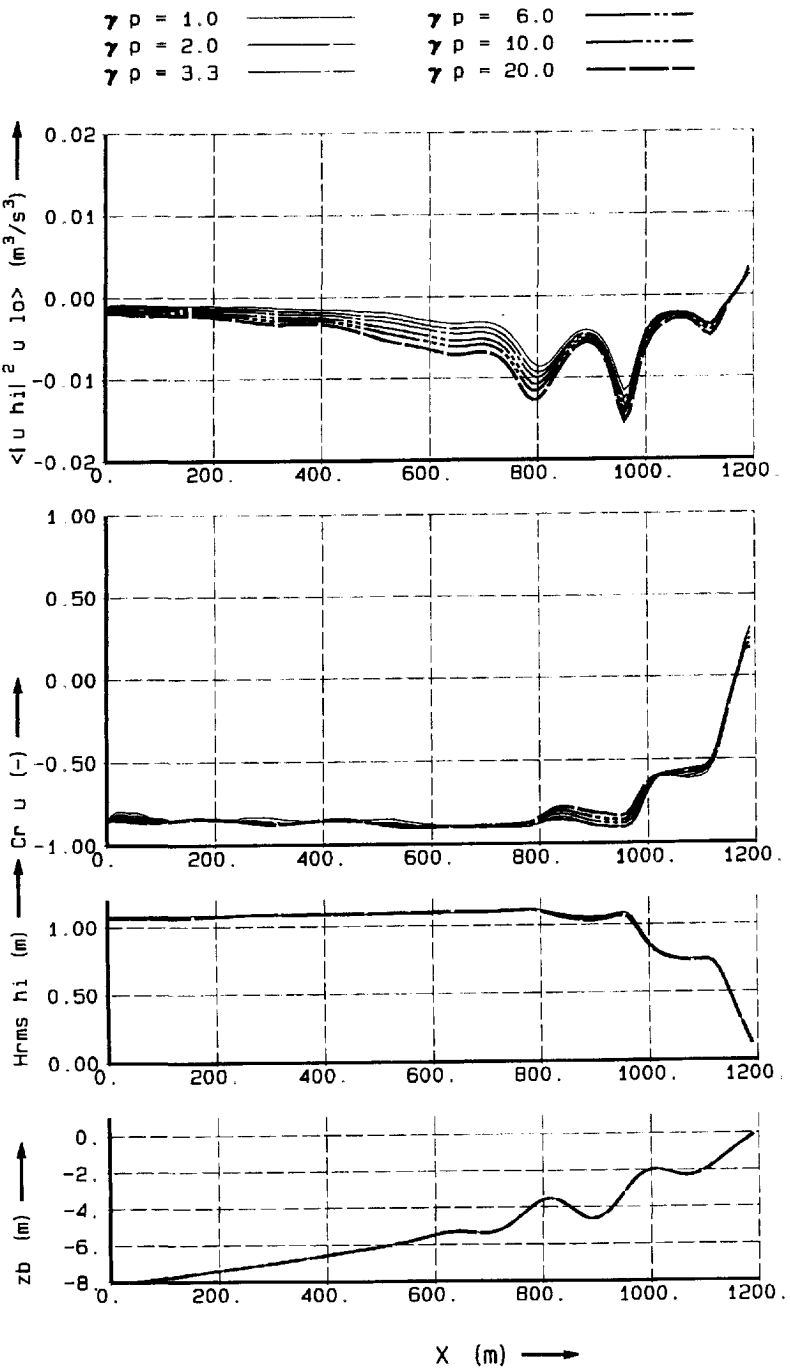

Figure 6.16 *Sensitivity of wind wave height $H_{rms,hi}$, correlation coefficient $C_{r,u}$ and long wave - short wave interaction term $\langle |u_{hi}|^2 u_{lo} \rangle$ to variation of the spectral peak enhancement factor γ_p; H_{rms} = 1.0 m*

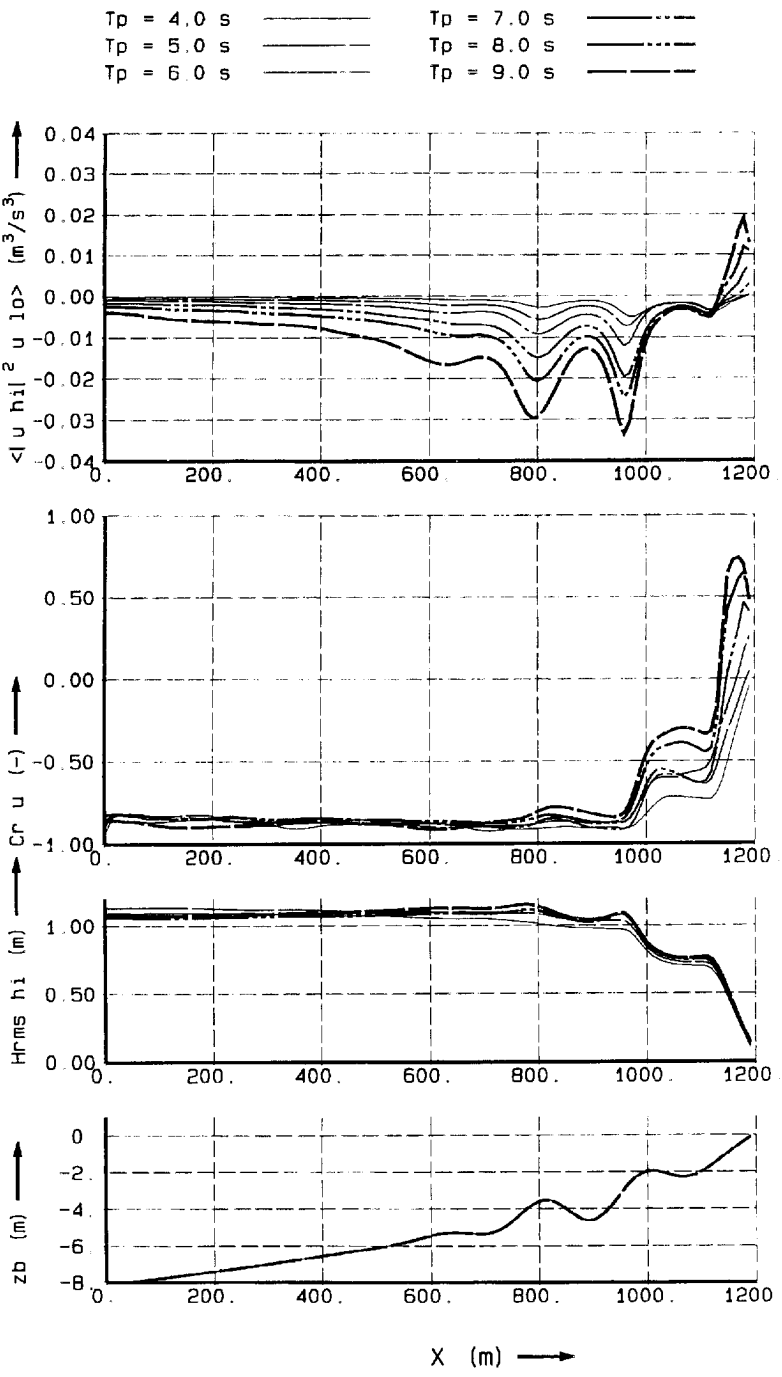

Figure 6.17 *Sensitivity of wind wave height $H_{rms,hi}$, correlation coefficient $C_{r,u}$ and long wave - short wave interaction term $\langle|u_{hi}|^2 u_{lo}\rangle$ to variation of the peak period T_p; H_{rms} = 1.0 m*

7. CONCLUSIONS AND RECOMMENDATIONS

7.1 Surf beat

In this thesis we describe the development, calibration and validation of a predictive model, code named "SURFBEAT", which describes the propagation of normally incident wave groups over a beach profile and their associated long wave motions.

The model formulations are based on the short wave averaged conservation equations for mass, momentum, wave action and wave density. Closure relations are derived from linear theory, except for those concerning dissipation terms. A new formulation for the time-varying, short wave averaged wave energy dissipation due to breaking is proposed. This formulation plays a key role in solving the conservation equations. Special attention is paid to the calibration of the parameters in the breaker formulation, and a set of constant parameter values is found for which the formulation is valid over a wide range of conditions.

A numerical method was designed to solve the non-linear system of conservation equations. In order to avoid a complicated treatment of the water line, the system of equations is transformed from a non-equidistant and time-varying physical domain to an equidistant and constant computational domain. A standard scheme of second-order accuracy is used to solve the transformed equations.

The applied numerical method has been tested against known analytical solutions of the non-linear shallow water equations. These solutions are reproduced accurately. The scheme is capable of accurately representing bore solutions of the shallow water equations; hence the model automatically represents the breaking of long waves.

The complete model is validated against data from three different wave flume experiments.

The first dataset concerns bichromatic waves incident on a plane sloping beach (Kostense, 1984). The measured quantities are the incident bound long wave amplitude and the reflected free long wave amplitude. The experiment contains series of tests covering either a range of group frequencies for constant incident wave amplitudes, or a range of incident wave amplitudes for a constant group frequency. Both weakly modulated and almost fully modulated incident waves are represented. The computer model is capable of predicting both the trends and the magnitude of the reflected free wave amplitudes with reasonable accuracy, both for the weakly modulated and for the almost fully modulated incident waves. The incident bound wave amplitudes are predicted accurately in all cases.

The second dataset was presented by Van Leeuwen (1992) and concerns random waves incident on a plane sloping beach. Here, time series of the water elevation measured in a number of points both on the horizontal stretch near the wave maker and on the sloping beach are available. An accurate method of generating boundary conditions for the model, based on a measured time series in a single point, has been developed and verified by the measurements. The predicted time series of the short wave energy and of the long wave elevation are in reasonable agreement with the measured time series throughout the flume when these accurate boundary conditions are applied. The main factor limiting the accuracy of these predicted time series is the assumption of a constant group velocity, which introduces phase errors in the predicted short wave energy and the long waves. The covariance function between the short wave energy and the total long wave elevation is however predicted accurately throughout the surf zone. This covariance function is a good indicator of the model's capability of predicting overall parameters of the interaction between groups of short waves and the associated long waves.

The third dataset was presented by Roelvink and Stive (1989) and concerns surface elevation and near-bed velocity measurements in a wave flume with random waves incident on a sandy beach of an initially plane slope which develops into a barred profile. The data available are time-averaged parameters of the incident wave field, the long waves and the interaction between short waves and long waves. The short wave parameters (wave heights and orbital velocities) are predicted with good accuracy. The long wave velocities and the correlation between the short wave velocity variance and the long wave velocity are also predicted accurately throughout the surf zone. The contributions of the interaction between short waves and long waves to the third and fourth order odd velocity moments are predicted with reasonable accuracy; deviations are generally not more than 30 % of the peak values. These errors are transferred linearly to errors in cross-shore transport predictions and are acceptable given the accuracy of the available transport models. All the observed trends in the measured parameters are reproduced faithfully by the model.

From the bichromatic test case the conclusion may be drawn that the model contains the necessary physics to describe long wave generation in the surf zone, although the calibration of the dissipation model has not been carried out systematically for the case of bichromatic waves.

The validation of the model for the random wave cases was carried out using the standard values for the empirical parameters that were determined in the calibration phase, for different cases. We may therefore conclude that in the context of cross-shore transport modelling the model presented here is an accurate enough predictive model

for the propagation and decay of normally incident random wave groups and their associated long wave motions over an arbitrary beach profile. The use of the non-linear shallow water equations for the long wave motion enables application of the model to severe conditions where the long waves have high amplitudes or may even be breaking.

7.2 Effect of surf beat on cross-shore profiles

In Section 1.2 we have discussed the possible mechanisms through which surf beat can affect cross-shore profiles: on the one hand the effect of the drift velocity pattern associated with standing long waves, and on the other hand the effect of the interaction between the short wave orbital velocity fluctuations and the long wave velocity. We conclude that the latter effect must be dominant, and further focus on describing this effect.

An important factor governing the morphodynamic behaviour of the profile is, to what extent the sediment transport distribution over the profile is sensitive to profile changes. This has been clarified in two schematic examples in Section 6.1.

From these two examples it follows that the dynamic morphological behaviour of a coastal profile is determined partly by patterns apparent on the undisturbed profile, and partly by the sensitivity of the transport pattern to profile changes. Both these aspects can be studied without actually computing the time-dependent dynamic behaviour in a complete morphological model.

The sensitivity of the transport pattern due to the interaction between short and long waves to changes in the bar topography has been established by schematizing the profile shape to a realistic, parametric form of which the parameters can be varied in a systematic way. By means of numerical simulations the sensitivity of the long wave - short wave interaction term to the spacing, position and amplitude of longshore bars has been studied, in relation to the basic pattern on an unbarred "equilibrium" profile.

This was carried out for two typical wave conditions. Separately, the sensitivity of the result for a typical barred profile to incident wave conditions was investigated, in order to verify that the conclusions are generally valid, and to identify the most important parameters of the incident wave field.

The main conclusions regarding the long waves themselves are that the most important incident wave parameters are wave height and period. Long wave amplitudes increase strongly near the shore, as opposed to short wave amplitudes. Long wave amplitudes keep increasing for increasing short wave period; with increasing wave height for a

constant wave period the long wave amplitudes first increase strongly, after which a saturation takes place. However, since generally the wave period increases with increasing wave height, the long wave amplitudes on the beach will keep growing with increasing wave height.

Over a wide range of realistic wave and profile characteristics, we find no evidence of resonance conditions.

Due to the absence of strong resonance effects on time-averaged long wave parameters on the barred profiles considered here, and due to the broad-bandedness of the low-frequency spectrum, phase coupling between the short wave envelope and the **reflected** long waves is generally very weak. As a result, the velocity moments are dominated by the phase coupling between **incoming** long waves and the short wave envelope. This phase coupling results in a seaward directed effect, except very near the shoreline. Since both long wave velocity and short wave velocity variance increase over bar crests, the velocity moments are strongest on or just seaward of the bar crests. This effect increases for increasing bar amplitudes, and is found irrespective of bar length and location.

The morphological effect of cross-shore long waves is therefore generally to increase offshore transport, except very near the shoreline, and to move bars in seaward direction, while reducing their amplitude.

The most important incident wave parameters governing these processes are the wave height, and to an even greater extent, the wave period, while the spectral shape has a very limited effect.

The hypothesis that bar formation is to an important extent related to cross-shore long waves is not supported by this study. Although we find that the cross-shore long wave motion plays an important role in bar evolution, it is generally a destructive role.

However, these conclusions are only applicable to cross-shore long wave modes; for the effect of edge waves forced by groups of obliquely incident short waves, the conclusions may be quite different.

7.3 Recommendations

The accuracy of time series of short wave energy and long wave elevation predicted by the SURFBEAT model presented here may be improved by allowing the short wave frequency to vary slowly, and by taking into account the effect of the long wave velocity on the propagation of the short wave groups. The main problems to solve in

this case are the prescription of boundary conditions for the short wave frequency, both at the seaward and at the landward boundary.

For real-life applications, it is essential to extend the model to the two-dimensional case. A first step in this direction has been presented by Reniers (1992). This model is however restricted to periodic wave groups on a beach which is uniform alongshore. It should be possible to extend this model to a full spectral model, although the use of linearised equations may seriously limit its applicability.

For non-uniform coasts a possibility is to include a description of the surf zone in the two-dimensional model COLOSSYS (Liu and Dingemans, 1989), which is currently under development. It must be investigated whether the present dissipation formulation can be incorporated in this model.

The strength of the third-order evolution equations used in COLOSSYS lies in the accurate description of the propagation of wave groups and long waves over large distances. For coastal areas where the area of interest is in the order of some group lengths, the relatively simple treatment of the short wave propagation in the present SURFBEAT model may be accurate enough; these formulations can be extended to two dimensions in a relatively straightforward manner. In both cases, generation of accurate boundary conditions will be an important problem to solve.

The validation of such two-dimensional models will require extensive and costly field measurement campaigns or wave basin experiments.

ACKNOWLEDGEMENTS

The research presented in this thesis was carried out as part of the G8 Coastal Morphodynamics research programme. It was funded jointly by the Netherlands' Rijkswaterstaat, in the framework of the "Coastal Genesis (Kustgenese)" programme, and the Commission of the European Communities, Directorate General for Science, Research and Development, under contract no. MAST-0035 and MAS2-CT92-0027.

I would like to thank Marcel Stive for introducing me to this area of research in a very stimulating way.

Henri Petit has helped me enormously with numerical aspects of the model; I'm very grateful for the mistakes I haven't made because of this.

I thank my colleagues Gert Klopman, Maarten Dingemans, Jan Karel Kostense and Ad Reniers for many fruitful discussions and suggestions.

Peter Jan van Leeuwen at Delft University of Technology has been very generous in making his data available at an early stage; I thank him for that and for valuable advices.

I also thank my supervisor Prof. Jurjen Battjes for his insight and his ability to indicate not only what is wrong, but also how to mend it.

Finally, I'm very grateful for having the parents I have, and for having Hesseltje to share my life with.

REFERENCES

Abdelrahman and Thornton (1987). *Changes in the short wave amplitude and wave-number due to the presence of infragravity waves. Proc. Specialty Conf. on Coastal Hydrodynamics, pp. 458-478, ASCE, New York, 1987.*

Bagnold, R.A. (1966). *An approach to the sediment transport problem from general physics. US Geological Survey, Professional Paper 422-I, 37 p.*

Bailard, J.A. (1981). *An energetics total load sediment transport model for a plane sloping beach. J. Geophys. Res., Vol. 86, pp. 10,938-10,954.*

Bakker, W.T. and J.H. de Vroeg (1988). *Is de kust veilig? Analyse van het gedrag van de Hollandse kust in de laatste 20 jaar. (Is the coast safe? Analysis of the behaviour of the Dutch coast over the last 20 years; in Dutch). Rijkswaterstaat, Tidal Waters Division, The Hague, Nota GWAO 88.017.*

Battjes, J.A. and J.P.F.M. Janssen (1978). *Energy loss and set-up due to breaking in random waves. Proc. 16th Int. Conf. on Coastal Eng., ASCE, pp. 569-587.*

Battjes, J.A. and M.J.F. Stive (1985). *Calibration and verification of a dissipation model for random breaking waves. J. Geophys. Res., vol. 90, No. C5, pp. 9159-9167.*

Bowen, A.J. (1980). *Simple models of nearshore sedimentation: beach profiles and longshore bars. in: The Coastline of Canada, edited by S.B. McCann, pp. 1-11, Geological survey of Canada, Ottawa, 1980.*

Bowen, A.J. and R.T. Guza (1978). *Edge waves and surf beat. J. Geophys. Res., Vol. 83, pp. 1913-1920.*

Bruun, P. (1954). *Coast erosion and the development of beach profiles. U.S. Army Corps of Engineers, Beach Erosion Board, Tech. Memo., No. 44.*

Carrier, G.F. and H.P. Greenspan (1958). *Water waves of finite amplitude on a sloping beach. J. Fluid Mech., Vol. 4, pp. 97-109.*

Dean, R.G. (1977). *Equilibrium beach profiles: US Atlantic and Gulf Coasts. Newark (Delaware), Univ. of Delaware, Dept. of Civil Engineering, Ocean Engineering report No. 12.*

Dingemans, M.J.F., H.A.H. Petit, Th.J.G.P. Meijer and J.K. Kostense (1991). *Numerical evaluation of the third-order evolution equations for weakly nonlinear water waves propagating over uneven bottoms. In: Computer modelling in Ocean Engineering 91, Arcilla et al. (eds), Balkema, Rotterdam.*

Gallagher, B. (1971). *Generation of surf beat by non-linear wave interactions. J. Fluid Mech., Vol. 49, part 1, pp. 1-20.*

Hibberd, S. and D.H. Peregrine (1979). *Surf and run-up on a beach: a uniform bore. J. Fluid Mech., Vol. 95, pp. 323-345.*

Holman, R.A. and A.J. Bowen (1982). *Bars, bumps and holes: models for the generation of complex beach topography. J. Geophys. Res., Vol. 87, No. C1, pp. 457-468.*

Huntley, D.A., R.T. Guza and E.B. Thornton (1981). *Field observations of surf beat, 1. Progressive edge waves. J. Geophys. Res., Vol. 86, pp. 6451-6466.*

Klopman, G. and P.J. van Leeuwen (1990). *An efficient method for the reproduction of nonlinear random waves. Proc. 22nd Int. Conf. on Coastal Eng., pp. 478-488, ASCE, New York.*

Kostense, J.K. (1984). *Measurements of surf beat and set-down beneath wave groups. Proc. 19th Int. Conf. on Coastal Eng., pp. 724-740, ASCE, New York.*

Lippmann, T.C. and R.A. Holman (1990). *The spatial and temporal variability of sand bar morphology. J. Geophys. Res., Vol. 95, C7, pp. 11575-11590.*

List, J.H. (1986). *Wave groupiness as a source of nearshore long waves. Proc. 20th Int. Conf. on Coastal Eng., ASCE, New York.*

List, J.H. (1992). *A model for the generation of two-dimensional surf beat. J. Geophys. Res., Vol. 97, pp. 5623-5635.*

Liu, Ph.L.-F. and M.W. Dingemans (1989). *Derivation of the third-order evolution equations for weakly nonlinear water waves propagating over uneven bottoms. Wave Motion, Vol. 11, pp. 41-64, Elsevier.*

Lo, J-M. (1981). *Surf beat: numerical and theoretical analysis. Ph.D. dissertation, Univ. of Delaware.*

Longuet-Higgins, M.S. and R.W. Stewart (1962). *Radiation stress and mass transport in gravity waves, with applications to 'surf beats'. J. Fluid Mech., Vol. 8, pp. 565-583.*

Longuet-Higgins, M.S. and R.W. Stewart (1964). *Radiation stresses in water waves; a physical discussion, with applications. Deep Sea Res., Vol. 11, pp. 529-562.*

Munk, W.H. (1949). *Surf beat. EOS Trans. AGU, Vol. 30, pp. 849-854.*

Nakaza, E. and M. Hino (1991). *Bore-like surf beat in a reef zone caused by wave groups of incident short period waves. Fluid Dynamics Res., 7, pp. 89-100.*

Nakaza, E., S. Tsukayama and M. Hino (1990). *Bore-like surf beats on reef coasts. Proc. 22nd Int. Conf. on Coastal Eng., pp. 1743-1756, ASCE, New York.*

Osborne, P.D. and B. Greenwood (1992a). *Frequency dependent cross-shore suspended sediment transport. 1. A non-barred shoreface. Marine Geology, Vol. 106, pp. 1-24.*

Osborne, P.D. and B. Greenwood (1992b). *Frequency dependent cross-shore suspended sediment transport. 2. A barred shoreface. Marine Geology, Vol. 106, pp. 25-51.*

Phillips, O.M. (1977). *The dynamics of the upper ocean. 2nd Edition, Cambridge Univ. Press.*

Reniers, A.J.H.M. (1992). *Long wave generation due to obliquely incident, grouped short waves. Delft Hydraulics Report H840.70, II, March 1992.*

Roelvink, J.A. (1991). *Modelling of cross-shore flow and morphology. Proc. ASCE Specialty Conf. "Coastal Sediments", ASCE, New York, pp. 603-617.*

Roelvink, J.A. and M.J.F. Stive (1989). *Bar-generating cross-shore flow mechanisms on a beach. J. Geophys. Res., Vol. 94, No. C4, pp. 4785-4800.*

Sand, S.E. (1981). *Long wave problems in laboratory models. J. Waterway, Port, Coastal and Ocean Div., Vol. 104, No. WW4, pp.492-503, ASCE, New York.*

Sato, S. and N. Mitsunobu (1991). *A numerical model of beach profile change due to random waves. Proc. ASCE Specialty Conf. "Coastal Sediments '91", pp. 674-687, Seattle.*

Sato, S., M. Ozaki and T. Shibayama (1990). *Breaking conditions of composite and random waves. Coastal Engineering in Japan, Vol. 33, No. 2, pp. 133-143.*

Schäffer, H.A. and I.G. Jonsson (1990). *Theory versus experiments in two-dimensional surf beat. Proc. 22nd Int. Conf. on Coastal Eng., pp. 1131-1143, ASCE, New York.*

Schäffer, H.A. and I. Svendsen (1988). *Surf beat generation on a mild-slope beach. Proc. 21st Int. Conf. on Coastal Eng., pp. 1058-1072, ASCE, New York.*

Shi, N.C. and L.H. Larsen (1984). *Reverse sediment transport by amplitude-modulated waves. Marine Geology, Vol. 54 (1983/1984) pp. 181-200.*

Stive, M.J.F. and M.W. Dingemans (1984). *Calibration and verification of a one-dimensional wave energy decay model. Delft Hydraulics Laboratory, report on investigation M 1882.*

Symonds, G. and K.P. Black (1991). *Numerical simulation of infragravity response in the nearshore. Proc. 10th Australasian Coastal and Ocean Eng. Conf., Auckland, pp. 339-344.*

Symonds, G. and A.J. Bowen (1984). *Interactions of nearshore bars with incoming wave groups. J. Geophys. Res., Vol. 89, no. C2, pp. 1953-1959.*

Symonds, G., D.A. Huntley and A.J. Bowen (1982). *Two-dimensional surf beat: long wave generation by a time-varying breakpoint. J. Geophys. Res., Vol. 87, no.C1, pp. 492-498.*

Thornton, E.B. and R.T. Guza (1983). *Transformation of wave height distribution. J. Geophys. Res., Vol. 88, pp. 5925-5938.*

Tucker, M.J. (1950). *Surf beats: sea waves of 1 to 5 minutes' period. Proc. Royal Soc. London Ser. A 202, pp. 565-573.*

Ursell, F. (1952). *Edge waves on a sloping beach. Proc. Royal Soc. London Ser. A 214, pp. 79-94.*

Van Leeuwen, P.J. (1992). *Low frequency wave generation due to breaking wind waves. Ph D. Thesis, Delft Univ. of Technology.*

Whitham, G.B. (1974). *Linear and non-linear waves. Wiley, New York.*

APPENDIX A

The transformation equations (3.2) and (3.3) are of the form:

$$\tau = t \tag{A1}$$

$$\xi = \xi(t,x) \tag{A2}$$

We can directly see that

$$\frac{\partial \tau}{\partial t} = 1$$

$$\frac{\partial \tau}{\partial x} = 0$$

The property $\frac{\partial \tau}{\partial t}\frac{\partial \xi}{\partial x} - \frac{\partial \tau}{\partial x}\frac{\partial \xi}{\partial t} = \frac{\partial \xi}{\partial x} \neq 0$ implies that $x(\tau,\xi)$ and $t(\tau,\xi)(\equiv \tau)$ exist.

Obviously the inverse transformation has the property:

$$\frac{\partial t}{\partial \tau} = 1$$

$$\frac{\partial t}{\partial \xi} = 0$$

Since $\frac{\partial t}{\partial \xi} = 0$ we find:

$1 = \frac{\partial \xi}{\partial \xi} = \frac{\partial \xi}{\partial x}\frac{\partial x}{\partial \xi} + \frac{\partial \xi}{\partial t}\frac{\partial t}{\partial \xi} = \frac{\partial \xi}{\partial x}\frac{\partial x}{\partial \xi}$, resulting in:

$$\frac{\partial \xi}{\partial x} = \left(\frac{\partial x}{\partial \xi}\right)^{-1} \tag{A3}$$

Since $\frac{\partial \tau}{\partial t} = 1$ and x and t are independent we have:

$0 = \frac{\partial x}{\partial t} = \frac{\partial x}{\partial \xi}\frac{\partial \xi}{\partial t} + \frac{\partial x}{\partial \tau}\frac{\partial \tau}{\partial t} = \frac{\partial x}{\partial \xi}\frac{\partial \xi}{\partial t} + \frac{\partial x}{\partial \tau}$, resulting in:

$$\frac{\partial \xi}{\partial t} = -\frac{\partial x}{\partial \tau}\left(\frac{\partial x}{\partial \xi}\right)^{-1} \tag{A4}$$

The differential equation:

$$\frac{\partial v}{\partial t}+\frac{\partial f}{\partial x}=r,$$

which is one of the components of Eq.(3.8), (3.9) and (3.12), can now directly be written as:

$$\frac{\partial \hat{v}}{\partial \xi}\frac{\partial \xi}{\partial t}+\frac{\partial \hat{v}}{\partial \tau}\frac{\partial \tau}{\partial t}+\frac{\partial \hat{f}}{\partial \xi}\frac{\partial \xi}{\partial x}+\frac{\partial \hat{f}}{\partial \tau}\frac{\partial \tau}{\partial x}=\hat{r},$$

where $\hat{v}(\tau,\xi)=v(\tau,x(\tau,\xi))$ and $\hat{f}=f(\hat{v}(\tau,\xi))$.

With the use of Eqs.(A1),(A2),(A3) and (A4) this becomes:

$$-\frac{\partial x}{\partial \tau}(\frac{\partial x}{\partial \xi})^{-1}\frac{\partial \hat{v}}{\partial \xi}+\frac{\partial \hat{v}}{\partial \tau}+(\frac{\partial x}{\partial \xi})^{-1}\frac{\partial \hat{f}}{\partial \xi}=\hat{r}.$$

Multiplication with $\frac{\partial x}{\partial \xi}$ yields:

$$-\frac{\partial x}{\partial \tau}\frac{\partial \hat{v}}{\partial \xi}+\frac{\partial x}{\partial \xi}\frac{\partial \hat{v}}{\partial \tau}+\frac{\partial \hat{f}}{\partial \xi}=\frac{\partial x}{\partial \xi}\hat{r},$$

which can be written as:

$$\frac{\partial}{\partial \tau}(\frac{\partial x}{\partial \xi}\hat{v})+\frac{\partial}{\partial \xi}(-\frac{\partial x}{\partial \tau}\hat{v}+\hat{f})=\frac{\partial x}{\partial \xi}\hat{r} \qquad \text{(A5)}$$

With the use of the expressions:

$$\frac{\partial \xi}{\partial t}=-\frac{\int_0^x W(\zeta)d\zeta}{(\int_0^{X_r(t)} W(\zeta)d\zeta)^2}W(X_r(t))\frac{dX_r}{dt}$$

$$\frac{\partial \xi}{\partial x}=\frac{W(x)}{\int_0^{X_r(t)} W(\zeta)d\zeta}$$

and the relations (A3) and (A4), equation (3.5) emerges from (A5)

APPENDIX B

Dissipation in random wave groups incident on a beach

reprinted from:

Coastal Engineering, Vol. 19 (1993) pp. 127-150

Coastal Engineering, 19 (1993) 127–150
Elsevier Science Publishers B.V., Amsterdam

Dissipation in random wave groups incident on a beach

J.A. Roelvink
Delft Hydraulics, P.O. Box 152, 8300 AD Emmeloord, Netherlands

(Received 19 February 1992; accepted after revision 20 August 1992)

ABSTRACT

Roelvink, J.A., 1993. Dissipation in random wave groups incident on a beach. *Coastal Eng.*, 19: 127–150.

Variations in short-wave properties on the time-scale of wave groups provide important mechanisms in the generation of long waves. An essential component of models that describe the propagation of wave groups is the description of the slowly varying dissipation due to wave breaking. A model is proposed for the time-varying dissipation rate.

As the time-varying dissipation rate cannot be obtained from direct measurements, calibration and verification is performed in an indirect way. The formulation is incorporated in several models of the time-averaged dissipation by combining it with a number of theoretical probability distributions for the wave energy. These models predict measurable quantities such as the mean dissipation, the fraction of breaking waves and some statistical wave height parameters. The parameters in the dissipation formulation are calibrated against some available measurements of the mean wave energy. A verification is then performed for some internal parameters in the models and for other datasets.

The calibrated models of the mean dissipation rate in random waves show some improvements in the prediction of internal parameters. The usefulness of these models is also enhanced because the calibration coefficients can be kept constant over a wide range of conditions.

The calibrated formulation of the time-varying dissipation rate is quite simple and can be readily used in wave propagation models that take into account variations on the time-scale of wave groups.

INTRODUCTION

The transformation of certain parameters of an incident random wave train across the surf zone has been the subject of much study and modelling effort. In recent literature, two classes of models have been developed, which are both based on the wave energy balance or the wave action equation, but use markedly different approaches.

In the first, *parametric*, class of models (Battjes and Janssen, 1978; Thornton and Guza, 1983), a shape of the breaking wave height distribution is as-

Correspondence to: J.A. Roelvink, Delft Hydraulics, P.O. Box 152, 8300 AD Emmeloord, Netherlands.

sumed, with parameters that are a function of local, time-averaged wave parameters. The dissipation per breaking wave is modelled using the analogy between fully breaking waves and bores, which was first pointed out by Le Mehaute (1962). By combination of the breaking wave height distribution and the dissipation function, the average dissipation as a function of local wave parameters is obtained. By solving the wave energy balance equation, these local wave parameters can be computed over an arbitrary profile, given the conditions at a seaward boundary.

The second, *probabilistic*, class of models takes the probability density function of wave height (and sometimes wave period) at a seaward boundary, schematizes it to a discrete number of wave height (period) classes, and assumes that each class behaves like a periodic sub-group that propagates independently of the others (Mizuguchi, 1982; Mase and Iwagaki, 1982; Dally et al., 1984). The wave energy balance equation is then solved separately for all waves. As a result, at each point along the profile, the wave height distribution can be determined. All models in this class separate the description for each wave into its behaviour before and after its breakpoint.

Both classes of models, when calibrated, may serve well to predict the transformation of certain properties of the wave height distribution across the surf zone. Also, wave-averaged parameters such as radiation stress and mass flux, required for the prediction of the mean set-up and the undertow, are predicted satisfactorily by both classes of models.

Recently, there has been a growing recognition of the importance of variations in short-wave properties on the time-scale of wave groups. Such variations can force long-wave motions that may be important in themselves or through their interaction with wave groups (Symonds et al., 1982; Symonds and Bowen, 1984; List, 1992; Schäffer and Jonsson, 1990). A new class of *dynamic* models (Sato and Mitsunobu, 1991; Roelvink, 1991; Symonds and Black, 1991) takes into account variations on this time-scale. The dissipation of the short-wave motion in this class of models is slowly varying on the time-scale of the wave groups. Although the propagation and decay of wave groups, and hence the excited long-wave motions, often depend critically on the formulation of this dissipation term, a satisfactory formulation has not yet been presented.

The main goal of this study is to develop a suitable formulation for the time-varying dissipation due to wave breaking. As it is impossible to measure the time-varying dissipation directly, the formulation can only be checked by building it into models that predict measurable parameters, such as the average dissipation, the fraction of breaking waves and the mean wave energy, and by verifying these models both externally and internally.

For this purpose, one wave propagation model of the probabilistic class and three models of the parametric class were formulated, calibrated and verified in this study, all based on the same dissipation formulation. Although it has

not been the primary goal of the study, these models are an interesting by-product in themselves.

The main product, however, is a calibrated formulation for the dissipation of short-wave energy as a function of energy and water depth, which can be easily implemented in models that are time-dependent on the wave-group scale.

DISSIPATION MODEL

Basic concept

In a random wave train, the process of energy dissipation due to wave breaking is extremely complex. If it were possible to plot a time series of the instantaneous dissipation rate at a given location, this would show intermittent peaks with random height and spacing, which cannot be described in a deterministic way. Even when a moving average is applied over some short-wave periods, the slowly varying dissipation rate will still have a random component. However, we can expect that this slowly varying dissipation rate will also have a systematic component which depends on slowly varying characteristics of the short waves, in particular the wave energy. This systematic component, which is the expected value of the dissipation rate per unit area, D, can itself be seen as the product of two components:

$$D = P_b D_b \tag{1}$$

where P_b is the probability that a wave is breaking and D_b the expected value of the dissipation rate in a breaking wave, given that its energy density is E. Both P_b and D_b vary on the time-scale of the wave groups.

Dissipation in a breaking wave

In order to model the dissipation D_b in a breaking wave, we use the well-known analogy between breaking waves and bores, which results in the following approximate expression (Battjes and Janssen, 1978):

$$D_b = \frac{\alpha}{4} \rho g f \frac{H^3}{h} \tag{2}$$

where f is the frequency, H is the height of the breaking wave, h the water depth and α a calibration coefficient. Battjes and Janssen assume all breaking waves to have the maximum wave height H_m; as this maximum wave height is of the order of the water depth, the expression reduces to:

$$D_b = \frac{\alpha}{4} \rho g f H_m^2 \tag{3}$$

As in our case the height of breaking waves is allowed to be considerably smaller than the maximum wave height, eq. (2) should be used in principle. However, it can be argued (Stive and Dingemans, 1984), that the water depth in eq. (2) should rather be seen as a "penetration depth", which is of the order of the wave height. In this case, the dissipation can be written as a simple function of the energy of the breaking waves:

$$D_b = 2\alpha f_p E \tag{4}$$

where the peak frequency f_p has been taken as a characteristic measure of the frequency.

Probability of breaking

In general, waves break when locally the wave front becomes too steep. For irregular waves this may be the result of several mechanisms, such as interaction between short waves, interaction between wave and bottom or between wave and current or wind. For simplicity, we shall not consider the effects of current or wind on wave breaking. Even then, the processes involved are extremely complex and no accurate model is available to predict the probability of breaking in irregular waves. Therefore, a simple empirical approach is chosen, based on some crude assumptions.

These assumptions are:

1. The probability of breaking depends only on local and instantaneous wave parameters. In reality, it also depends on the history of the individual waves, but the breaking process, especially in random waves, has a time-scale which is short compared to the wave group scale, so this effect can be neglected.

2. The basic parameters governing the probability of breaking are the local and instantaneous wave energy and the water depth.

3. In principle, waves of any energy may be breaking or non-breaking. However, the probability of breaking should increase monotonically towards 1 for increasing energy or decreasing water depth.

Thornton and Guza (1983) propose the following empirical "weighting function", which can be interpreted as the probability of breaking:

$$P_b = \left[\frac{H_{rms}}{\gamma h}\right]^n \left[1 - \exp\left[-\left[\frac{H}{\gamma h}\right]^2\right]\right] \leq 1 \tag{5}$$

According to this expression, the probability that a particular wave in an irregular wave train is breaking not only depends on the height of this wave relative to the water depth, but also on a characteristic height parameter of the whole wave train (i.c. H_{rms}). This would imply that the breaking process in a given wave group is influenced by events on a much greater time-scale, which seems unlikely and is in contradiction with our assumption 1. We therefore propose a different form:

$$P_b(E,h) = 1 - \exp\left[-\left(\frac{E}{\gamma^2 E_{ref}}\right)^{n/2}\right] \tag{6}$$

with:

$$E_{ref} = \frac{1}{8}\rho g h^2$$

where γ and n are coefficients. In Fig. 1 this function is plotted for several values of n. It can be seen that the steepness of the function increases with increasing n. The two coefficients γ and n will have to be determined empirically.

Conditional expected dissipation rate for waves with given energy

The expected dissipation rate, given a specific value of E, is now simply found by substituting eqs. (4) and (6) into eq. (1), which leads to:

$$D = \left[1 - \exp\left[-\left(\frac{E}{\gamma^2 E_{ref}}\right)^{n/2}\right]\right] 2\alpha f_p E \tag{7}$$

This equation describes the dissipation rate for a given (random) wave energy and water depth, as is the the main goal of this study. The calibration of the coefficients α, γ and n and the verification of the formulation as such is described in the following sections.

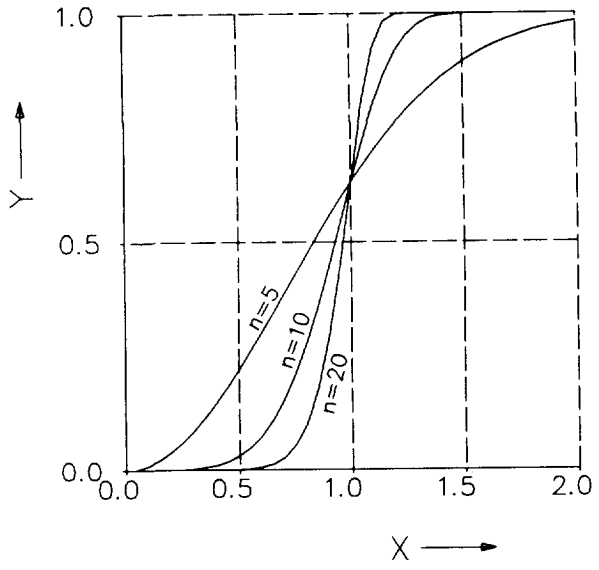

Fig. 1. Plot of the function $Y = 1 - \exp(-X^{n/2})$ for $n = 5, 10, 20$.

TRANSFORMATION OF WAVE ENERGY DISTRIBUTION

Probabilistic model

The formulation for the *probabilistic* approach can be derived readily from the wave action equation by assuming that the slowly varying cross-shore velocity is small compared to the group velocity C_g. This is a reasonable assumption, except for a limited area near the swash zone, where the group velocity goes to zero and long-wave velocities cannot be neglected.

Under this assumption, the wave action equation reduces to the wave energy balance:

$$\frac{\partial E}{\partial t}+\frac{\partial}{\partial x}(EC_g)=-D \tag{8}$$

Assuming C_g to be constant in time, the rate of change of the energy flux of a (part of a) wave group as it travels towards the shore is described by:

$$\frac{\mathrm{d}}{\mathrm{d}x}(EC_g)=-D \tag{9}$$

The dissipation rate D depends on local wave parameters and the slowly varying water depth. Except, again, for the swash zone, the slow fluctuations in the water level can be neglected. In this case, the time-dependence vanishes from the equation, so it can be solved for any given (seaward) boundary value of E. In other words, we can follow any part of a wave group through the surf zone using this equation. As a result, we can also compute the transformation of the energy distribution through the surf zone, starting from a given distribution of E in deep water.

In deep water, it is reasonable to assume a Rayleigh distribution for the wave height; this is equivalent to an exponential distribution for the wave energy:

$$P(\underline{E}<E)=1-\exp\left(-\frac{E}{\bar{E}}\right) \tag{10}$$

where $\underline{E}$ is the stochastic variable, E is a specified level of the wave energy, $\bar{E}$ is the time-averaged wave energy and P_b is the probability of non-exceedance.

In order to compute the transformation of this distribution, the distribution in deep water is given as a number of energy levels with decreasing probability of exceedance. For each deep water energy level, eq. (9) is solved by explicit numerical integration. The result is a number of wave energy decay lines, which cannot cross each other. This is due to the assumptions made in this model, namely a constant group velocity and a dissipation model which is monotonically dependent on the local wave energy.

As a result, a line which starts at an energy level with a certain probability of exceedance will represent this probability throughout the surf zone. At any computation point along the profile, the distribution of the wave energy can be reassembled from these lines. The mean wave energy can be computed from this distribution. Also, the total fraction of breaking waves can be deduced from the model.

The distribution of wave energy can be used to predict the wave height distribution by means of a suitable non-linear local wave model, which uses energy, peak frequency and water depth as input. Here, we apply the high-order stream function method as described by Rienecker and Fenton (1981). Results are presented below.

Parametric models

Basic concept

In the *parametric* class of models, the energy balance equation (8) is averaged over a time scale which is large compared with the wave group time scale:

$$\overline{\frac{\partial \bar{E}}{\partial t}} + \overline{\frac{\partial}{\partial x}(EC_g)} = \overline{-D} \tag{11}$$

Assuming a stationary wave field and no correlation between wave energy and group velocity, this equation reduces to:

$$\frac{\partial}{\partial x}(\bar{E}\bar{C}_g) = -\bar{D} \tag{12}$$

The mean dissipation can be described as the weighted average of the dissipation function:

$$\bar{D} = \int_0^\infty p(E)D(E)\mathrm{d}E \tag{13}$$

where $p(E)$ is the local probability density function (pdf) of the wave energy. In order to close the equations, an assumption must be made regarding the shape of this function, depending on the local wave parameters. The scaling of the function then follows from the requirements that the function is a pdf:

$$\int_o^\infty p(E)\mathrm{d}E = 1 \tag{14}$$

and that the first moment equals the mean energy:

$$\int_0^\infty p(E)E\mathrm{d}E=\bar{E} \tag{15}$$

In the following, three parametric probability density functions are discussed, viz. a depth-limited Weibull-distribution, the Rayleigh-distribution and the clipped Rayleigh-distribution according to Battjes and Janssen (1978).

The following parameters will be used in order to simplify the equations:

$$E_{\mathrm{ref}}=\frac{1}{8}\rho g h^2,\quad \sigma=\sqrt{(\bar{E}/E_{\mathrm{ref}})},\quad E_*=\frac{E}{\bar{E}},\quad Q_{\mathrm{b}}=\int_0^\infty P_{\mathrm{b}}(E)p(E)\mathrm{d}E$$

Weibull distribution

Klopman and Stive (1989) propose a wave height distribution, based upon a shape originally proposed by Glukhovskiy (1966), which degenerates to a Rayleigh-distribution in deep water, but has a depth-limitation resulting in a gradual deformation of the distribution for decreasing water depth. In terms of wave energy, this distribution can be written as:

$$P(E<E)=1-\exp\{-A(E/\bar{E})^m\} \tag{16}$$

Here, m is a free parameter for which Klopman and Stive propose a formulation, which is rewritten here in terms of energy:

$$m=1+0.7\tan^2\left(\frac{\pi}{2}\frac{1}{\gamma_2}\sqrt{\bar{E}/E_{\mathrm{ref}}}\right)=1+0.7\tan^2\left(\frac{\pi}{2}\frac{\sigma}{\gamma_2}\right) \tag{17}$$

The value of γ_2 as given by Klopman and Stive is the theoretical maximum of the wave height over depth ratio, 0.833. The maximum value for the energy-related σ-value as defined above is in the order of 30% lower, due to the non-linearity of depth-limited waves. Therefore a value of 0.65 has been used here.

The parameter A is linked to m through the requirement given by eq. (15):

$$A=\left[\Gamma\left(1+\frac{1}{m}\right)\right]^m \tag{18}$$

where Γ is the gamma function.

The probability density function is found by differentiating eq. (16):

$$p(E)=\frac{mA}{\bar{E}}(E/\bar{E})^{m-1}\exp\{-A(E/\bar{E})^m\} \tag{19}$$

The mean dissipation is now found by integration of eq. (13):

$$\bar{D}=\int_0^\infty p(E)P_b(E)D_b(E)\mathrm{d}E=$$

$$=\int_0^\infty \frac{mA}{\bar{E}}(E/\bar{E})^{m-1}\exp\{-A(E/\bar{E})^m\}\left[1-\exp\left[-\left(\frac{E}{\gamma^2 E_{ref}}\right)^{n/2}\right]\right]*2\alpha f_p E\mathrm{d}E$$

$$=2\alpha f_p \bar{E} mA\int_0^\infty E_*^m\exp(-AE_*^m)\left[1-\exp\left[-\left(\frac{\sigma^2}{\gamma^2}E_*\right)^{n/2}\right]\right]\mathrm{d}E_*$$

$$=2\alpha f_p \bar{E} f_1(\sigma,\gamma,n) \qquad (20)$$

The result is that the mean dissipation is the dissipation in waves with the mean energy, times a function of the wave energy relative to the water depth. This function f_1 is less than or equal to 1, and depends on the local wave height to water depth ratio σ and on the empirical coefficients γ and n.

Rayleigh distribution

The Rayleigh distribution is a special case of eq. (16) for m equal to 1. It has been used by Thornton and Guza (1983), in combination with a slightly different formulation for the dissipation. The mean dissipation follows immediately from eq. (20) and is given by:

$$\bar{D}=2\alpha f_p \bar{E}\int_0^\infty E_*\exp(-E_*)\left[1-\exp\left[-\left(\frac{\sigma^2}{\gamma^2}\right)^{n/2}\right]\right]\mathrm{d}E_*=2\alpha f_p \bar{E} f_2(\sigma,\gamma,n) \qquad (21)$$

Clipped Rayleigh distribution

The clipped Rayleigh distribution as proposed by Battjes and Janssen (1978) is based on the assumptions that the wave heights are Rayleigh-distributed up to a maximum wave height, that all higher waves are simply cut off to this height, that all waves having this maximum height are breaking and that only these waves are breaking. This can be translated to our concept by letting the value of n in the probability of breaking go to infinity, in which case the function becomes a step function: zero for $E/E_{ref} < \gamma^2$, unity for $E/E_{ref} \geqslant \gamma^2$. The maximum wave energy is defined by:

$$E_m=\gamma^2 E_{ref} \qquad (22)$$

Since the probability density function has a "spike" at $E=E_m$, with an area equal to the fraction of breaking waves Q_b, and since the probability of breaking equals unity at this energy, we get for the mean dissipation:

$$\bar{D}=\int_0^\infty p(E)P_b(E)D_b(E)\mathrm{d}E=Q_bD_b(E_m)$$

$$=Q_b2\alpha f_pE_m=2\alpha f_p\bar{E}\frac{\gamma^2}{\sigma^2}Q_b \tag{23}$$

In the clipped Rayleigh distribution, the fraction of breaking waves is defined by the implicit relation:

$$Q_b=\exp\left[-\frac{1-Q_b}{\bar{E}/E_m}\right] \tag{24}$$

This relation yields a unique function of $\bar{E}/E_m=\sigma^2/\gamma^2$, so:

$$\bar{D}=2\alpha f_p\bar{E}f_3(\sigma,\gamma) \tag{25}$$

For the three parametric energy distributions, we get similar expressions for the mean dissipation. For given values of the calibration parameters γ and n the functions f_1, f_2 and f_3 depend only on σ. Therefore it is easy to generate tables of these functions and to interpolate from these tables when solving the mean energy balance equation.

CALIBRATION OF THE MODELS

Three datasets, containing a total of 11 tests, were used to calibrate the probabilistic model and the parametric models, viz. those reported in Battjes and Janssen (1978), Stive (1985) and Hotta and Mizuguchi (1980). A summary of the characteristics of the profile and incident wave conditions is given in Table 1. All sets pertain to irregular waves incident perpendicular to a beach. The letter L under "Type" stands for laboratory test, F stands for field test.

The parameter for which the calibration was performed is the overall energy-based wave height often (confusingly) referred to as H_{rms}. Here it will be termed H_E:

$$H_E=\sqrt{(8\bar{E}/\rho g)} \tag{26}$$

In deep water, H_E is equal to the root-mean-square wave height H_{rms}; in shallow water, due to non-linearity of the waves, the parameters deviate from each other.

The seawardmost data point, having a wave height $H_{E,0}$ and a water depth h_0, is used as a boundary condition for the models. For a given set of calibration points, the energy distribution across each profile is computed and compared to the measured distribution. Two indicators of the overall accuracy of the models are computed, viz. the root-mean-square relative error ϵ_{rms} and the relative bias (mean error) ϵ_{mean}:

TABLE 1

Experimental parameters calibration sets

Test	Source	Type	h_0 (m)	$H_{E,0}$ (m)	f_p (Hz)
MS10	Stive (1985)	L, plane	0.70	0.142	0.341
MS40	Stive (1985)	L, plane	0.70	0.135	0.633
BJ2	Battjes and Janssen (1978)	L, plane	0.70	0.144	0.511
BJ3	Battjes and Janssen (1978)	L, plane	0.70	0.122	0.383
BJ4	Battjes and Janssen (1978)	L, plane	0.70	0.143	0.435
BJ11	Battjes and Janssen (1978)	L, barred	0.70	0.137	0.450
BJ12	Battjes and Janssen (1978)	L, barred	0.70	0.121	0.443
BJ13	Battjes and Janssen (1978)	L, barred	0.70	0.104	0.467
BJ14	Battjes and Janssen (1978)	L, barred	0.70	0.118	0.481
BJ15	Battjes and Janssen (1978)	L, barred	0.70	0.143	0.498
HotMiz	Hotta and Mizuguchi (1980)	F, barred	1.65	0.527	0.113

$$\epsilon_{\text{rms}} = \sqrt{\frac{1}{N}\sum\left[\frac{H_{E,\text{comp}}}{H_{E,O}} - \frac{H_{E,\text{meas}}}{H_{E,O}}\right)^2} \Big/ \frac{1}{N}\sum\frac{H_{E,\text{meas}}}{H_{E,O}} \tag{27}$$

$$\epsilon_{\text{mean}} = \sum\left[\frac{H_{E,\text{comp}}}{H_{E,O}} - \frac{H_{E,\text{meas}}}{H_{E,O}}\right] \Big/ \sum\frac{H_{E,\text{meas}}}{H_{E,O}} \tag{28}$$

As is apparent from the formulae, the errors were scaled with the incident wave height; this is to give data points comparable weights regardless of the scale of the tests or the incident conditions.

From preliminary computations, it turned out that the results were not very sensitive to the value of n, which indicates the steepness of the curve which describes the probability of breaking. Realistic results were obtained both for $n=10$ and for $n=20$.

TABLE 2

Optimum γ-values and relative rms error for $\alpha=1$ and $n=10$, 20. 11 datasets. 159 points

Model	n	α	γ	ϵ_{rms}	Fig.
Probabilistic	10	1.0	0.55	0.045	2a
	20	1.0	0.53	0.054	2b
Weibull	10	1.0	0.54	0.057	2c
	20	1.0	0.52	0.057	2d
Rayleigh	10	1.0	0.57	0.062	2e
	20	1.0	0.57	0.063	2f
Clipped Rayleigh	-	1.0	0.66	0.056	2g

The optimum combination of the coefficients α and γ was obtained by drawing isolines of the error indicators in the α,γ plane, for both values of n, and visually determining the approximate location of zero mean error and minimum rms error. Plots of these isolines are given in Figs. 2a to 2g. By refining the α,γ grid locally and looking at the numerical output, a more accurate location of this optimum was then found.

In all cases the optimum α,γ-combination is found close to the line $\alpha=1$. As a constant value of α facilitates the comparison of the different models, the value of α was fixed at 1, and optimum γ-values were determined for each model and n-value. The results are given in Table 2.

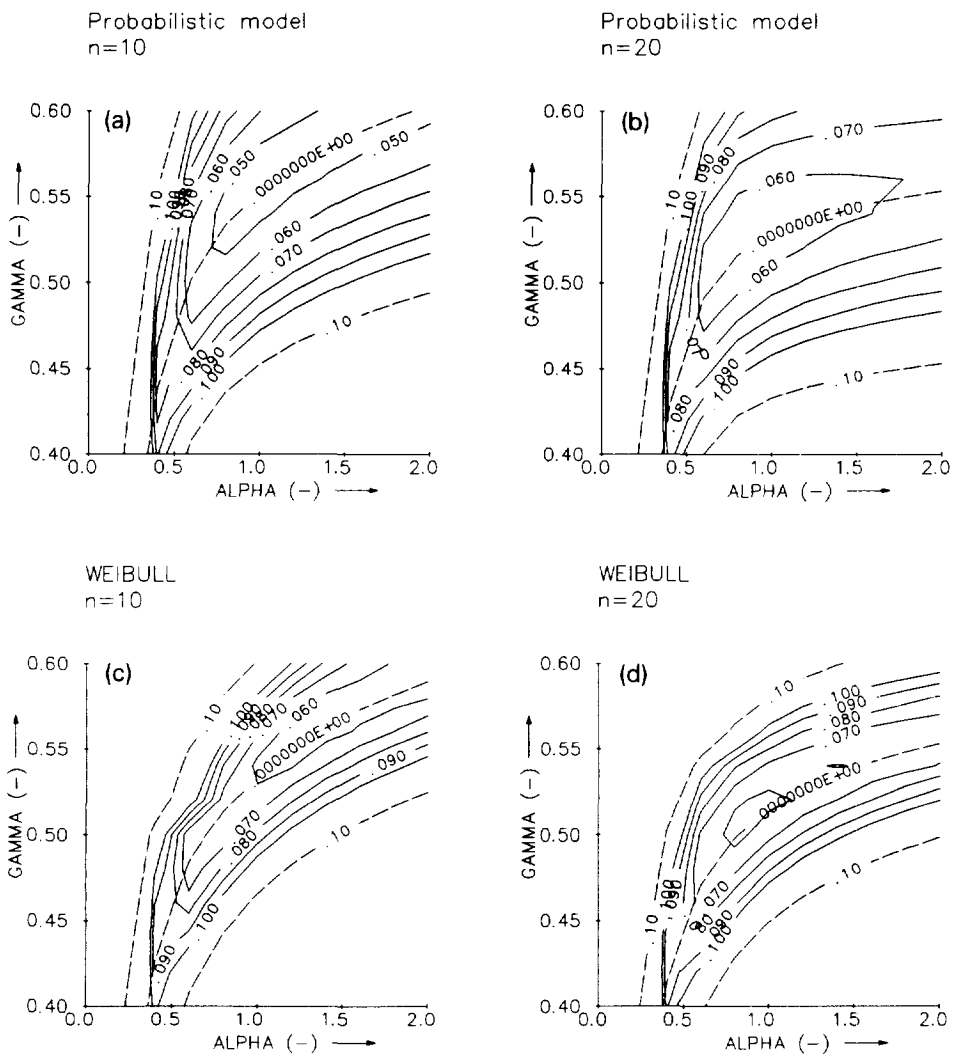

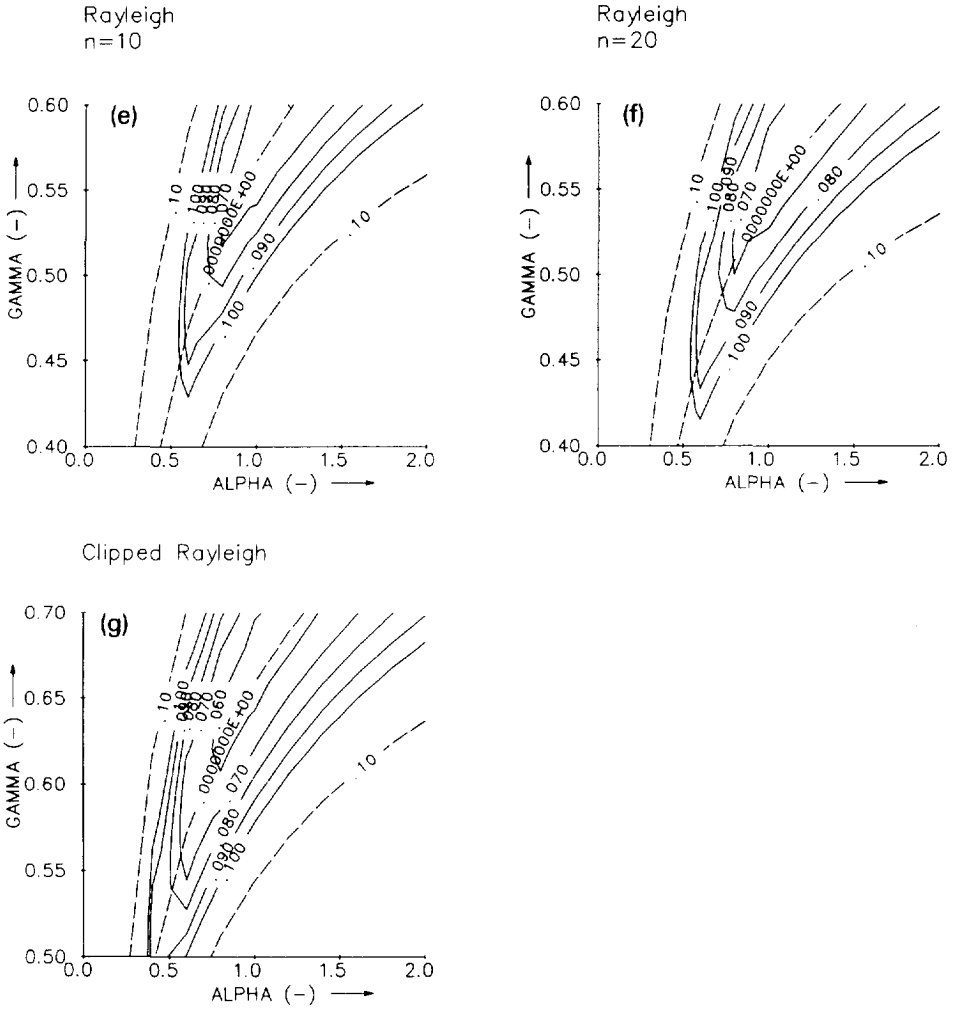

Fig. 2. (a–g) Isolines of rms-error (drawn lines) and mean error (interrupted lines) for all points in calibration sets.

Apparently, all models can be calibrated to give reasonably accurate predictions of the spatial wave energy variation for a fixed combination of calibration coefficients. The probabilistic model seems to be the most accurate, whereas the parametric Rayleigh model with n set at 10 or 20 gives the greatest error.

The clipped Rayleigh model ($n=\infty$) seems to do well with a constant α,γ-combination. Battjes and Stive (1985) used an expression for the maximum wave height which includes the effect of wave steepness; consequently they found that the calibration coefficient γ showed a dependence of the deep water

wave steepness. It seems that using the simpler relation (22) removes this dependence. The optimum γ-values for the Weibull parametric model and the probabilistic model agree closely, which indicates that the energy distributions resulting from the probabilistic model are similar to the shape assumed beforehand in the parametric model.

In the Rayleigh model with finite n, higher wave energy is possible than in the Weibull model, so the probability of breaking for a given energy must

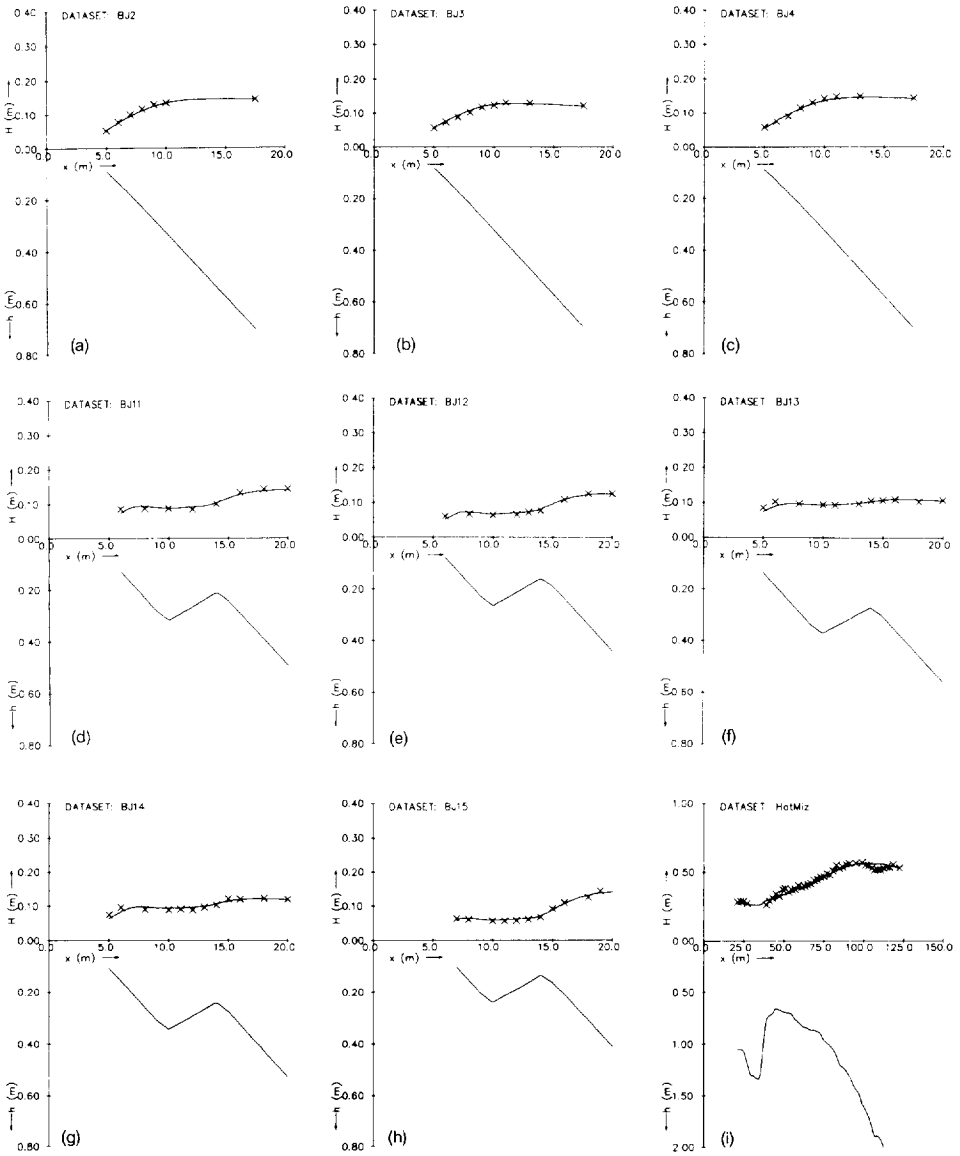

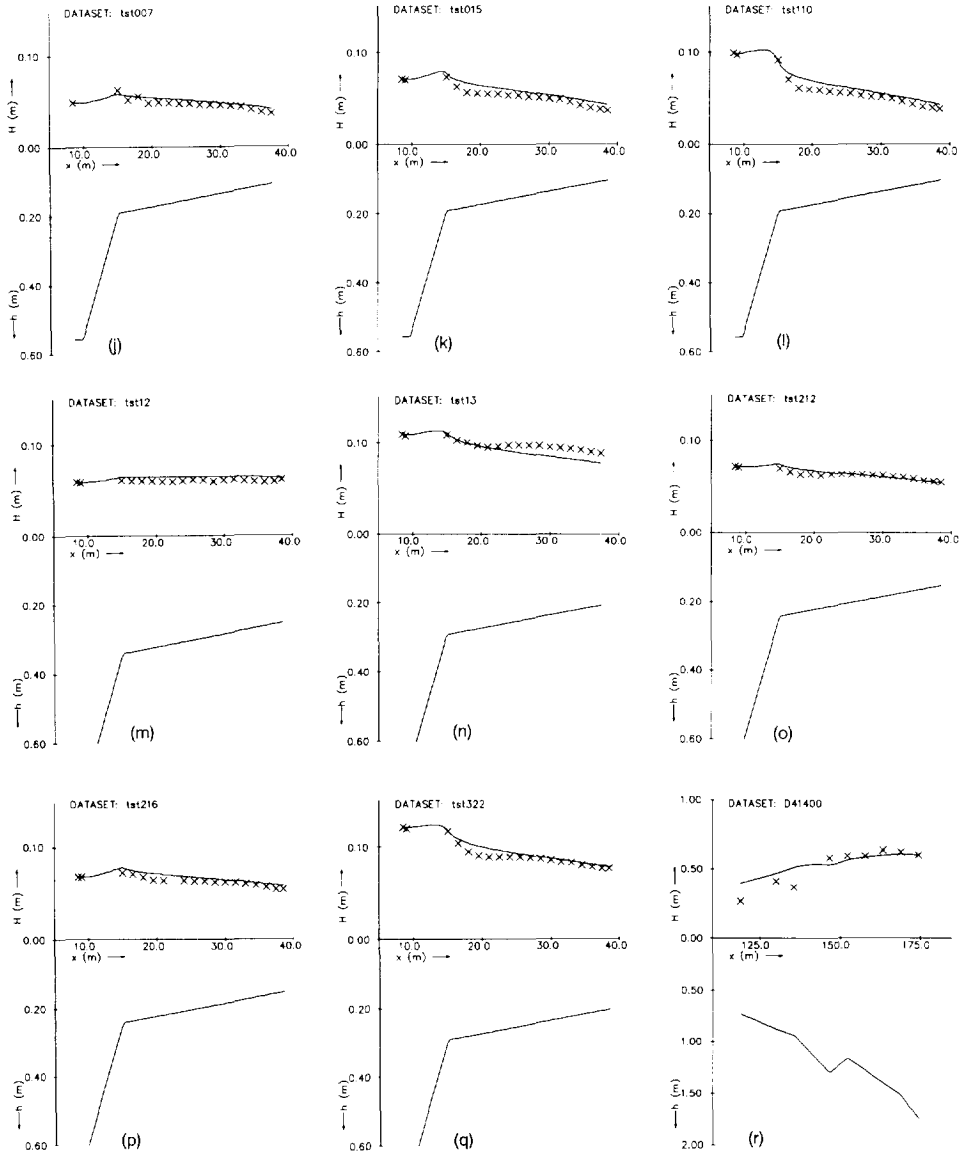

Fig. 3. (a–z) Comparison of measured and computed spatial distribution of H_E, calibration sets and verification sets (continued on p. 142).

decrease in order to get the same mean dissipation. This results in a higher optimum value of γ.

In the clipped Rayleigh model, it is assumed that all breaking waves have the maximum wave energy. The γ-value in this case indicates the level where

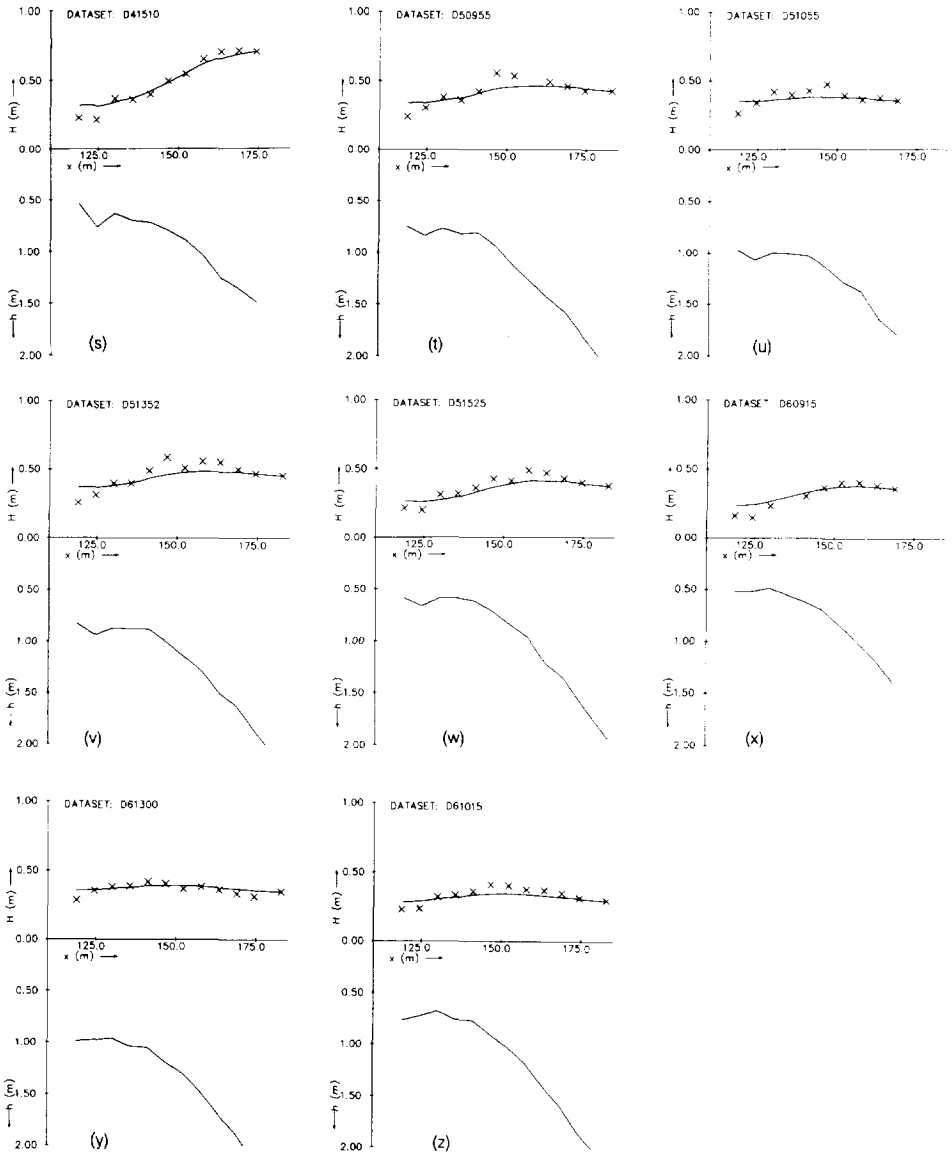

Fig. 3 (continued).

most dissipation takes place. The optimum value of 0.66 is not in contradiction with the other models.

A value of n equal to 10 gives slightly better results than n equal to 20; for the probabilistic model a value of 5 was tried but produced no better results. The value of n was kept at 10 in all further computations.

In Figs. 3a through 3i, the wave height profiles as computed with the probabilistic model, for $n = 10$, are compared with the measured wave height profiles, for all calibration tests. The agreement is quite good, especially considering that all computations were performed with the same set of coefficients.

VERIFICATION

The primary goal of this study is to formulate the time-varying dissipation as a function of local wave parameters. As this is only one of the internal parameters in the models described above, the fact that the mean wave energy (the external parameter) is predicted accurately is not sufficient; errors in internal parameters may be cancelled out by each other.

The dependence scheme in Fig. 4. indicates which other internal parameters must be checked in order to gain confidence in the formulation of the expected value of the slowly varying dissipation.

In the following sections, the numbered items in the dependence scheme will be discussed seperately; afterwards, conclusions are drawn on the accuracy of the model of the expected slowly varying dissipation.

Average dissipation

As has been shown in the previous Section, the average dissipation is modelled accurately. An independent verification is given by two additional datasets, viz. those reported by Ebersole and Hughes (1987) and by Van der Meer (1990). The incident wave conditions are given in Table 3.

The dataset by Ebersole and Hughes was obtained in the field during the DUCK85 campaign. It concerns long-period swell incident perpendicular to an almost prismatic beach. The measurements were carried out with the photopole technique (Hotta and Mizuguchi, 1980). The measurements have been studied in detail by Dally (1990). A problem with hindcasting these experi-

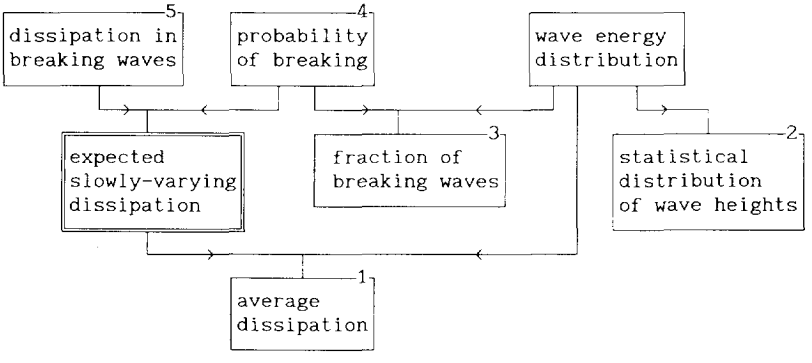

Fig. 4. Dependence scheme dissipation model.

TABLE 3

Experimental parameters verification sets

Test	Source	Type	h_0 (m)	$H_{E,0}$ (m)	f_p (Hz)
D41400	Ebersole and Hughes (1987)	F, barred	1.75	0.600	0.089
D41510	Ebersole and Hughes (1987)	F, barred	1.49	0.706	0.089
D50955	Ebersole and Hughes (1987)	F, barred	2.14	0.431	0.088
D51055	Ebersole and Hughes (1987)	F, barred	1.80	0.353	0.089
D51352	Ebersole and Hughes (1987)	F, barred	2.19	0.452	0.092
D51525	Ebersole and Hughes (1987)	F, barred	1.94	0.374	0.090
D60915	Ebersole and Hughes (1987)	F, barred	1.40	0.360	0.078
D61015	Ebersole and Hughes (1987)	F, barred	2.14	0.296	0.076
D61300	Ebersole and Hughes (1987)	F, barred	2.43	0.346	0.099
T007	Van der Meer (1990)	L, step	0.56	0.049	0.403
T015	Van der Meer (1990)	L, step	0.56	0.071	0.438
T110	Van der Meer (1990)	L, step	0.56	0.099	0.513
T12	Van der Meer (1990)	L, step	0.71	0.059	0.488
T13	Van der Meer (1990)	L, step	0.66	0.109	0.488
T212	Van der Meer (1990)	L, step	0.61	0.072	0.645
T216	Van der Meer (1990)	L, step	0.61	0.068	0.403
T322	Van der Meer (1990)	L, step	0.66	0.121	0.513

ments with the present model is that the wave height distributions at the outermost measuring point deviate significantly from either Rayleigh or Weibull distributions; therefore we cannot expect very good agreement. Still, the measurements have been included as a severe test case. The models were applied with their pre-calibrated coefficient values: $\alpha = 1$, $n = 10$ and γ as in Table 2. Model performance was reasonable for all models: for the 9 experiments, the mean error was less than 2% for all models and the rms error was in the order of 13%. The probabilistic model was not significantly better than the parametric models.

The dataset by Van der Meer concerns laboratory cases of waves incident on a profile with a steep step followed by a very gently sloping bottom. Here, the parametric models show a mean error in the order of 1% and a rms error in the order of 11% over a total of 8 tests. The probabilistic model shows a

TABLE 4

Relative mean and rms error. 28 tests, 389 points

Model	n	α	γ	ϵ_{mean}	ϵ_{rms}
Probabilistic	10	1.0	0.55	0.013	0.088
Weibull	10	1.0	0.54	0.000	0.099
Rayleigh	10	1.0	0.57	0.011	0.099
Clipped Rayleigh	–	1.0	0.66	0.000	0.096

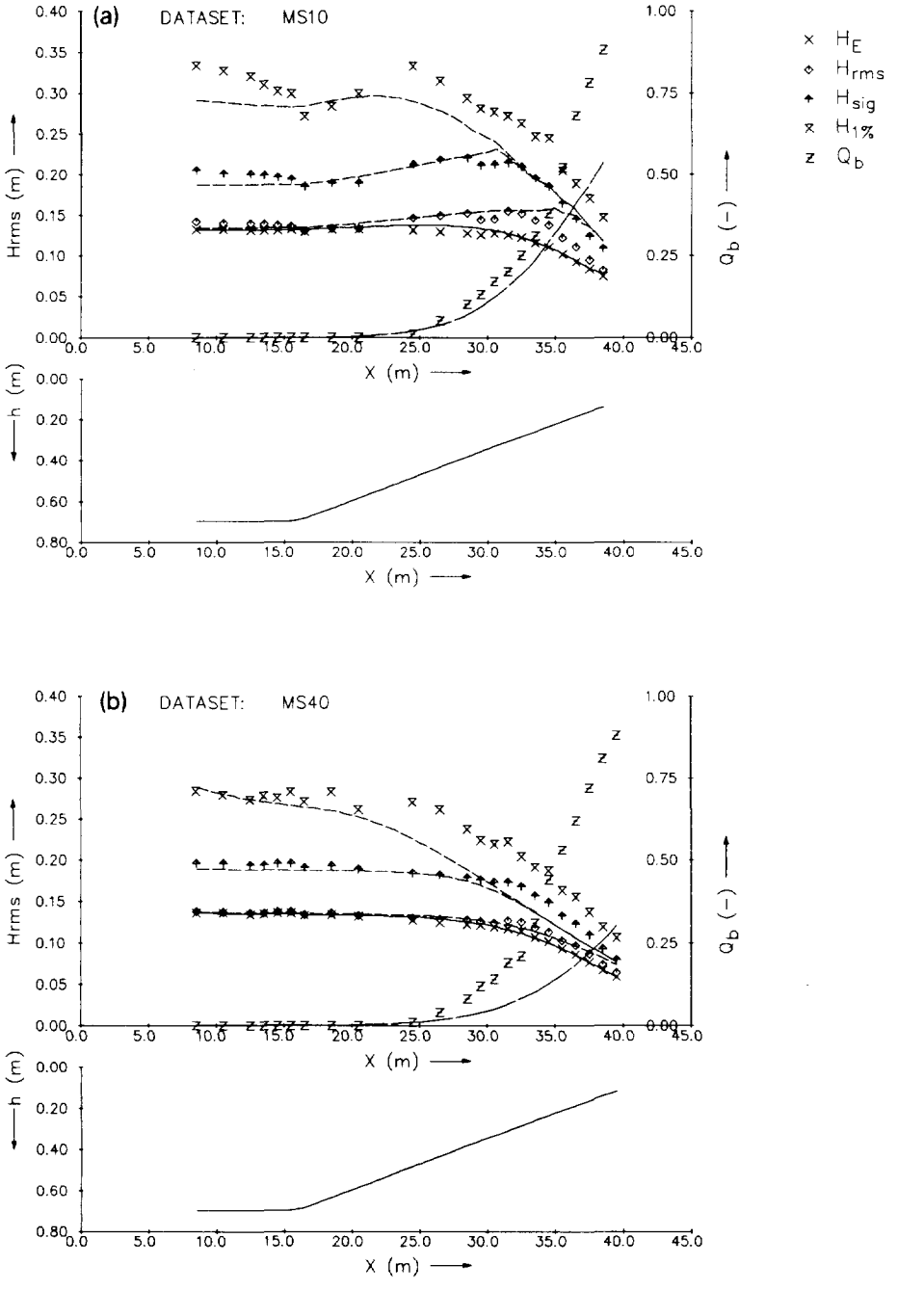

Fig. 5. (a, b) Measured vs. computed values of H_E, H_{rms}, H_{sig}, $H_{1\%}$ and Q; tests from Stive (1985).

mean error of almost 5%, but a lower rms error of 8%. The general shape of the energy distributions over the profile is represented best by the probabilistic model; hence the lower rms error.

The error indicators were also computed over all tests considered in this study; the results are given in Table 4.

All models can be used to predict the variation of the mean wave energy over the profile; the probabilistic model is slightly more accurate in this respect. A comparison between the measured wave height profiles and those computed with the probabilistic model is given in Figs. 3a to 3z.

Statistical distribution of wave heights

At present, no data are available on the probability distribution of the wave energy; data on wave height probability distributions are available. With the help of non-linear theory, wave heights can be estimated from wave energy levels. If the variation of statistical wave height parameters over the profile is predicted correctly, the underlying energy probability distributions are likely to be correct as well.

The statistical wave height parameters are deduced from the predicted wave energy probability distribution by the following method. The distribution of the linear estimate of the wave height, H_l, was derived from the wave energy distribution, where $H_l = \sqrt{(8E/\rho g)}$. The statistical parameters $H_{l,rms}$, $H_{l,sig}$ and $H_{l,1\%}$ were computed from this distribution, using the usual definitions. The matching non-linear crest-to-trough heights were then computed with the help of Rienecker and Fenton's (1981) stream function method.

The dataset used is from Stive (1985), tests MS10 and MS40. In Figs. 5a and 5b, the distributions of the rms wave height H_{rms}, the significant wave height H_{sig} and the wave height exceeded 1% of the time, $H_{1\%}$, as measured and as computed, are given. Qualitatively, the agreement is quite good; quantitatively, the values of $H_{1\%}$ are underestimated within the surf zone. This may be due to the presence of long waves; the higher waves are limited in the model by the mean depth, whereas in reality they are limited by the slowly fluctuating depth. Also within the surf zone, as can be expected, the values of the rms wave height are overpredicted by non-linear theory, due to the decoupling of the higher harmonics. Still, the wave height distributions are predicted well enough to lend some confidence to the computed energy distributions. Further study is required to confirm this.

Fraction of breaking waves

The fraction of breaking waves, Q_b, is the integral of the product of the energy distribution and the probability of breaking at a given energy. Therefore, if the energy distribution is modelled correctly, the fraction of breaking waves can only be correct if the probability of breaking is correct too. In the

same two tests from Stive (1985), the fraction of breaking waves was counted visually; measured and predicted values are shown in Figs. 5a and 5b. For test MS10, the agreement is quite good, although well inside the surf zone Q_b is somewhat underpredicted, by up to 30%. For test MS40, the underprediction is much more serious: up to a factor 3. This seems strange since the dissipation is modelled so well.

A possible explanation is that the peak period during this test was twice as short as during test MS10. The waves therefore tended to be spilling, whereas the bore model only really applies to fully breaking waves with a roller over the whole wave front. In such a case, the criterion that a breaking wave is "a wave with foam on it" will overestimate the fraction of bore-like breaking waves.

The question is, whether this analysis should lead to an adjustment of the definition of "breaking wave" or to an adjustment of the model of the dissipation in a breaking wave. This should be resolved in further study; for now, the computed fraction of breaking waves should be interpreted as the fraction of fully breaking, bore-like waves.

Probability of breaking

The probability of breaking as a function of wave height has been investigated by some authors (Thornton and Guza, 1983; Dally, 1990). This gives a qualitative check on the shape of this probability as a function of energy. However, the available data do not enable a direct plot of the probability of breaking against the wave energy, for given water depths, so a direct quantitative check cannot be made. As is also apparent from the previous Section, further study is required on this aspect of the model.

Dissipation in breaking waves

An interesting verification of the formulation of the dissipation in breaking waves is obtained from the measurements of Stive (1984), for regular waves. On page 109 of his paper, he presents graphs of a non-dimensional dissipation A_ϵ, defined as the ratio of the dissipation rate derived from measured energy flux gradients and the dissipation according to a hydraulic jump:

$$D_b = A_\epsilon \frac{1}{4} \rho g f H^3 \frac{h}{d_1 d_2} \tag{29}$$

where d_1 is the depth in front of the breaker and d_2 is the depth at the crest. The values of A_ϵ are in the range of 1.5 to 2.5. If we now assume:

$$\frac{Hh}{d_1 d_2} = \gamma_3 \tag{30}$$

we get a similar expression to our eq. (4) if $\alpha = A_\epsilon \gamma_3$. With the order of magnitude estimates $H/h \simeq 0.5$, $d_1/h \simeq 0.8$ and $d_2/h \simeq 1.3$, γ_3 is in the order of 0.5, which leads to an α-value in the order of 1. This is in agreement with the optimum value found in the calibration.

Conclusions on verification

From the verification presented here we may draw the conclusion that the mean dissipation is modelled correctly and that there are indications that the wave energy distribution is also modelled correctly; therefore, the expected time-varying dissipation must be reasonably accurate. This term is again composed of two terms, viz. the time-varying dissipation in breaking waves and the probability of breaking. There is an indication that the first of these terms is modelled correctly; on the probability of breaking there is still some uncertainty. Qualitatively, there is agreement between measured and predicted fractions of breaking waves; quantitatively, they are somewhat underpredicted, although of the right order of magnitude.

CONCLUSIONS

The existing parametric model according to Battjes and Janssen has been improved in the sense that the internal parameters are more realistic; also, the dependence of the calibration coefficients on wave steepness has vanished. A parametric model based on a Weibull distribution has been added to this class of models, for which the distributions closely resemble those resulting from the probabilistic model. All three parametric models can be used to predict with reasonable accuracy the spatial distribution of the mean wave energy; the one based on a Weibull distribution is the most accurate, and the model based on the Rayleigh distribution the least accurate.

The probabilistic model presented has been shown to follow from the wave action equation if the group velocity is assumed to be constant in time and effects of surfbeat can be neglected. These restrictions are less severe than those for the earlier models in this class, which require a negligible variation of the propagation velocity of individual waves. One set of equations is used throughout the shoaling and breaking region, as opposed to earlier models in this class. The model can be used to predict the transformation of the probability distribution of the wave energy through the surf zone. With the help of a non-linear wave theory, wave height characteristics can be derived from the energy distributions.

The calibrated and verified eq. (7) for the expected time-varying dissipation can be readily used in wave propagation models that take into account variations on the time-scale of wave groups.

ACKNOWLEDGEMENTS

This work was undertaken as part of the MAST G6 Coastal Morphodynamics research programme. It was funded jointly by the Coastal Genesis programme of The Netherlands' Rijkswaterstaat and by the Commission of the European Communities, Directorate General for Science, Research and Development, under MAST contract no. 0035. The author would like to thank Prof. J.A. Battjes and his colleagues M.J.F. Stive and M.W. Dingemans for their constructive remarks on a draft version of this paper.

REFERENCES

Battjes, J.A. and Janssen, J.P.F.M., 1978. Energy loss and set-up due to breaking of random waves. In: Proc. 16th Int. Conf. Coastal Engineering, ASCE, New York, pp. 569–587.

Battjes, J.A. and Stive, M.J.F., 1985. Calibration and verification of a dissipation model for random breaking waves. J. Geophys. Res., 90(C5): 9159–9167.

Dally, W.R., 1990. Random breaking waves: Field verification of a wave-by-wavealgorithm for engineering application. Coastal Eng., 16: 369–397.

Dally, W.R., Dean, R.G. and Dalrymple, R.A., 1984. A model for breaker decay on beaches. Proc. 19th Int. Conf. Coastal Engineering, ASCE, New York, pp. 82–98.

Ebersole, B.A. and Hughes, S.A., 1987. Duck85 photopole experiment. U.S. Army Waterways Experiment Station, misc. paper CERC-87-18, Vicksburg, MS.

Glukhovskiy, B.Kh., 1966. Issledovaniye morskogo vetrovogo volneniya (investigation of sea wind waves). Gidrometeoizdat, St. Petersburg, Leningrad, 1966.

Hotta, S. and Mizuguchi, M., 1980. A field study of waves in the surf zone. Coastal Engineering in Japan, Vol. XXIII, Japan Soc. of Civil Engineers, Tokyo.

Klopman, G. and Stive, M.J.F., 1989. Extreme waves and wave loading in shallow water. Paper presented at E&P Forum Workshop "Wave and current kinematics and loading", Paris, 25–26 Oct. 1989.

Le Mehaute, B., 1962. On non-saturated breakers and the wave run-up. In: Proc. 8th Int. Conf. Coastal Engineering, ASCE, New York, pp. 1178–1191.

List, J.H., 1992. A model for two-dimensional surf beat. J. Geophys. Res., 97: 5623–5635.

Mase, H. and Iwagaki, Y., 1982. Wave height distributions and wave grouping in surf zone. In: Proc. 18th Int. Conf. Coastal Engineering, ASCE, New York, pp. 58–76.

Mizuguchi, M., 1982. Individual wave analysis of irregular wave deformation in the nearshore zone. In: Proc. 18th Int. Conf. Coastal Engineering, ASCE, New York, pp. 485–504.

Rienecker, M.M. and Fenton, J.D. 1981. A Fourier approximation method for steady water waves. J. Fluid Mech., 104: 119–137.

Roelvink, J.A., 1991. Modelling of cross-shore flow and morphology. In: Proc. ASCE Specialty Conf. "Coastal Sediments", Seattle, WA. ASCE, New York, pp. 603–617.

Sato, S. and Mitsunobu, N., 1991. A numerical model of beach profile change due to random waves. In: Proc. ASCE Specialty Conf. "Coastal Sediments", Seattle, WA, pp. 674–687.

Schäffer, H.A. and Jonsson, I.G., 1990. Theory versus experiments in two-dimensional surf beats. In: Proc. 22nd Int. Conf. Coastal Engineering, Delft, pp. 1131–1143.

Stive, M.J.F., 1984. Energy dissipation in waves breaking on gentle slopes. Coastal Eng., 8: 99–127.

Stive, M.J.F., 1985. A scale comparison of waves breaking on a beach. Coastal Eng., 9: 151–158.

Stive, M.J.F. and Dingemans, M.W., 1984. Calibration and verification of a one-dimensional wave energy decay model. Delft Hydraulics Laboratory, report on investigation M 1882.

Symonds, G. and Black, K.P., 1991. Numerical simulation of infragravity response in the nearshore. In: Proc. 10th Australasian Coastal and Ocean Eng. Conf., Auckland, pp. 339–344.

Symonds, G. and Bowen, A.J., 1984. Interactions of nearshore bars with incoming wave groups. J. Geophys. Res., 89(C2): 1953–1959.

Symonds, G., Huntley, D.A. and Bowen, A.J., 1982. Two-dimensional surf beat: long wave generation by a time-varying breakpoint. J. Geophys. Res., 87(C1): 492–498.

Thornton, E.B. and Guza, R.T., 1983. Transformation of wave height distribution. J. Geophys. Res., 88: 5925–5938.

Van der Meer, J.W., 1990. Golfhoogtes van brekende golven op een flauw talud (Wave heights for breaking waves on a flat slope, in Dutch). Delft Hydraulics report no. H462-IV, Delft.